The Philosophical Magazine

FIRST PUBLISHED IN 1798

A Journal of Theoretical Experimental and Applied Physics

Vol. 6 September 1961 No. 69
Eighth Series

25s. 0d., plus postage
Annual Subscription £13 10s. 0d., payable in advance

Printed and Published by
TAYLOR & FRANCIS LTD
RED LION COURT, FLEET STREET, LONDON, E.C.4

THE PHILOSOPHICAL MAGAZINE

Authors wishing to submit papers for publication in the Journal should send manuscripts directly to the Publishers.

Manuscripts should be typed in *double* spacing on one side of quarto (8×10 in.) paper, and authors are urged to aim at absolute clarity of meaning and an attractive presentation of their texts.

References should be listed at the end in alphabetical order of authors and should be cited in the text in terms of author's name and date. Diagrams should normally be in Indian ink on white card, with lettering in soft pencil, the captions being typed on a separate sheet.

A leaflet giving detailed instructions to authors on the preparation of papers is available on request from the Publishers.

Authors are entitled to receive 25 offprints of a paper in the Journal free of charge, and additional offprints can be obtained from the Publishers.

The *Philosophical Magazine* and its companion journal, *Advances in Physics*, will accept papers for publication in experimental and theoretical physics. The *Philosophical Magazine* publishes contributions describing new results, letters to the editor and book reviews. *Advances in Physics* publishes articles surveying the present state of knowledge in any branch of the science in which recent progress has been made. The editors welcome contributions from overseas as well as from the United Kingdom, and papers may be published in English, French and German.

The Growth of Ice Crystals on Freshly Cleaved Covellite Surfaces

By J. Hallett
Department of Meteorology, Imperial College, London†

[Received January 23, 1961]

Abstract

Oriented ice crystals growing as thin plates on freshly cleaved surfaces of covellite, when examined by reflected light, show interference colours which give a measure of the crystal thickness. Some growing crystals remain constant in colour, failing to thicken in a direction normal to the basal plane. Growth can be initiated on the basal plane by contact with a thicker crystal, by increase of the excess vapour density, or by causing mechanical damage to the surface.

When two crystals of different thickness touch, layers grow from the point of contact across the thinner crystal, with velocity inversely proportional to the thickness, for thickness 200 to 1000 Å. This implies that the layers are growing primarily by surface diffusion of adsorbed molecules to their edges. This surface diffusion is characterized by a distance x, from which a growing layer collects molecules; measurements indicate that x has a maximum value of 7·5 μ at -6°c. The shape of layers and crystals are circular, polygonal, or dendritic depending on their thickness, and the excess vapour density of the environment. The relevance of the results to the variation of ice crystal habit with temperature is examined.

§ 1. Introduction

In a previous investigation of the epitaxial growth of ice crystals on single crystalline substrates (Bryant *et al.* 1959), it was discovered that crystals growing on freshly cleaved surfaces of covellite (natural cupric sulphide) were often very thin, and gave rise to brilliant interference colours when viewed by a microscope with vertical illumination. As each crystal grows vertically the colour changes, enabling its rate of growth to be found. In the present investigation this technique has been exploited to select crystals which do not grow perpendicular to the basal plane, and to investigate the relation between the rate of growth of discrete layers across the crystal, and the layer thickness. Previous observations had shown that layers growing on p-toluidene (Kowarski 1935) and cadmium (McNutt and Mehl 1955) crystals grown from the vapour, and on KH_2PO_4 crystals grown from solution (Bunn and Emmett 1949) propagated with a velocity inversely related to their thickness. Other substances, however, for example, crystals of sucrose growing from solution (Albon and Dunning 1959) had

† Present address: Department of Meteorology, University of California, Los Angeles.

layers whose growth velocity was independent of thickness. By observing the growth rate, shape, thickness, and spacing of the layers on ice crystals we hoped to learn something about the growth mechanism which would throw some light on the changes of crystal habit with temperature exhibited by ice crystals growing from the vapour (Hallett and Mason 1958).

§ 2. Experimental Technique

The principle of the apparatus is similar to that used in the previous investigation. The substrate crystal rested on the flat end of a brass rod which dipped into a vacuum flask containing liquid nitrogen (fig. 1†). Its temperature was controlled by a resistance heater soldered just below the surface. The environmental conditions were controlled by the temperature of an ice-lined outer brass chamber, also cooled by liquid nitrogen. Its temperature was controlled by a second heater, and could be kept constant to within 0·2°C. It was measured by a copper–constantan thermocouple in contact with the ice surface. An estimate of the substrate crystal temperature was obtained from a thermocouple 40 s.w.g. copper–constantan, which lay alongside the crystal. This gave a value which was too low, since it had a higher thermal conductivity than the substrate crystal and both were heated by the warmer environment. A correction was made empirically by observing the temperature difference when ice crystals neither grew nor evaporated, which should have occurred when the crystal and environment temperatures were just equal. The maximum correction was about 4°C. This effect was partly caused by the proximity of the warm objective. In practice this limited the working distance to a minimum of 4 mm. The vapour density excess or deficiency $\Delta\rho$, was calculated from the difference of the equilibrium vapour density over ice at the environment and substrate temperatures. An error of 0·2°C in either temperature would give rise to an error of 10^{-7} g cm^{-3} in the excess vapour density near 0°C, and 10^{-8} g cm^{-3} near -20°C. The whole cold unit rested on the stage of the microscope and could be moved with the usual vernier adjustments, about $\frac{1}{2}$ cm in each direction.

The optical system employed a 16 mm bloomed metallurgical objective. The object was illuminated by a tungsten lamp through a vertical illuminator, viewed by a $\times 20$ eyepiece, and recorded simultaneously via a part silvered mirror on 35 or 16 mm colour film, Superanscochrome, Type PN 1 226 (tungsten).

In performing an experiment, the current in each heater was adjusted to give any desired value of crystal and environment temperature, and hence vapour density difference. A freshly cleaved specimen of covellite about $3 \times 3 \times 0{\cdot}5$ mm^3 was selected, placed in position with a pair of tweezers, where it came into thermal equilibrium with its surroundings in a few seconds. The microscope was then moved into place for viewing and photography.

† Figures 2, 5, 8, 9, 10 and 15 are shown as plates.

Fig. 1

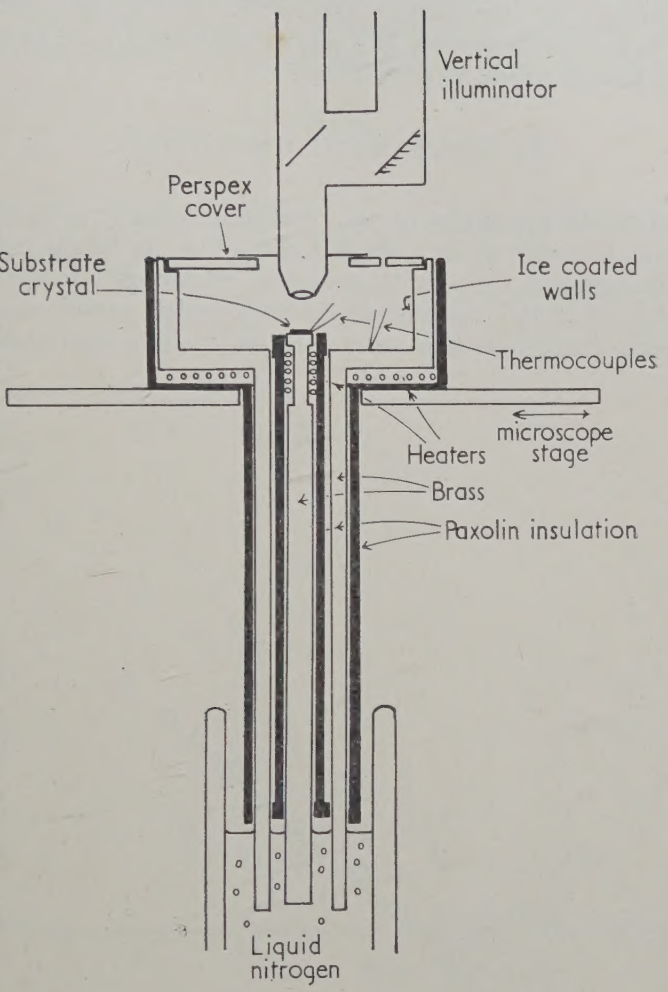

The experimental apparatus.

§ 3. Measurement of Ice Crystal Thickness

Events took place too quickly for accurate visual observation, and all measurements were made from frames of 16 mm film, taken each second. A calibration slide was made of Newton's rings produced by freezing a lens of known radius of curvature on a surface of covellite whose surface had been tested against an optically flat surface, using white (tungsten) light for illumination. Under these conditions, each order of interference

had a characteristic colour and with a little practice the actual thickness of any crystal could be estimated to an accuracy of 150 to 200 Å. As crystals became thicker, the interference colours were fainter, and could not be distinguished when the crystal thickness exceeded about 2 μ, beyond which all crystals became a uniform pink colour.

§ 4. Experimental Observations

4.1

The first crystals to appear on the covellite invariably grew along those steps in the substrate which exceeded about 0·1 μ in height (see fig. 10). All crystals assumed a constant orientation related only to the substrate crystal and not to the direction of the step, which varied continuously. The presence of steps less than 0·1 μ in height could be seen when crystals,

Fig. 3

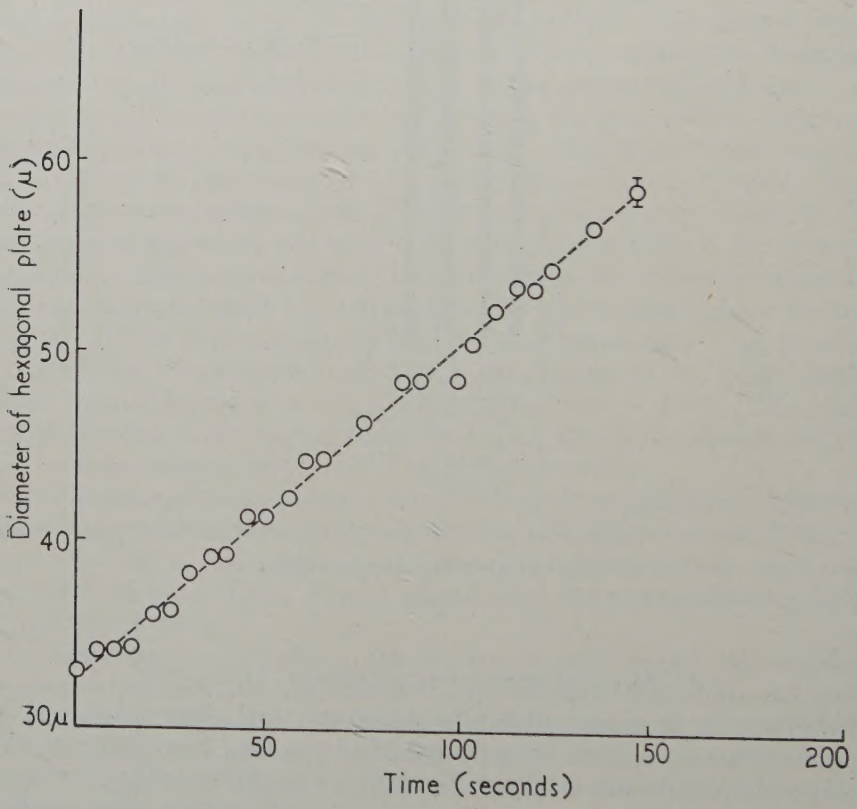

The rate of growth of a hexagonal plate of constant thickness 6000 Å. Temperature −14°c. Excess vapour density $0{\cdot}39 \times 10^{-6}$ g cm^{-3}.

nucleated elsewhere, grew across them, and showed a change of hue. This is clearly shown by the large crystal in the upper part of fig. 2, which has grown across steps of height 800 to 300 Å. The total thickness of this crystal was about 5000 Å. Crystals subsequently grew on flat areas of the surface, particularly when the excess vapour density was large.

Fig. 4

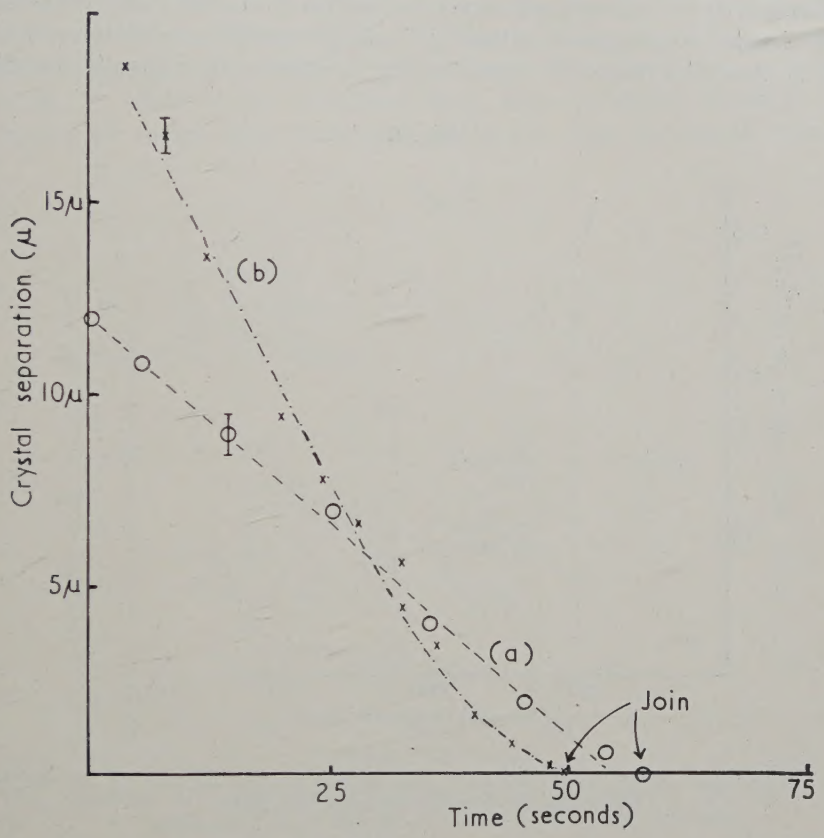

The approach of two hexagonal plates. Temperature −18°c. Excess vapour density $0{\cdot}2 \times 10^{-6}$ g cm^{-3}. (*a*) Plates of constant thickness; (*b*) plates growing vertically.

All crystals which originated at steps, and most others, grew uniformly in thickness until they became pink. At low values of excess vapour density, however, a few isolated crystals increased only in diameter, the colour and thickness remaining constant. The growth rate of a typical crystal is shown in fig. 3. Measurement made on about 50 such crystals showed that the crystal diameter increases linearly with time between 15 and 100 μ. Crystals which thickened invariably grew more slowly in diameter. Figure 4 shows that the rate of approach of two plates of

constant, nearly equal thickness does not decrease as they become close together and finally join. Curve (*b*) shows that the rate of approach does decrease when the crystals are thickening in the vertical direction.

The rate of vertical growth depended also on temperature, and prism-type crystals often appeared below $-25°$C and above $-8°$C.

4.2. *Crystal Shape*

The shape of the ice crystals depended on the crystal thickness, changing from circular to polygonal as the thickness increased from 3000 to 5000 Å. This is shown by the lower crystal in fig. 2, which was originally circular,

Fig. 6

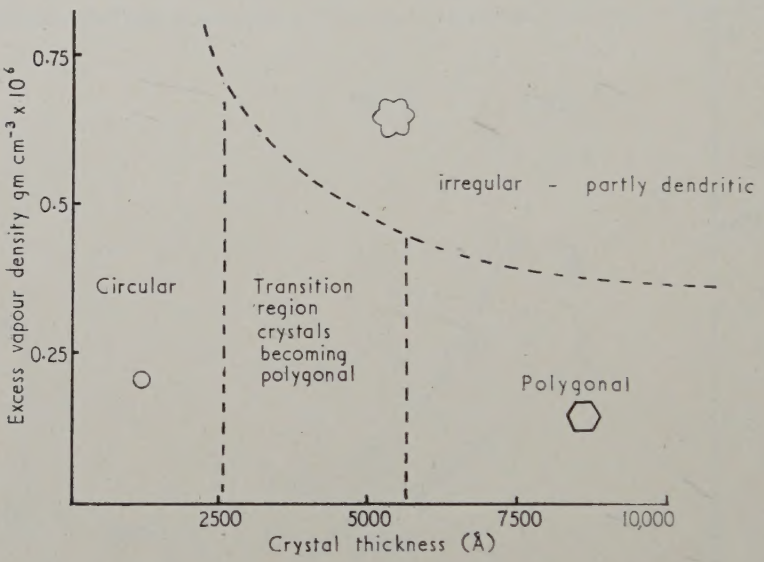

The variation of shape with thickness and excess vapour density of ice crystals growing on freshly cleaved covellite.

and is beginning to take polygonal form as it thickens. At high values of excess vapour density, the crystal shape became very irregular, as in fig. 5, and finally took a roughly dendritic form with branches lying along $\langle 11\bar{2}0 \rangle$ directions. These changes are summarized in fig. 6. There was not any dependence of shape on crystal diameter from 15 to 100 μ.

4.3. *Ageing of the Covellite Surface*

If a piece of covellite which had not been freshly cleaved was used as the substrate crystal, the type of growth was quite different from that described above. As the ice crystal diameter increased beyond about 20 μ, it began to grow upwards from the surface, forming a hollow hexagonal

cup. The covellite behaved in this way after about 10 min exposure to the (London) atmosphere.

4.4. *Growth of Ice Layers*

Ice layers were occasionally seen spreading over flat ice crystals already growing on the substrate. These layers were often initiated as two crystals of different thickness grew laterally, and joined. If one crystal was much thicker than the other, say 2000 Å and 10 μ, a succession of discrete layers of different thickness often spread out from the point of contact, and grew across the thinner crystal (fig. 5). The shape of these layers depended upon their thickness and the excess vapour density of the environment as shown in fig. 7. Thin layers, less than 300 Å, were invariably circular (fig. 5, crystal in upper left), becoming polygonal with increasing thickness.

Fig. 7

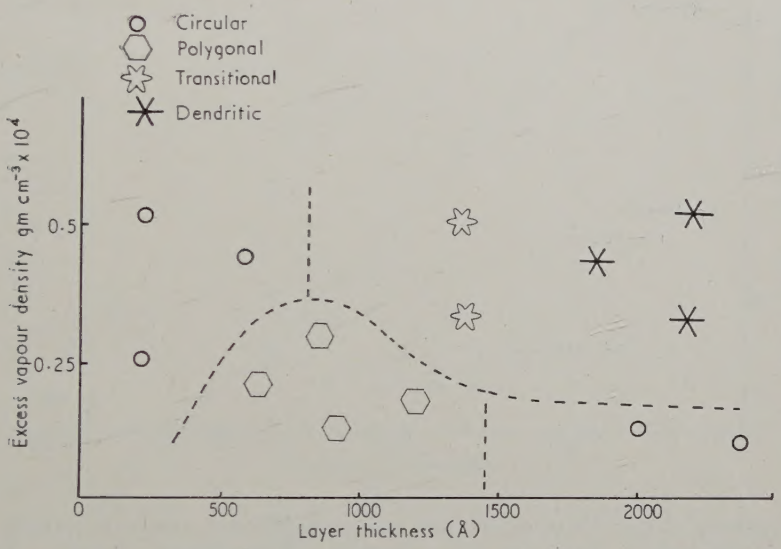

The variation of shape with thickness and excess vapour density of layers spreading from the point of contact of two crystals.

Layers between 800 Å and 2000 Å spread first around the edge of the crystal, and then inwards towards the centre (fig. 8). This effect appears to be related to the increasing importance of diffusion of water vapour through the air as the step height exceeds the mean free path of air molecules, about 0·1 μ. Layers of thickness greater than 2000 Å spread with a sloping front, and usually have a greater velocity of growth in the $\langle 11\bar{2}0 \rangle$ directions, giving in effect a three dimensional dendrite (see fig. 2, lower crystal, and figs. 9, 10). When the touching crystals were of almost the same thickness, the thickening appeared to take place uniformly over the whole crystal. As soon as the difference exceeded 800 Å, however, the thickening took place first around the edge as described above.

Layers were also occasionally initiated remote from the edge of a crystal, possibly by the inclusion of a foreign particle as the crystal grew. In this case layers of thickness up to 2000 Å spread out in circular form. As soon as any layer greater than 800 Å reached the crystal edge, however, it spread around the edge, as if it had been initiated there and then filled in toward the centre.

Observations of the rate of growth of layers were made from time lapse films. For layers whose thickness lay between 200 and 1000 Å, the velocity

Fig. 11

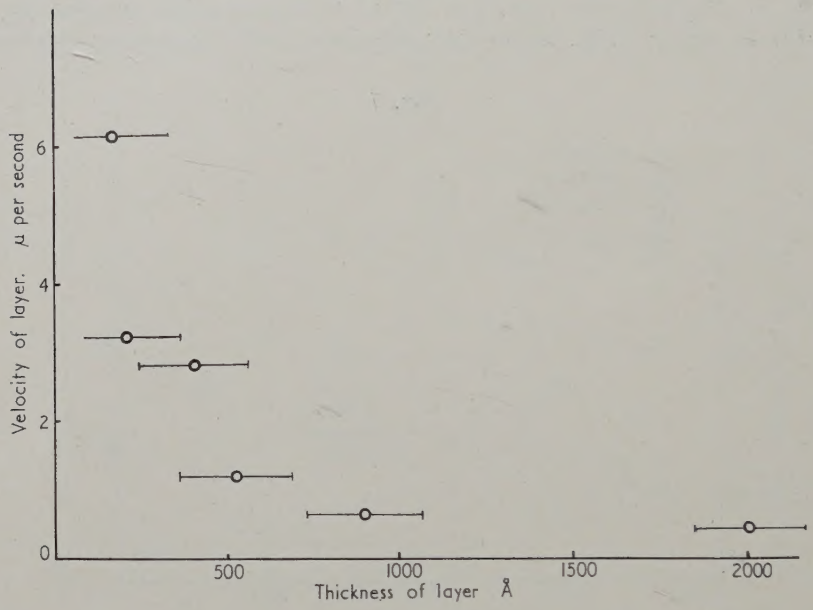

The velocity of growth of a series of layers of different thickness, which were initiated at the edge of a crystal. Temperature $-6{\cdot}0°$C. Excess vapour density $0{\cdot}22 \times 10^{-6}$ g cm^{-3}.

was found to be inversely proportional to the layer thickness. A typical set of measurements are shown in fig. 11. The velocity of layer growth increased with the excess vapour density, until a value of $0{\cdot}2 \times 10^{-6}$ g cm^{-3} was reached, when the growth rate became nearly constant. If a crystal were thickening uniformly however, its rate of growth was approximately proportional to the excess vapour density.

It was found that the rate of growth of circular layers was constant for radii from 10 μ to at least 80 μ. A typical example of the growth of such a layer is shown in fig. 12. As in the case of complete ice crystals, the growth rate is reduced when the layer is also increasing in thickness. The

resolution was not sufficient to make measurements on layers with radius less than about 10 μ.

4.5. *Influence of Temperature on Velocity of Ice Layers*

In view of the strong dependence of ice crystal habit on temperature (Hallett and Mason 1958), an investigation of the influence of temperature on the rate of layer propagation was made. The initiation of layers was a very uncertain event, and many growths were examined before a layer

Fig. 12

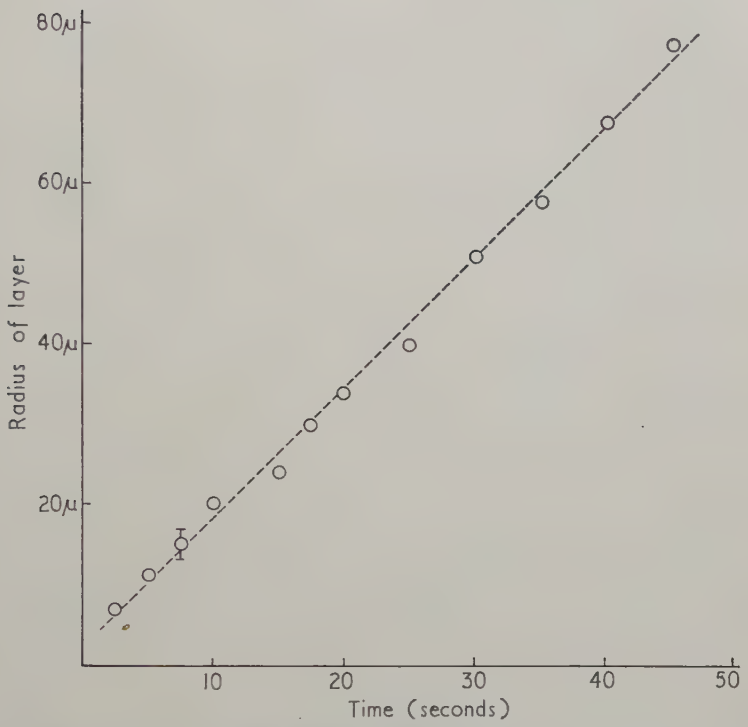

Rate of growth of a circular layer initiated at a crystal edge. Temperature $-17{\cdot}5$°C. Excess vapour density $0{\cdot}25 \times 10^{-6}$ g cm^{-3}.

suitable for measurement was obtained. Hence, to facilitate this investigation, use was made of the above relationship between layer thickness and velocity. The velocity of any layers of thickness between 200 and 1000 Å was measured, and the velocity of a layer of 250 Å thickness deduced. All measurements were made with an excess vapour pressure of $0{\cdot}25 \pm 0{\cdot}05 \times 10^{-6}$ g cm^{-3}. It was very difficult to obtain observations of layers at temperatures greater than about -5°C, as crystals would not nucleate on the covellite surface. It was necessary to begin the experiment

with the substrate at about $-10°$C, and increase the temperature to the required value after nucleation had occurred. This took about one minute to reach a steady value, and usually any plates present had grown vertically in the high excess vapour density. It was not practicable to change the environment temperature because of the large thermal inertia of the outer walls. The results are shown in fig. 13, with the dashed part of the curve representing the less certain results at higher temperatures.

Fig. 13

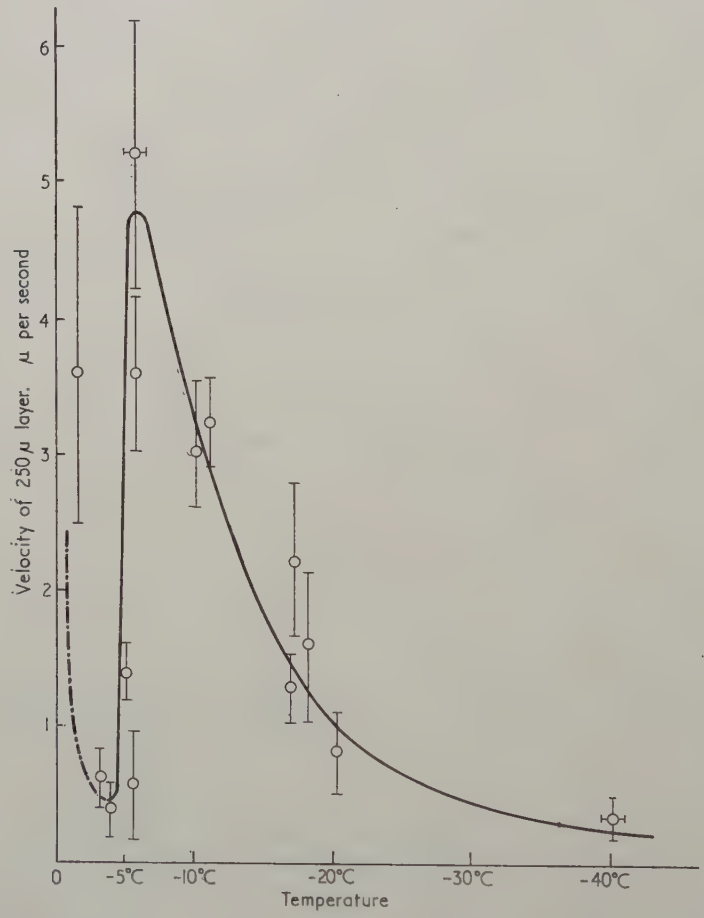

The temperature variation of the rate of growth of a layer 250 Å thick. Excess vapour density $0{\cdot}25 \times 10^{-6}$ g cm^{-3}.

The initiation of layers described above usually resulted in the distance between layers of order 30 μ. Occasionally, however, when a thin layer formed after a thick layer, it would spread with a corresponding greater

velocity and eventually catch up the first to give a thicker, more slowly moving layer. This event happened very rarely, and only two cases have been recorded on film. It was found that as the layers approached each other, at a definite distance apart, each began to move more slowly,

Fig. 14

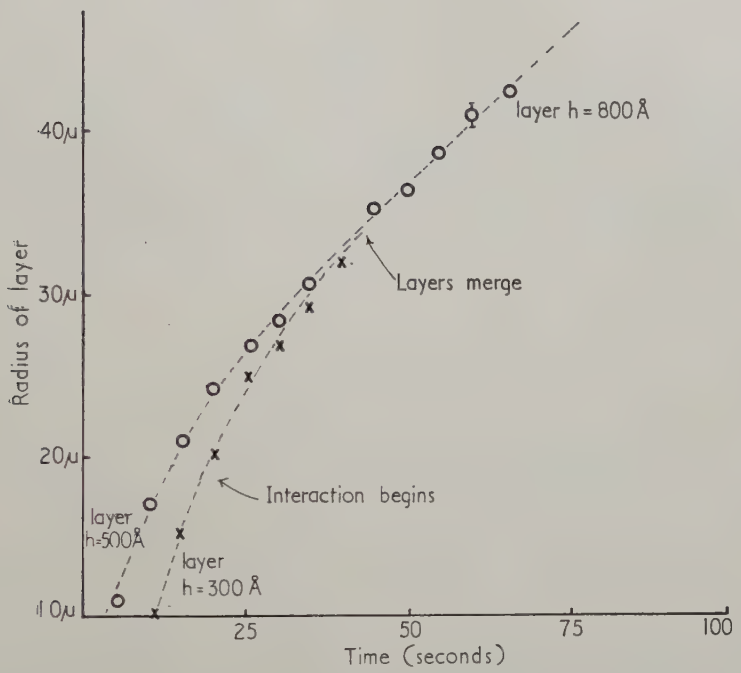

The interaction between two ice layers of different thickness. Temperature $-17{\cdot}5°$C. Excess vapour density $0{\cdot}25 \times 10^{-6}$ g cm^{-3}.

until the two merged (fig. 14) and the resulting thicker layer again moved with a constant velocity. The interaction distance was about 5μ at $-17{\cdot}5°$C, and about 10μ at $-10°$C with excess vapour density $0{\cdot}2 \times 10^{-6}$ g cm^{-3}.

4.6. *Evaporation*

Evaporation studies of ice crystals on covellite were difficult because of the inability to change the temperatures sufficiently quickly, and observations could only be made while crystals were increasing in temperature. Evaporation first began at corners and edges and eventually the crystal took the shape of a spherical cap. Layers present when evaporation began, usually evaporated as discrete layers before the remainder of the crystal. Occasionally crystals evaporated by the initiation of layers at the edge.

4.7. *Mechanical Damage of Crystals*

A piece of 36 s.w.g. stainless steel wire was cemented to the base of the objective so that the tip was just in the field of view. This was then racked down to a suitable crystal which was not thickening, and a scratch made in the surface by moving the crystal beneath the wire. This caused the crystal to grow vertically over its whole surface, the line of the scratch filling in slowly.

§ 5. Discussion. Evidence for Surface Migration of Water Molecules

5.1. *The Variation of the Velocity of Ice Layers with Thickness*

Consider a crystal layer growing only parallel to the basal plane both by direct deposition of molecules from the vapour, and also by the collection of mobile molecules from the surface layer within a distance x of the growing edge.

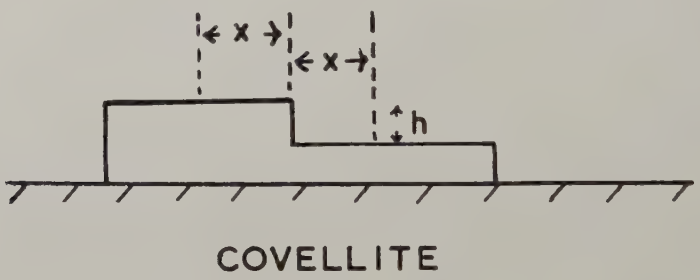

If the density of surface molecules is small, then x represents the mean free path of a molecule on the surface. The velocity of advance of a straight step, U, of constant height h, is given by

$$U = \frac{A}{\rho_1}\frac{(2x+h)}{h} \quad . \quad . \quad . \quad . \quad . \quad . \quad . \quad . \quad (1)$$

where A = mass flux of vapour $cm^{-2}\,sec^{-1}$, ρ_i = density of ice. This result is in agreement with the experimental result that $U = \text{const}/h$ for values of h between 200 and 1000 Å when $2x \gg h$. We can therefore conclude that surface diffusion is important for layer growth under these conditions. The condition that $2x \gg h$ is shown to be valid by an independent determination of the value of x (see next section).

5.2. *Rate of Growth of Layers*

Consider the rate of growth of a circular layer, radius r, of constant thickness, by direct deposition and by surface migration of molecules from a distance x on either side. We take $h \ll x$, neglecting growth by direct deposition.

There are two cases:

1. $r < x$. If m is the mass of the layer,

$$\frac{dm}{dt} = 2\pi\rho_i hr\frac{dr}{dt} = A\pi(r+x)^2 \quad \text{when} \quad \frac{dr}{dt} = \text{const}\,\frac{(r+x)^2}{r}. \qquad (2)$$

2. $r > x$.

$$\frac{dm}{dt} = 4A\pi rx \quad \text{when} \quad \frac{dr}{dt} = \text{constant}. \qquad (3)$$

Experimentally it is found that $dr/dt = \text{constant}$ for layers $r > 10\,\mu$, accurate measurements not being possible for smaller radii. This sets an upper limit of $10\,\mu$ to the migration distance.

It may be pointed out that as the whole crystal is subject to the ambient supersaturation, those parts remote from the growing edge must be returning as many molecules to the vapour as leave it—and must have a vapour pressure *larger* than the value for the ice step at this particular temperature.

The lack of variation of layer velocity beyond a critical value of the excess vapour pressure would imply that the surface layer had reached an equilibrium and become saturated.

Direct evidence for the absolute value of x for the ice surface comes from the two observations of the interaction of approaching layers: $5\,\mu$ at $-17{\cdot}5$°C and $10\,\mu$ at -12°C at $\Delta\rho = 0{\cdot}2 \times 10^{-6}$ g cm^{-3}, which gives values of x of $2{\cdot}5\,\mu$ and $5\,\mu$ respectively.

In the case of growth of crystals directly on the substrate, we suppose that molecules will be collected from a distance x on the ice and a distance x_c on the covellite. In the case $r > x$, this again leads to the result $dr/dt = \text{constant}$. This is observed for crystals whose radius is greater than about $7\,\mu$. It is also found that two approaching crystals do not interact until they are separated by at least $2\,\mu$, so that we conclude that $x_c < 1\,\mu$.

5.3. *The Influence of Temperature*

If we consider the growth rate of a layer of constant thickness and at constant flux, then eqn. (1) gives $U = \text{const.}\ x$. Hence it is possible to interpret the variation of growth rate with temperature (fig. 13) as a variation of x with temperature. The two values of x obtained in § 5.2 above, enable a scale to be placed on this curve, to give a maximum value of x of about $7{\cdot}5\,\mu$ at a temperature of $-6 \pm \frac{1}{2}$°C.

This temperature dependence differs significantly from the rapid increase with decrease of temperature suggested by Burton *et al.* (1951) for growth directly from the vapour in the absence of air. In view of the importance of this result it would be desirable to obtain further information by direct measurements of x from layer interaction over a wide range of temperature and also in the absence of air.

§ 6. The Influence of the Substrate on Crystal Growth

If we intend to apply the results obtained in the previous section to crystals growing freely in the atmosphere or in a diffusion chamber, it will be necessary to investigate the effect, if any, of the substrate.

As was shown in a previous paper (Bryant *et al.* 1959), the substrate reduces the supersaturation required for nucleation and determines the orientation of the crystal. In the case of freshly cleaved covellite, however, some crystals grow which do not thicken in a direction perpendicular to the basal plane. We can interpret this as being caused by an absence of suitable sites for growth in this direction—a hypothesis which is supported by the sudden growth of these crystals when large excess vapour densities are produced, suggesting that homogeneous nucleation of layers is taking place—and also by the initiation of growth (at low excess vapour density) when the crystal is subject to mechanical damage. It appears that exposure to the atmosphere leads either to a deposit of particulate matter or an adsorption of gaseous impurities on the covellite surface. This causes regions of strain in the overlying ice crystal, which ultimately lead to the formation of imperfections in the basal plane, and consequent growth in the prism direction. Crystals perfect in the basal plane have not been observed on old covellite surfaces, or on other substrates, and although crystals are occasionally sufficiently thin to show interference colours, they quickly grow in thickness and become colourless.

§ 7. Crystals and Layer Shape

It is difficult to interpret the changes of crystal and layer shape shown in figs. 6 and 7 without a knowledge of the structure of the surface layer. The transition from polygonal and circular growth to dendritic growth with increase of excess vapour density takes place much more completely for layers on an ice surface than for crystals growing on covellite, and suggests that the surface layer on ice is quite different from that on covellite. This is confirmed by the lack of interaction between approaching crystals when growing on a covellite surface. The growth of dendritic layers on ice resembles more closely that which has been observed on freshly cleaved muscovite mica (fig. 15) and also on biotite mica (Kleber and Weis 1958), indicating that the migration distance of water molecules on mica is comparable with that on ice, a point which requires further experimental investigation.

§ 8. Ice Crystal Growth

These results show that ice crystals can grow on a covellite substrate without growth taking place perpendicular to the basal plane, irrespective of the temperature, from -4 to -40°C, providing the vapour density excess is not too large. This is in striking contrast to the habit variation with temperature observed for crystals growing in the atmosphere and the diffusion chamber, and also for the majority of crystals growing on the

covellite surface. In all these cases, sites for growth parallel to the c axis must be produced, possibly by stresses of a solid impurity built into the lattice, or by thermal stresses occurring during growth.

In all cases, there are present sites for growth parallel to the basal plane. These may be imperfections in the ice itself, or the step between the ice and the covellite surface. The habit of a crystal containing growth sites in both prism and basal plane may therefore depend upon the relative rates of surface diffusion on the two faces, providing the growth site concentration is not large. The dependence of habit on a surface parameter of this kind is to be expected in view of the immediate change of habit as the crystal temperature is changed during growth in the diffusion chamber—which does not occur for the 'perfect' crystals growing on the covellite surface.

The present experimental results only give the variation with temperature of x on the basal plane, so that a complete explanation of the complex habit temperature relation in ice must await an experimental determination of the corresponding parameter on the prism face.

Acknowledgment

This work was carried out as part of the Imperial College Interdepartmental Research Programme on the Physics and Chemistry of Water, under the direction of Dr. B. J. Mason, and with the financial support of the Department of Scientific and Industrial Research and written whilst the author was employed on National Science Foundation grant No. 5095 at the Meteorology Department, University of California, Los Angeles.

References

Albon, N., and Dunning, W. J., 1959, *Acta cryst., Camb.*, **12,** 219.
Burton, W. K., Cabrera, N., and Frank, F. C., 1951, *Phil. Trans.*, **243,** 299.
Bryant, G. W., Hallett, J., and Mason, B. J., 1959, *J. Phys. Chem. Solids*, **12,** 189.
Bunn, C. W., and Emmett, H., 1949, *Disc. Faraday Soc.*, No. 5, 119, Crystal Growth.
Hallett, J., and Mason, B. J., 1958, *Proc. roy. Soc.* A, **247,** 440.
Kleber, W., and Weis, J., 1958, *Z. Krist.*, **110,** 1.
Kowarski, L., 1935, *J. Chim. phys.*, **32,** 303.
McNutt, J. E., and Mehl, R. F., 1955, *Trans. Amer. Soc. Metals*, **50,** 1006.

Steep-sided Trigons on Diamonds

By Eileen M. Wilks
Clarendon Laboratory, Oxford

[Received February 6, 1961]

Abstract

The natural octahedron surfaces of diamond exhibit many small triangular-shaped cavities or trigons. The majority are low-angle pyramids, but there is another variety which has steep sides and a flat base. Contour measurements on the pyramidal form have already been reported; similar measurements have now been made on the steep-sided variety. It is found that the sides of these trigons are octahedron planes. Thus the steep-sided trigons must arise by some quite different mechanism from the etch process responsible for the low-angle pyramids.

§ 1. Introduction

Triangular-shaped cavities, commonly called trigons, have long been observed on the natural octahedron faces of diamonds. They are oppositely oriented to the octahedron face, and the majority have sides which are inclined to the surrounding octahedron surface at angles of a few degrees. Not all of these low-angle trigons are simple pyramids, some are truncated with flat bases, and some have slightly concave sides (Tolansky 1955). The morphology of trigons is of interest in connection with theories of crystal growth and dissolution, and we have described the contours of these low-angle trigons in a previous paper (Frank *et al.* 1958). In addition, there is another type of trigon, found on natural octahedron surfaces, which has steep sides and a flat base; it is with this type that we are here concerned. Examples of the two forms are shown on fig. 1†, trigon X is a low-angle pyramid, while trigon Y has steep sides and a flat base. The latter type is not as common as the pyramidal form, although it has been observed on all the diamonds we have studied. For example, on one typical stone there were more than 100 pyramidal trigons deeper than 100 Å, but only eight steep-sided ones. (If trigons have depths less than about 100 Å, it becomes difficult to make an accurate estimate of their shape.)

The differences in outline between the two types of trigon may be seen from multiple-beam interferograms. In fig. 2 the fringes cross a steep-sided trigon; there is an abrupt change of depth at the edge. Figure 3 shows fringes crossing a low-angle trigon; the sides slope down to the apex at the

† Figures 1, 2, 3 and 5 are shown as plates.

centre. As mentioned above, contour measurements have already been made on the pyramids; we have now made similar measurements on the steep-sided trigons, and this paper describes results obtained on one of the stones previously used in studying the pyramidal trigons; a good quality 'blue white' regular octahedron of about 1 carat.

§ 2. Experimental Method

To determine the inclinations to the octahedron surface of the sides of a steep-sided trigon, two measurements are required: the depth t and the lateral dimension a as illustrated in fig. 4.

Fig. 4

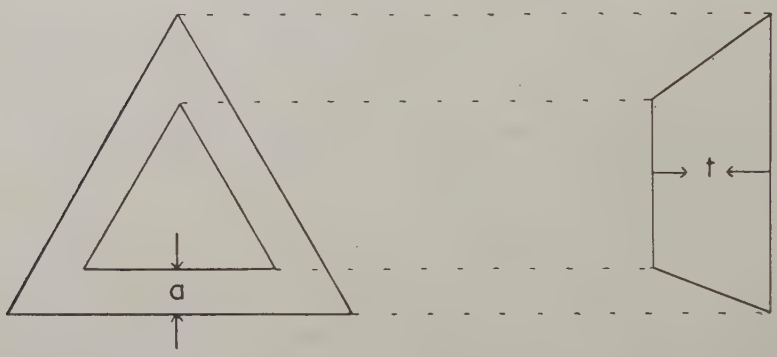

Plan and side views of a steep-sided trigon showing the dimensions a and t required to determine the inclination of the sides to the octahedron surface.

It was not possible to determine these dimensions on all the available trigons owing to several limitations imposed by the method of measurement. The dimension a could be found from photomicrographs at a magnification of 3000 to within $\pm 0{\cdot}3$ micron, and by taking some 20 readings on each photomicrograph we obtain a value of a accurate to $\pm 0{\cdot}1$ micron. This sets the lower limit to our measurement and we have only investigated trigons with values of a greater than $1{\cdot}2$ micron. Additional restrictions were also introduced by the interference method of determining the depth. To determine the correspondence between orders, the trigons had to have a large-enough surface area so that at least two fringes could be observed within the trigon, and also the method becomes difficult for depths greater than about 7 microns. (For trigons deeper than about 15 microns ordinary microscopy was used.) Again many trigons are located near to the edges of the octahedron surface, and some of these were obscured by the opposite octahedron surface when viewed by transmitted light in order to determine the correspondence between orders. As a result of these restrictions the number of available trigons on any given face was rather limited. Thus on the face shown in fig. 5, there are about 18 trigons, but measurements could only be made on six of them: and on the other face

studied, measurements could be made on three out of a total of 12 trigons. The results for these nine trigons are given in the table below.

§ 3. Results

Face	Trigon number	Depth (microns)	Side length (microns)	Inclination (degrees)
A	1	4·5	52	75
A	2	5·4	62	70
A	3	17·5	109	75
A	4	6·7	41	68
A	5	5·9	64	70
A	6	25·0	114	68
B	7	5·7	100	70
B	8	5·4	81	74
B	9	5·7	90	71

The accuracy of these results is estimated to be about 6°. As the angle between two intersecting octahedron planes is 70° 39′; the results show that to within the accuracy of measurement the steep-sided trigons have sides which correspond to octahedron planes. These results are in marked contrast to those found for the pyramidal trigons where the sides are inclined to the octahedron surface by angles no greater than about 2°. It was also apparent from the Fizeau fringes that the base of a steep-sided trigon is parallel to the octahedron surface. We have already noted that our method of measurement severely restricts the size and depth of trigons available for inspection. Therefore no significance is to be attached to the narrow range of depths in our results. There is a suggestion that the deeper steep-sided trigons have also larger surface areas but this again is probably not significant.

§ 4. Discussion

The present results together with those previously obtained (Frank *et al.*) show that the trigons observed on diamond consist of two distinctly different types: the pyramidal form with shallow non-crystallographic sides and a flat-based form whose sides are octahedron planes. This distinction is relevant to recent discussions as to whether natural trigons are the result of etch or growth processes. Tolansky (1955) argued that all natural trigons are due to growth because trigons produced in etching experiments (Fersmann and Goldschmidt 1911, Williams 1932, Omar *et al.* 1954) are oppositely oriented to the natural ones. In addition he pointed out that edges of etched trigons in the octahedron surfaces are generally rounded in contrast to the straight sides of natural trigons (although trigons with straight edges have since been obtained by etching (Omar and Kenawi 1957 and Tolansky and Patel 1957.) Other support for a growth mechanism

was deduced by Tolansky and Wilcock (1947) from a study of a flat-based trigon, the base of which lay very exactly in the same plane as did the surface of the stone some distance away. However, we have recently presented arguments, based on surface features associated with pyramidal trigons in contact, which imply that this type of trigon is due to etch (Frank *et al.* 1958). Subsequently, pyramidal trigons oriented in the same way as the natural ones have been obtained by etching (Frank and Puttick 1958). Thus, although it seems that pyramidal trigons with non-crystallographic sides are due to dissolution, the flat-based trigons with octahedron sides must arise by a different mechanism.

Acknowledgments

My thanks are due to Industrial Distributors (Sales) Limited both for the loan of the diamond used in this investigation and for a research grant.

References

Fersmann, A., and Goldschmidt, V., 1911, *Der Diamant.*
Frank, F. C., and Puttick, K. E., 1958, *Phil. Mag.*, **3,** 1273.
Frank, F. C., Puttick, K. E., and Wilks, E. M., 1958, *Phil. Mag.*, **3,** 1262.
Omar, M., and Kenawi, M., 1957, *Phil. Mag.*, **2,** 859.
Omar, M., Pandya, N. S., and Tolansky, S., 1954, *Proc. roy. Soc.* A, **225,** 33.
Tolansky, S., 1955, *Microstructure of Diamond Surfaces* (London: N.A.G. Press).
Tolansky, S., and Patel, A. R., 1957, *Phil. Mag.*, **2,** 1003.
Tolansky, S., and Wilcock, W. L., 1947, *Proc. roy. Soc.* A, **191,** 182.
Williams, A. F., 1932, *The Genesis of the Diamond* (London: Ernest Benn).

The High Temperature Electrical Resistance of Iron–Aluminium Alloys

By R. Feder†, P. H. Thornton‡ and R. W. Cahn
Department of Physical Metallurgy, University of Birmingham

[Received March 2, 1961]

Abstract

Electrical resistance, at temperatures from −196 to 700°c, was used as an indicator of crystallographic order to test the reality of certain anomalies in the long-range order in solid solutions near the composition Fe_3Al, which had previously been detected by x-ray diffraction. Resistance anomalies were found in three of the five alloys tested, containing 22·9, 23·5 and 24·8 at.% aluminium, but not in the alloys containing 22·2 and 25·5 at. % aluminium. Their significance is briefly discussed.

§ 1. Introduction

The experiments to be described here were carried out to confirm the reality of an anomaly in the ordering behaviour of iron–aluminium solid solutions, originally discovered during an investigation of these alloys by x-ray diffraction (Lawley and Cahn 1961). It was found that from several of the alloys, the intensity of superlattice lines was higher if the alloys were slow-cooled all the way from above the critical ordering temperature T_c than if they were rapidly cooled through a range of temperatures near T_c, and then slow-cooled. Figure 1 shows an example of this kind of behaviour. It implies that the rapid cooling through T_c (termed *transcritical fast cooling*) works some not readily reversible structural change in the alloy which prevents it from reaching full equilibrium order. Only a subsequent anneal well above 600°c restores to the alloy the capacity to attain equilibrium order, corresponding to the upper curve in fig. 1. For this reason the alloy is said to possess a *thermal memory*.

Electrical resistance is a good index of atomic order and therefore, if this effect is genuine, then the resistance–temperature relation should be sensitive to thermal history. The investigation included alloys containing 25·5, 24·8, 23·5, 22·9 and 22·2 at. % aluminium. X-ray diffraction studies of the first three of these had revealed a thermal memory effect, while the last two, which gave no superlattice lines and are subject to short-range ordering only, were included to test whether these alloys can also show

† Now at I.B.M., Watson Research Center, Yorktown Heights, New York, U.S.A.

‡ Now at Mellon Institute, Pittsburgh, Pennsylvania, U.S.A.

signs of thermal memory. The results of studies of an alloy containing 19·4 at. % aluminium, which shows highly unusual resistivity properties, will be published separately (Feder *et al.* 1962).

Fig. 1

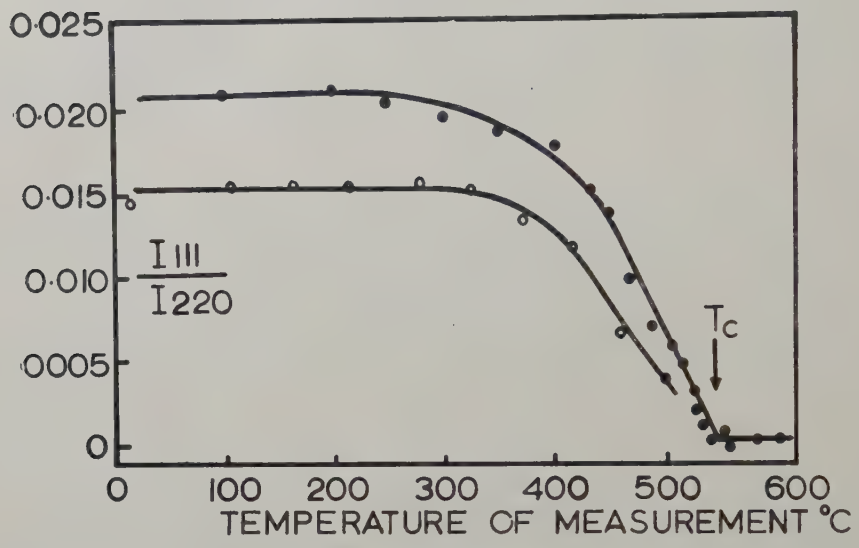

The intensity ratio of the (111) superlattice line and the (220) fundamental line, as a function of temperature, for the 24·8 at. % alloy. ●, equilibrium; ○, after transcritical fast cool. (From Lawley and Cahn 1961.)

§ 2. Experimental Methods

Samples were milled in zigzag form from vacuum-cast and hot-rolled sheet about 1 mm thick, as for previous resistance studies (Feder and Cahn 1960, Cahn and Feder 1960). This shape provided an adequate total resistance (0·2–0·3 ohm at room temperature) but kept the sample compact and thus made it easy to hold its temperature uniform. This was further assisted by enclosing the sample, insulated by thin mica sheets, in a slotted copper furnace block.

For resistance measurements, the sample was heated or cooled continuously in an electric furnace, in air, at a rate of 1–2°c/min, which was slow enough to maintain equilibrium at temperatures down to about 300°c (Lawley and Cahn 1961). At 700°c, oxidation of the samples was negligible; anneals at 800°c were normally carried out in a vacuum, but occasional anneals in air at this temperature had no permanent effect on the resistance (and therefore on the composition) of the samples.

Resistance was measured by a double potentiometer method, with due precautions to eliminate thermoelectric e.m.f.'s, to an accuracy of

~0·2 mohm, at intervals of 10–15°C. In view of the complicated shape of the samples, no attempt was made to calculate absolute resistivities.

Since the test furnace was not adapted for rapid cooling, the *effect* of a rapid transcritical cool through T_c (= 525–550°C according to composition, from X-ray data for those alloys which possess long-range order) was achieved by first water-quenching the sample from an auxiliary furnace held at 600°C or higher, and then placing it in the test furnace, which had been preheated to about 500°C, so that it rapidly attained this temperature.

The programme of heat treatments given to each sample is indicated by the inset diagram in the corresponding figure. A sloping line here indicates heating or cooling at 1–2°C/min, vertical lines indicate rapid heating or cooling. Continuous lines indicate heating or cooling in air, dashed lines indicate heating or cooling in vacuum. For each sample some provision was made in the design of the experiment for testing the reproducibility of the resistance–temperature curves.

§ 3. Results

Figures 2–6 show the results obtained with the five experimental samples. Individual experimental points are not shown for lack of space; experimental scatter was of the order of the thickness of the curves as drawn. Reproducibility of similar runs was good throughout.

Figure 2 shows quite clear evidence of the influence of a transcritical fast cool, and of the existence of a thermal memory. The resistance after a transcritical fast cool† (curve A) is higher at all temperatures than it is in equilibrium (curve B). Moreover, anneals at a series of temperatures up to 620°C do not remove the effect of the transcritical fast cool; that is to say, a thermal memory of the transcritical fast cool persists in the alloy. A heat treatment at 800°C however suffices to remove the thermal memory. The sequence of experiments was carefully designed to make sure that any irreversible changes in the state of the specimen (e.g. oxidation) would have been detected. The degree of order corresponding to equilibrium (curve B) is higher than after the transcritical fast cool (curve A), in accord with the conclusions drawn from the X-ray diffraction data.

The slow heating of the quenched sample (curve C) shows that ordering is sufficiently rapid above about 300°C to maintain equilibrium. The slight dip of curve C below curve B is not thought to imply the existence of an abnormally high degree of order, for theoretical analysis of the resistance–temperature curve (Cahn and Feder 1960) shows that at *high* temperatures there is no assurance than an increase of order will lead to a reduction of resistance.

In fig. 3, the results for the 25·5 at. % alloy show no evidence that transcritical fast cooling has any effect, and there is no thermal memory. The magnitude of the effect detected by X-rays in this alloy was rather smaller

† The term is used to represent the equivalent heat treatment referred to above.

than in the 24·8 at. % alloy (except in the range 400–500°C) and the consequent effect upon the resistivity might be below the limit of detection. It is also possible that the filings used for the x-ray work were slightly poorer in aluminium than the solid alloy, from which both the filings and the resistance specimens were made. This would help to account for the null effect in fig. 3, since the order anomaly rapidly decreases with increasing aluminium content (Lawley and Cahn 1961).

Fig. 2

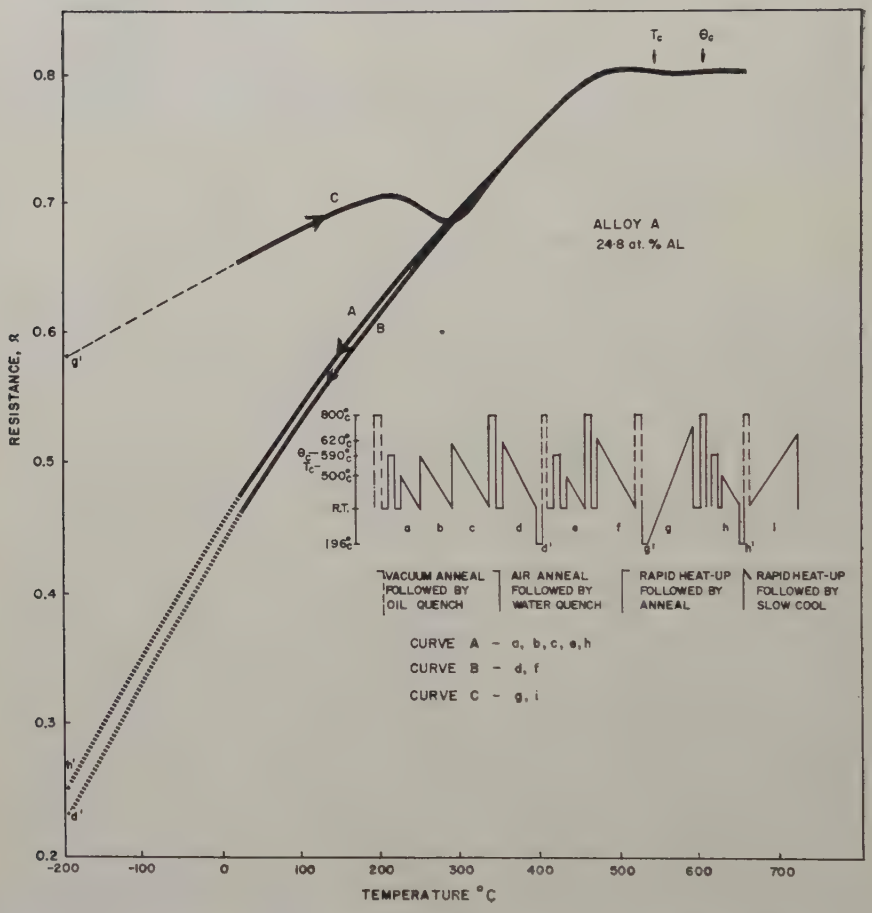

Resistance–temperature curves for 24·8 at. % alloy. T_c is the critical ordering temperature and θ_c is the ferromagnetic Curie temperatures.

The 23·5 at. % alloy again showed a marked influence arising from a transcritical fast cool. Curve *a* (fig. 4) defines the equilibrium behaviour, and curve *b* the perturbation due to transcritical fast cooling. Here, the effect of the transcritical fast cool on resistivity shows most just below the critical temperatures, and fades away towards room temperature. Since

the effect of order on resistivity is always most pronounced at low temperatures, this behaviour suggests that the difference in state of order induced by the transcritical fast cool rapidly diminishes on continued cooling†. Nevertheless, its latent influence (i.e. thermal memory) persists, for on reheating (curve *c*) the path of curve *b* is almost exactly retraced. The reheat to 680°C (end of curve *c*) suffices to erase the thermal memory, and curve *d* is once again close to curve *a*.

It is striking that in this alloy, the resistance during slow heating of the disordered sample (curve *e*) follows the path of the *anomalous* state of the

Fig. 3

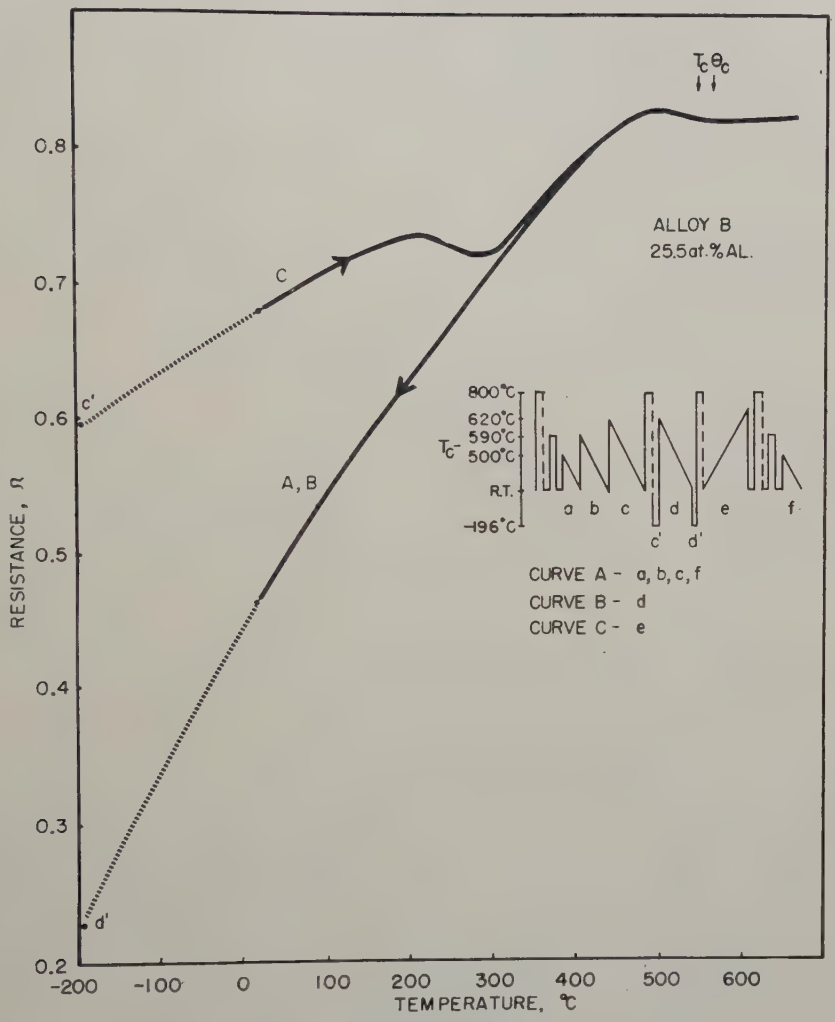

Resistance–temperature curves for 25·5 at. % alloy.

† This is again in accord with x-ray data, which reveal a large order anomaly in the range 400–500°C only.

alloy rather than the equilibrium path. This peculiar behaviour was also found to a pronounced degree during an examination of an alloy containing 19·4 at. % aluminium (Feder *et al.* 1962).

The 22·9 at. % alloy had showed no detectable long-range ordering when examined by x-ray diffraction, but the 8% difference in room temperature resistance between quenched and slow-cooled samples (fig. 5) suggest that very slight long-range ordering may in fact exist, and have been missed in the earlier study. However, it is equally plausible that the resistance difference can be explained entirely in terms of short-range order. The inversion of resistance as between curves *a* and *d* in the range 170–270°c is presumably merely a trivial consequence of the smaller temperature coefficient of resistivity of disordered alloys (Cahn and Feder 1960), coupled with the sluggishness of diffusion, and therefore of ordering, below ~250°c. It is noteworthy that the ordering, when it comes, leads to a sharp *increase* of the resistance, which lends support to the view that we are concerned with short-range rather than long-range order.

Fig. 4

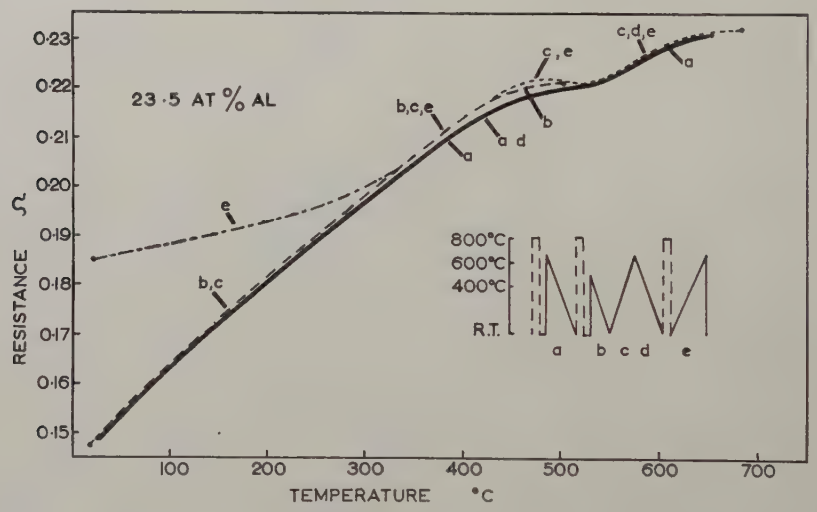

Resistance–temperature curves for 23·5 at. % alloy.

Irrespective of whether the ordering in question here is long range or short range, the heat treatment programme used did lead to very pronounced resistance anomalies. The fact that these anomalies more or less disappear at 500°c suggests, by analogy with fig. 4, that if there is indeed any long-range order, then the critical temperature is near 500°c.

The resistance of the 22·2 at. % alloy (fig. 6) is virtually unaffected by heat treatment; in the quenched condition it has a very slightly lower resistance than in the slow-cooled condition. This alloy had shown only short-range order when examined by x-rays (Lawley and Cahn 1961). However, this short-range order was quite pronounced and it is surprising that it has so little effect on the resistance.

Fig. 5

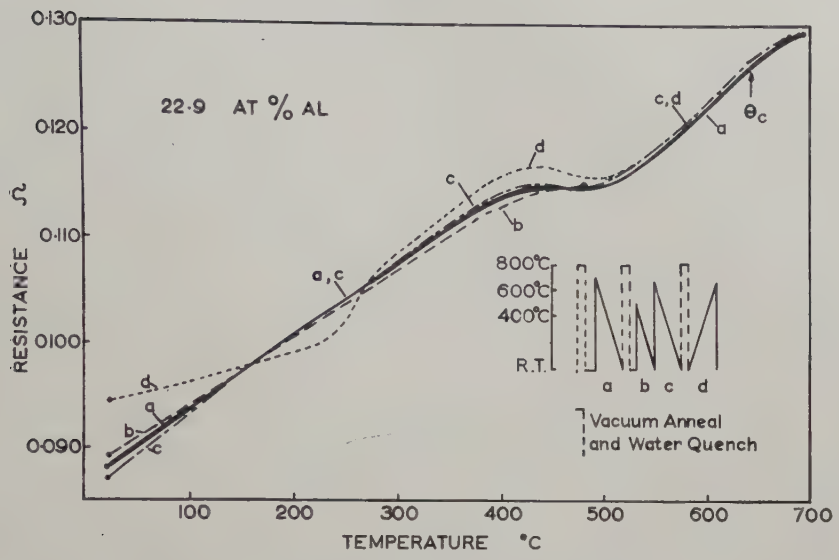

Resistance–temperature curves for 22·9 at. % alloy.

Fig. 6

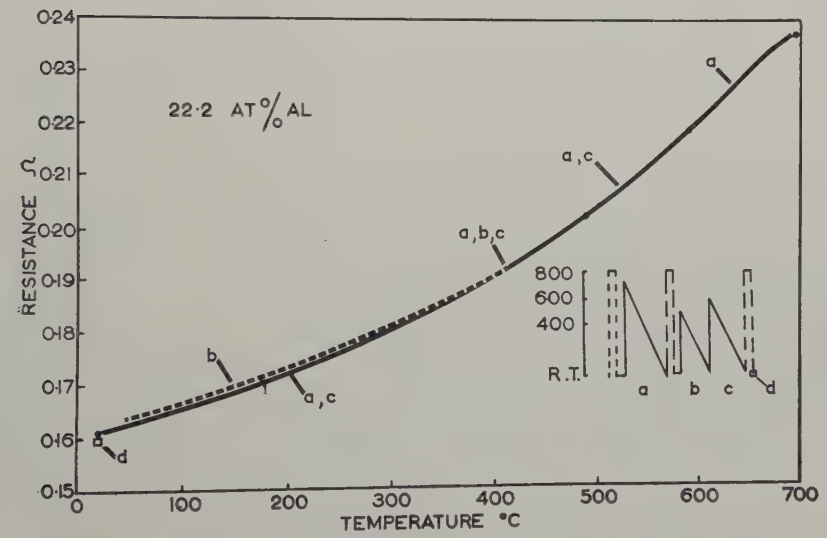

Resistance–temperature curves for 22·2 at. % alloy.

§ 4. Discussion

The experiments described above confirm the reality of the transcritical fast cool effect, originally discovered during the x-ray diffraction experiments, and also confirm the persistence of a thermal memory in the samples. In detail, there are some points of disagreement with the x-ray results, but in evaluating there it has to be remembered that we have little knowledge of the relation between order and resistance for the various alloys; only for the stoichiometric alloy have the details been worked out (Cahn and Feder 1960). Indeed, one cannot even be sure whether in the temperature range just below T_c, a rise in resistance corresponds to an increase or a decrease of the degree of order. For this reason no firm conclusions can be drawn, from the resistance data alone, about the extent and even the sense of the order anomalies produced by the heat treatments used. It is beyond doubt, however, that the order anomalies exist. Moreover, in spite of the slow heating and cooling rates used, the various resistance curves did not merge; this confirms the important conclusion, drawn from the results of the x-ray work, that the anomalous states of order resulting from transcritical fast cooling were metastable and not simply a result of sluggish diffusion. Indeed, near 400°c isothermal ordering is complete in a matter of minutes (Lawley and Cahn 1960, Feder and Cahn 1960, McQueen and Kuczynski 1959), so that slowness of diffusion cannot account for the separation of the various curves at 400°c, in figs. 4 and 5.

A tentative interpretation of the transcritical fast cooling effect and of thermal memory, in terms of competition between long or short-range order and the supplementary *directional order* caused by ferromagnetic influences, has been proposed elsewhere (Lawley and Cahn 1961), and the reader is referred to that paper.

The present resistance–temperature curves have been compared with those published by Bennett (1952), although the compositions studied by him were not identical with ours, and he was concerned only with simple heat treatments. Allowing for the small differences in composition, the forms of the equilibrium resistance curves in the two studies agreed quite well. It is of interest, however, that Bennett's 21·5 at. % alloy showed a much greater difference in resistance between the quenched and the slow cooled conditions than did our 22·2 at. % alloy. Masumoto and Saito (1952) also found a considerable resistance difference between the quenched and the slow-cooled conditions of a 22·0 at. % alloy. It can only be pointed out, in explanation of these differences, that the fine structure of the alloys varies rapidly with composition in this range (Lawley and Cahn 1961), and that moreover it is not easy to get reliable chemical analyses of these alloys, so that published compositions should be treated with some reserve.

Acknowledgments

We are indebted to Professor G. V. Raynor, F.R.S. for the provision of laboratory facilities and for his support during this work, to Professor J. D. Fast of Philips Research Laboratories for casting some of the alloys used,

and to the Secretary of the U.S. Army for a Fellowship awarded to one of us (R.F.), during the tenure of which most of this work was carried out.

References

Bennett, W. D., 1952, *J. Iron St. Inst.*, **171,** 372.
Cahn, R. W., and Feder, R., 1960, *Phil. Mag.*, **5,** 451.
Feder, R., and Cahn, R. W., 1960, *Phil. Mag.*, **5,** 343.
Feder, R., Kramer, K., Levin, E., and Cahn, R. W., 1962 (to be submitted to *Phil. Mag.*).
Lawley, A., and Cahn, R. W., 1961, *J. Phys. Chem. Solids*, **20,** 204.
Masumoto, H., and Saito, H., 1952, *Sci. Rep. Res. Inst. Tôhoku Univ.* A, **4,** 321.
McQueen, H. J., and Kuczynski, G. C., 1959, *Trans. Met. Soc., A.I.M.E.*, **215,** 619.

Observations of Precipitation in Thin Foils of Aluminium + 4% Copper Alloy†

By G. Thomas‡
Metallurgy Department, Cambridge University
and M. J. Whelan
Crystallographic Laboratory, Cavendish Laboratory, Cambridge

[Received December 12, 1960]

Abstract

A high temperature specimen stage has been used to study precipitation in thin foils of Al + 4% Cu alloy directly in the electron microscope. Precipitates a few hundred Angstroms in size are observed to form in a few minutes at temperatures ~250° to 300°C. This initial precipitation has been identified by electron diffraction as the θ' phase, and is found to occur in a well-defined single orientation with respect to the matrix. The orientation observed is consistent with one of those of θ' formed in bulk material. The growth at higher temperatures of larger θ precipitates at the expense of the θ' precipitates has also been studied. The results show that precipitation in thin foils differs from that in bulk material due to the fact that the surfaces act as preferential nucleation sites. Most of the precipitates in the thin foils appear to be at the surfaces. In aged bulk material preferential precipitation occurs on helical dislocations formed from screw dislocations by vacancy climb. The precipitates are observed to go into solution at ~500°C. Measurement of the rate of dissolution by ciné techniques has enabled an estimate of the diffusion coefficient of copper in aluminium to be made. Other observations include the formation of regions denuded of small precipitates near grain boundaries and large precipitates, and the growth and dissolution of precipitates under a fluctuating temperature.

§ 1. Introduction

The stages of precipitation in the Al + Cu system (low copper content) have been extensively investigated in recent years, and much is now known about the various types of clusters (Guinier–Preston zones) and precipitates formed by ageing at different temperatures. Low temperature ageing (~100°C) of a quenched alloy generally produces 'zones' or plate-like clusters of copper atoms on the {100} planes of the matrix (Guinier 1942, 1956, Nicholson and Nutting 1958, Nicholson *et al.* 1959), while ageing at higher temperatures (~200°C and above) produces large precipitates of θ' $CuAl_2$ also on {100} planes, or the equilibrium θ $CuAl_2$ structure. For a review of the work on Al + Cu see Silcock *et al.* (1954), Hardy and Heal (1956) and Nicholson *et al.* (1959). All of the information obtained so far comes from experiments on bulk specimens examined either with x-rays or (after thinning) by transmission electron microscopy

† Communicated by the Authors.
‡ Now at the Department of Mineral Technology, Berkeley 4, California, U.S.A.

so that only the aged state of the bulk material is studied. A notable exception is the work of Castaing and Laborie (1954), who studied precipitation both in bulk specimens and in thin foils aged outside the electron microscope. These workers have emphasized the differences in precipitation behaviour expected by use of the two methods.

It was evident to the authors that much useful information might be obtained from a study of precipitation in thin foils aged inside the electron microscope during observation. A comparison of the ageing behaviour of thin foils ($< \sim 1\,\mu$ thick) and bulk material can therefore be made. The nature of the sites of nucleation of precipitates in thin foils is also open to investigation. The experiments reported in this paper have been carried out with this object in view.

§ 2. Experimental Technique

Foils of Al + 3·7 wt. % Cu alloy of total impurity 0·003% and 0·005 in. thick were prepared from thicker sheet by several stages of cold rolling with intermediate anneals. The foils were solution heat treated by water quenching from 540°C. Thin foils suitable for transmission electron microscopy were prepared by electropolishing in a phosphoric–chromic acid bath (Nicholson *et al.* 1958). The specimens were examined in a Siemens Elmiskop 1 electron microscope operated at 100 kv using the high temperature stage described by Whelan (1960). The accuracy of temperature measurement in these experiments is roughly estimated as ± 30°C. For dynamic experiments photographs were recorded on 16 mm ciné-film in a camera mounted outside the viewing window of the electron microscope.

§ 3. Experimental Results

3.1. *Examples of Precipitation Patterns Observed*

The experiments on the thin foils were carried out by ageing at temperatures ~250°C and above, where the θ' and θ phases are expected to form in the bulk material. Selected area electron diffraction patterns indicated that both these phases are also formed in the thin foils (see § 3.3). Figures 1 to 7 and fig. 13† are typical micrographs obtained from thin foils of the alloy aged at various temperatures showing the precipitation patterns observed. Figure 1 (*a*) and (*b*) is a micrograph of an area where the foil surface is approximately (112). Figure 1 (*a*) taken after ageing for a few minutes at ~270°C, shows rounded or irregular-shaped precipitates of average diameter ~500 Å with an areal density of $\sim 10^{10}$ cm^{-2}, while fig. 1 (*b*) shows the same area a few minutes later at a temperature of ~340°C. A marked coarsening of the precipitates is apparent. The density has decreased by a factor of three or more while the average diameter is greater than ~1000 Å. This coarsening is the result of growth of larger precipitates at the expense of smaller ones which disappear. Many of the small precipitates on fig. 1 (*a*) have shrunk and disappeared

† With the exception of fig. 14, all figures are shown as plates.

on fig. 1 (*b*), while others (e.g. A, B and C on fig. 1 (*a*) and (*b*)) have grown and assumed angular shapes. The small round or irregular-shaped precipitates first observed are hereafter referred to as the 'initial precipitation'. Electron diffraction patterns and dark field experiments (§ 3.3) have shown that the initial precipitation is the θ' phase of $CuAl_2$. The larger angular-shaped precipitates on fig. 1 (*b*) have been similarly identified as the θ phase. Figures 3 and 4 are micrographs of areas of approximately (110) orientation where the contrasting morphology of θ' and θ precipitates is evident.

The change from the small θ' precipitates to the angular θ precipitates occurs very slowly below about 300°C. Electron diffraction patterns (§ 3.3) show only θ' spots below this temperature for ageing times of several minutes. However, many of the θ precipitates in fig. 1 (*b*) can be recognized as rather large precipitates on fig. 1 (*a*). In some cases dark field micrographs (§ 3.3) have shown that even at temperatures ~250°C these larger precipitates are not the θ' phase. It appears therefore that the θ phase is present even at the lower temperatures although the quantity is insufficient to give appreciable diffraction. It is also unknown whether θ is formed by transformation from θ' or whether it nucleates independently. The growth of θ precipitates at the expense of θ' precipitates occurs fairly rapidly above ~350°C.

A considerable amount of evidence has accumulated which suggests that much of the initial precipitation and of the subsequently formed θ phase is nucleated preferentially at the foil surfaces. The facts are as follows:

(*a*) Features of the initial precipitation (e.g. areal density, size and shape of precipitates) depend markedly on orientation, i.e. on the crystallographic nature of the foil surface, and vary from grain to grain in the same specimen. When the foil surface is near (100) the initial precipitation is usually slow to appear, very irregular, and is difficult to see clearly in the early stages. Figure 2 (*a*) is a micrograph of a foil with a (100) surface aged for about 10 min at ~270°C. Two types of precipitate are visible. The first includes the large θ' platelets on {100} viewed edge-on; in this case they are known to have nucleated in the interior on dislocations previously observed but out of contrast in fig. 2 (*a*) (see § 3.2). The second type (also θ' phase) includes the irregular precipitates of poorer visibility which are thought to lie at the surface. This type is always characteristic of (100) areas not containing internal centres of nucleation such as dislocations. Regions of near (112) and (110) orientations are shown in fig. 1 (*a*) and (*b*) and in figs. 3 and 4 respectively. In these micrographs the θ' precipitates assume a more rounded shape.

(*b*) A study has been made of the early stages of the initial precipitation in an attempt to detect any precipitate density variation with foil thickness, as expected if the precipitation is a volume effect. No noticeable effect has been observed except in thin regions (see below). This suggests that the density of precipitates depends on the surface area of the foil.

(*c*) Preferential precipitation has been observed at inclined grain boundaries running through the foil. Figure 5 (*a*) and (*b*) shows such a boundary at A. The precipitates are observed to form along the edges of the boundary B and C corresponding to the top and bottom surfaces of the foil.

(*d*) In areas of (100) orientation an extended type of precipitate pattern is produced at temperatures $\sim 330°$C. Figure 2 (*b*) shows an example formed in a different area of the same grain as in fig. 2 (*a*). This extended pattern forms suddenly from the irregular precipitates of fig. 2 (*a*). It has been identified as the θ phase. These extended patterns are thought to be produced by coalescence of θ' plates lying on the (100) surface plane. Detailed inspection shows that the pattern consists of two overlapping patterns, one of which shows bend extinction contours (Heidenreich 1949) while the other shows no extinction contours. These probably represent extended precipitates on opposite surfaces of the foil. Furthermore dislocations have been observed to move in an unhindered manner through such areas.

(*e*) When θ precipitates dissolve at $\sim 500°$C (§ 3.4), marks are often observed on the image covering the areas previously occupied by precipitates. These marks are particularly noticeable if the foil has been held at high temperature for several minutes before the solution treatment. An example of these marks is visible in fig. 13 (*e*) around the large precipitate. The marks may be produced by increased oxidation of the foil at the site of the precipitate. Whatever the origin of the marks they are much more likely to be a surface than a volume effect since the interior of the metal would be homogeneous above the solution temperature.

It therefore seems probable that in thin foils the surfaces provide sites for preferential nucleation of precipitates and that many of the precipitates observed are at the surfaces. This is expected on the hypothesis of Seitz (1952) by which solute atoms are associated with vacancies and move with them. Quenched-in vacancies would be expected to diffuse to the surfaces of the thin foils on ageing and deposit copper at the surfaces, thereby providing nuclei for further precipitation. Surface diffusion of copper atoms would also account qualitatively for the rapid rate of changes which take place suddenly at comparatively low temperatures, e.g. for the change between fig. 2 (*a*) and (*b*) following a small rise of temperature. Precipitation in the interior of the foil is sometimes observed; e.g. the θ' plates viewed edge-on in fig. 2 (*a*) are undoubtedly nucleated in the interior. However, it is believed that these precipitates are characteristic of nucleation at dislocations (§ 3.2) and would be absent if dislocations were not present. Dislocations are usually observed in such cases.

In thin regions of the specimen near the edges of the foil, precipitates are often observed which run right through the foil. These precipitates are usually separated from the surface precipitation patterns of thicker regions by a zone denuded of surface precipitation. An example is shown in fig. 6 (*a*); the precipitates have been identified as the θ phase. The

boundary surfaces between matrix and precipitates are usually nearly perpendicular to the foil surface, so that the projected widths of the boundary planes are small. However, dark field images in the strong matrix reflections have shown that the areas occupied by these precipitates behave like holes in the foil, i.e. they scatter a negligible number of electrons into the matrix reflections. This proves that the precipitates run right through the foil. Figure 6 (*b*) shows a similar θ precipitate in a thicker region where the inclined boundary plane with thickness interference fringes is visible. Several different orientations of these precipitates occur in the same region but no systematic study has been made.

Regions denuded of precipitation are frequently observed near grain boundaries. Figure 5 (*a*) and (*b*) is a typical example at a triple grain boundary junction. Preferential precipitation has occurred at the grain boundaries leaving a denuded zone $\sim \frac{1}{2}\mu$ wide. Typically the denuded zone is observed to increase in width with ageing time, until ultimately most of the initial precipitation has disappeared leaving behind large precipitates at the grain boundaries and in the interior of the grains. Denuded regions also form around large precipitates in the interior of grains. Figure 7 (*a*) and (*b*) is a micrograph of the same area of a foil of unknown orientation. Figure 7 (*a*) taken after 30 min at $\sim 250°$C shows the initial precipitation. Figure 7 (*b*) shows the rather striking effect observed in this area after raising the temperature a few degrees. The initial precipitation coarsened rapidly and larger precipitates such as A and B suddenly formed leaving denuded regions around them. The large precipitates appear to run right through the foil with almost perpendicular boundaries. Ultimately all the initial precipitation disappeared leaving only a few of the large precipitates. Although the large precipitates were not identified in this case they are undoubtedly the θ phase. All these changes can be easily followed visually in the electron microscope.

3.2. *Comparison of Precipitation in Thin Foils and Bulk Material*

To test whether the precipitation observed in thin foils is a surface phenomenon, the following experiment was performed. A thin foil was prepared from quenched bulk material. The electropolished foil is generally only suitable for transmission microscopy in local areas near the edge of the foil; elsewhere it may be several microns thick and can be considered as bulk material. The specimen (i.e. thin parts and thick parts together) was then aged for a few minutes in high vacuum at 270°C to simulate conditions occurring on the electron microscope high temperature stage. Thin specimens were cut from the edge and were examined in the electron microscope. The micrographs were similar to those obtained from thin foils aged in the microscope at about this temperature (e.g. compare fig. 8 with fig. 1 (*a*)). The specimen was then electropolished again to remove several microns, i.e. a thin foil was prepared from what may be considered as aged bulk material. The micrographs obtained from this specimen were noticeably different and showed much larger

precipitates of θ' phase lying on {100} planes in Widmanstätten-type patterns similar to those previously observed by Thomas and Nutting (1955) using oxide replica techniques (see, for example, fig. 9). This experiment is fairly convincing proof that much of the initial precipitation in thin foils is characteristic of the surfaces of the specimen, and that thin foils differ appreciably from bulk material in ageing behaviour.

The precipitation patterns observed in aged thick specimens subsequently thinned as in fig. 9 are probably produced by preferential precipitation at dislocations. It is now known (Thomas and Whelan 1959) that quenched-in vacancies in Al + 4% Cu alloys migrate to screw dislocations and cause them to climb into helices. The segments of a helical dislocation have considerable edge component and it seems probable that if copper atoms migrate to the dislocations with vacancies they will segregate at the compression side of the dislocation, thereby relieving the strain and forming nuclei for further precipitation. Therefore, on ageing, a helical dislocation may give rise to the arrays of precipitates lying on {100} planes visible in fig. 9. Figure 10 shows an example of precipitation at helical dislocations in a bulk specimen aged for 2 min. at 270°C. This micrograph shows an earlier stage of precipitation than that visible in fig. 9. In this case the small precipitates A formed at the helical dislocations seem to be partially coherent and give rise to diffraction contrast effects due to strain in the surrounding matrix similar to those observed by Nicholson and Nutting (1958). The contrast effects are very similar to those observed at dislocation loops in quenched aluminium (Hirsch *et al.* 1958). The dislocation line B connecting the precipitates is clearly visible in fig. 10, but elsewhere (e.g. at C–C) it appears to be out of contrast (Hirsch *et al.* 1960).

3.3. *Identification of Precipitates*

The selected area diffraction technique has been used to identify the precipitates at various temperatures. The structure of the θ phase of $CuAl_2$ has been studied by Friauf (1927) and by Bradley and Jones (1933). The Bravais lattice is body-centred tetragonal with $a = 6{\cdot}054$ Å, $c = 4{\cdot}864$ Å (Bradley and Jones 1933). These lattice parameters have been used to compute d-spacings which were compared with observed spacings measured from electron diffraction patterns. The structure of the θ' phase is also based on a body-centred tetragonal lattice with $a = 4{\cdot}04$ Å, $c = 5{\cdot}8$ Å (Silcock *et al.* 1954, Silcock and Heal 1956). The a parameter is practically identical with that of the matrix. It was found in all cases that the electron diffraction spots could be interpreted by assuming that one or other (or both) of the above phases was present.

The dark field technique has been used to distinguish between the two phases when present together. A dark field micrograph taken with one of the known θ' or θ reflections serves to show up the location of many of the corresponding precipitates in a given area. In this way it has been possible to show that the large or angular shaped precipitates in figs. 1 (*b*), 2 (*b*), 3 and 4 are the θ phase and that the initial precipitation is the θ' phase.

Selected area diffraction patterns have shown that the initial precipitation formed on the first ageing invariably consists of precipitates of the same orientation. The orientation of θ' observed is that in which the c-axis makes the smallest angle with the normal to the foil. The orientation relationship usually holds over the whole grain. Figures 11 and 12 (a) are typical examples of electron diffraction patterns of the initial precipitation for foils with near (011) and (001) surfaces respectively, showing

Orientations of precipitates

Precipitate	Approximate foil surface	Number of cases examined	Approximate orientation of precipitate
θ'	(001)	several	$[001]_{\theta'}$ parallel to $[001]_{M}$† $[100]$ common to both.
θ'	(011)	3	$[011]_{\theta'}$ parallel to $[011]_{M}$ $[100]$ common to both.
θ'	(112)	3	$[111]_{\theta'}$ parallel to $[112]_{M}$ $[1\bar{1}0]$ common to both.
θ	(001)	several	$[001]_{\theta}$ parallel to $[001]_{M}$ $[100]_{\theta}$ parallel to $[110]_{M}$
θ	(011)	1	$[113]_{\theta}$ parallel to $[011]_{M}$ $[1\bar{1}0]_{\theta}$ parallel to $[100]_{M}$
θ	(011)	1	$[111]_{\theta}$ parallel to $[011]_{M}$ $[1\bar{1}0]_{\theta}$ parallel to $[100]_{M}$

† M denotes the matrix.

single crystal type patterns from θ' (selected area diameter $\sim 1\,\mu$). The table summarizes the results for three different foil surfaces. The orientations are approximate; the first parallelism quoted in each case may be in error by as much as $\sim 10°$. All the orientations of θ' in the table are consistent within the error with the well-known orientation of θ' in the bulk material, i.e. the tetragonal axes of θ' are parallel to the cubic axes of the matrix. The orientation of the θ phase formed after the disappearance of θ' has not been extensively studied except for foils with near (100) surfaces. In this case the observed orientation (see table) is the same as that reported previously by Guinier (1942) (Guinier's group 1 orientation) for θ formed from θ' in the bulk material. It is possible that the last two cases of the table for foils with near (011) surfaces represent this case also within the experimental error. Figure 12 (b) shows the diffraction pattern of the θ phase formed from the θ' phase of fig. 12 (a). Both these patterns were obtained from areas similar to those shown in fig. 2 (a) and (b).

Little can be said at present about the habit plane of the initial precipitates. In the case of foils of (100) orientation (fig. 2 (*a*) and (*b*)), the habit plane is believed to be the (100) surface. In some other orientations the θ' precipitates appear to have grown into the foil on an inclined plane which might be {100} after nucleating at the surface. The precipitates in fig. 1 (*b*) at D, E and other places lend support to this view. These rounded precipitates appear elongated in the $[\bar{1}10]$ direction as if they were roughly circular discs viewed at an angle. In this case this direction is parallel to the trace of the (001) plane perpendicular to the *c*-axis of θ' on the foil (112) surface One edge of each precipitate (parallel to this direction) is rather irregular suggesting that this is the intersection of the (001) habit plane with the irregular surface of the foil. Similarly in fig. 4 the large θ precipitates probably have the inclined (100) plane as habit plane and run right through the foil. However, in many other cases there is no clear indication of a habit plane.

3.4. *Dissolution of Precipitates at High Temperatures*

When the temperature of a thin foil containing precipitates is raised above ~ 400°C coarsening occurs rapidly, and ultimately at ~ 500°C all the precipitates go into solution. Figure 13 is a typical sequence of micrographs showing how the originally angular-shaped θ precipitates become rounded-off and shrink as the temperature is raised and eventually disappear. The foil surface is (100) and the precipitates in this case are probably thin plates lying at the foil surface. If the temperature is suddenly raised and held constant, the rounded precipitates are observed to shrink slowly at first when their diameters are large and then more rapidly as their diameters decrease.

The rates of solution of the last few remaining precipitates have been studied using ciné techniques. It has been found in three cases out of twelve examined that $d(r^2)/dt$ is approximately constant over the range of r ($r < \sim 2000$ Å) (r is the precipitate radius at time t). Figure 14 shows a plot of r^2 *versus* t in such a case. In the other cases however, similar plots are irregular or show a roughly linear variation for large particle radius but have negative values of $d^2(r^2)/dt^2$ for small particle radius. The linear variation can be understood on the basis of a diffusion-limited dissolution process. Several authors (Zener 1949, Wert and Zener 1950, Frank 1950, Ham 1958) have considered the reverse case of growth. For a precipitate of negligible initial dimensions in an initially uniform supersaturation, where the growth rate is determined by diffusion and not by any interfacial phenomenon, these authors have shown that the solution of the time-dependent diffusion equation leads to $r^2 = kDt$, where k is the rate constant and D is the coefficient for diffusion of material to the precipitate. Boundary conditions at large distances from the precipitate are assumed. Ham (1958) has also considered growth of a spheroidal precipitate (rod-like or plate-like) and has shown that a similar solution exists, the eccentricity of the precipitate remaining constant. The growth constant k depends on

the shape of the precipitate. Frank (1950) has given graphs from which k may be determined for the cases of spherical, cylindrical and one-dimensional diffusion in terms of the ratio $(\rho_s-\rho_e)/(\rho_c-\rho_s)$ where ρ_c, ρ_s and ρ_e are the concentrations of diffusing material inside, at the surface, and at a large distance from the precipitate. For small values of this ratio in the spherical case the rate constant k is $2(\rho_s-\rho_e)/(\rho_c-\rho_s)$, a result which can be obtained by an approximation using steady-state diffusion theory.

Fig. 14

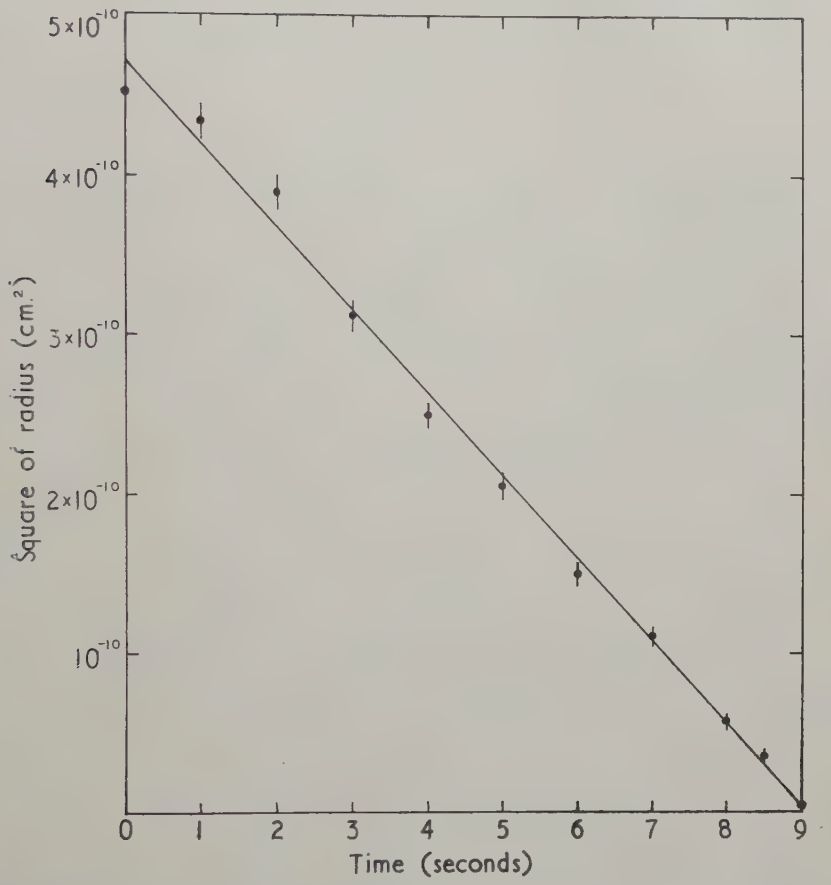

Plot of (radius)^2 versus time for the last few seconds of the lifetime of a shrinking precipitate. Measurements taken from ciné-film.

As far as the authors are aware, no exact solution of the dissolution problem has been given. When the rate constant is small however, it is expected that it will be the reverse of that in the growth case, i.e.

$$\frac{d(r^2)}{dt} = -kD, \qquad \ldots\ldots\ldots \quad (1)$$

The applicability of the above theory to precipitates in thin foils is questionable. The effects of the surfaces have been neglected. Even if the foil is thick compared with the precipitate diameter, the correct value of k is obscure since it depends on the precipitate shape. The influence of surface diffusion on dissolution of precipitates at the surface of the foil is also unknown. It is not surprising therefore that a linear variation is the exception rather than the rule. However, if it is assumed that in the cases where a linear variation is observed the precipitates are small spheres in the interior of a relatively thick foil it is possible to estimate the diffusion coefficient of Cu in Al from eqn. (1). Spherical precipitates satisfying this condition will probably be formed from θ precipitates which initially run right through the foil as in fig. 6 (*b*). For a sphere we have

$$D = -\tfrac{1}{2}\frac{(\rho_c-\rho_s)}{(\rho_s-\rho_e)}\frac{d(r^2)}{dt}\ ; \qquad \ldots\ldots \quad (2)$$

ρ_c, ρ_e and ρ_s can be taken approximately as the atomic per cent concentrations. Since nearly all the copper is in solution ρ_e is about equal to the concentration of copper in the alloy (1·6 at. %). ρ_s can be neglected in comparison with ρ_c in the numerator of eqn. (2). ρ_c is about 32·4 at. % $\rho_s-\rho_e$ can be obtained from the slope of the phase boundary on the equilibrium diagram if ΔT (the temperature increase above the equilibrium point at 1·6 at. % copper) is known. $\rho_s-\rho_e$ is about $1{\cdot}3\times10^{-2}\Delta T$ at. %. Putting $d(r^2)/dt$ equal to $\sim -5\times10^{-11}$ cm^2 sec^{-1} from the slope of fig. 14, we obtain $D\sim 6\times10^{-8}/\Delta T$ cm^2 sec^{-1}. For $\Delta T \sim 30$°C, D is $\sim 2\times10^{-9}$ cm^2 sec^{-1}, which is slightly larger than, but of the same order of magnitude as the values of the diffusion coefficients for copper in aluminium above 500°C reported in the literature (see Smithells 1955). The observed rate can therefore be understood on the basis of a diffusion-limited process. With further refinement the electron microscope method might provide a suitable method of measuring diffusion coefficients in other alloy systems. However, it appears to be limited at present by uncertainties in the theoretical interpretation, besides the purely practical difficulty of estimating the temperature accurately.

3.5. *Some Further General Observations*

Several other interesting observations have been made on the dissolution process. An experiment was performed in which precipitates were observed while the temperature was successively raised and lowered by about 20°C from ~500°C. In this way precipitates could be made to diminish in size (raising the temperature) or grow (lowering the temperature) at will, i.e. there is no difficulty in growth provided a site for precipitation is still available. However, if the precipitates are allowed to dissolve completely at 500°C, re-precipitation does not occur when the temperature is lowered by ~20°C. In order to cause precipitation after dissolution the temperature had to be lowered by about 100°C below the limit of solid solubility. The precipitates then formed were quite different morphologically, consisting mainly of extended patterns probably lying at the foil surfaces.

Most of the effects described in this paper have referred to the first ageing treatment. It has also been possible to quench-in the solid solution in thin foils from above the solubility limit†. From successive precipitation→dissolution→quenching→re-precipitation sequences carried out on the same specimen in the microscope it was found that the second and subsequent precipitation differed considerably from the first precipitation. In general much less θ' is produced by low temperature ageing during the second precipitation. Angular precipitates characteristic of the θ phase are often formed during the second precipitation. Figure 5 (*a*) and (*b*) is a micrograph (at low magnification) of the same region at $\sim 300°$C during the second and third precipitations. The density of the precipitates is lower than that during the first precipitation while their size is greater. Diffraction patterns of typical regions during the second precipitation showed spots belonging to θ' and θ of several orientations in contrast to the well-defined single orientation observed during the first precipitation. It was also found that the specimen has no memory regarding nucleation sites, i.e. by observing precipitates formed at a given temperature, dissolving them, quenching and by re-precipitating at the same temperature, keeping the same region in view, it was found that the new precipitates appeared to nucleate quite randomly (e.g. compare figs. 5 (*a*) and (*b*)). The differences between the first and subsequent precipitations are not understood at present and further work is required on this point. Finally, it may be stated that the observations described in this paper are most conveniently demonstrated by ciné-photography.

§ 4. Conclusions

1. The experiments have shown that it is possible to observe directly precipitation in thin foils of Al + 4% Cu alloy.

2. Precipitation in thin foils generally appears to differ from that in bulk material. Precipitation seems to occur preferentially at the foil surfaces, and this is probably due to the fact that solute atoms are associated with and migrate to the surfaces with quenched-in lattice vacancies. In contrast to this, precipitation in bulk specimens occurs preferentially at helical dislocations formed from screw dislocations by vacancy climb. Again this can be interpreted in terms of migration of solute atoms with vacancies.

3. During the first ageing treatment the first precipitates to appear at temperatures $\sim 250°$–$300°$c are of the θ' phase. Usually only one orientation of θ' is observed over a whole grain. The orientation observed is consistent with one of the three possible orientations of θ' in bulk material.

4. At temperatures $\sim 350°$c the small θ' precipitates disappear, while larger angular precipitates of the θ phase are formed. In a few cases examined the orientation of θ observed is consistent with one of the orientations of θ formed from θ' in bulk material.

† Switching off the heating current to the high temperature stage generally gave a sufficiently fast cooling rate to effect this.

5. At $\sim 500°$C the precipitates go into solution. In a few cases $d(r^2)/dt$ has been found to be constant. This result can be interpreted in terms of diffusion-limited dissolution and the diffusion coefficient can be roughly estimated.

6. Quenching and re-precipitation sequences have shown that subsequent precipitation differs considerably from the first precipitation.

Acknowledgments

The authors wish to express their thanks to Professor N. F. Mott, F.R.S., to Professor A. H. Cottrell, F.R.S., and to Dr. W. H. Taylor for their continued interest and encouragement. Thanks are also due to Professor J. Nutting, Drs. P. B. Hirsch F. S. Ham, J. W. Cahn and R. B. Nicholson for valuable discussions.

This work was carried out during the tenure of an I.C.I. Fellowship (G. T.), and Research Fellowships from Gonville and Caius College, Cambridge, from D.S.I.R. and from the Royal Society Mr. and Mrs. John Jaffé Donation (M. J. W.).

References

Bradley, A. J., and Jones, P., 1933, *J. Inst. Met.*, **51**, 131.
Castaing, R., and Laborie, P., 1954, *C. R. Acad. Sci., Paris*, **238**, 1885.
Frank, F. C., 1950, *Proc. roy. Soc.* A, **201**, 586.
Friauf, J. B., 1927, *J. Amer. chem. Soc.*, **49**, 3107.
Guinier, A., 1942, *J. phys. Radium*, **3**, 124; 1956, *Trans. Amer. Inst. min. (metall.) Engrs*, **206**, 673.
Ham, F. S., 1958, *J. Phys. Chem. Solids*, **6**, 335.
Hardy, H. K., and Heal, T. J., 1956, Institute of Metals Monograph and Report Series No. 18, p. 1.
Heidenreich, R. D., 1949, *J. appl. Phys.*, **20**, 993.
Hirsch, P. B., Silcox, J., Smallman, R. E., and Westmacott, K. H., 1958, *Phil. Mag.*, **3**, 897.
Hirsch, P. B., Howie, A., and Whelan, M. J., 1960, *Phil. Trans.* A, **252**, 499.
Nicholson, R. B., and Nutting, J., 1958, *Phil. Mag.*, **3**, 531.
Nicholson, R. B., Thomas, G., and Nutting, J., 1958, *Brit. J. appl. Phys.*, **9**, 23; 1959, *J. Inst. Met.*, **87**, 429.
Seitz, F., 1952, *Advanc. Phys.*, **1**, 43.
Silcock, J. M., Heal, T. J., and Hardy, H. K., 1954, *J. Inst. Met.*, **82**, 239.
Silcock, J. M., and Heal, T. J., 1956, *Acta cryst.*, **9**, 680.
Smithells, C. J., 1955, *Metals Reference Book*, Vol. 2 (London: Butterworths), p. 552.
Thomas, G., and Nutting, J., 1956, Institute of Metals Monograph and Report Series No. 18, p. 57.
Thomas, G., and Whelan, M. J., 1959, *Phil. Mag.*, **4**, 511.
Wert, C., and Zener, C., 1950, *J. appl. Phys.*, **21**, 5.
Whelan, M. J., 1960, *Report of the Fourth International Conference on Electron Microscopy*, Vol. 1 (Berlin: Springer-Verlag), p. 96.
Zener, C., 1949, *J. appl. Phys.*, **20**, 950.

Changes of Elastic Modulus associated with Internal Friction in Sodium Chloride

By R. W. Whitworth
Department of Metallurgy, Imperial College, London†

[Received February 28, 1961]

Abstract

Previous measurements of the amplitude-dependent internal friction of NaCl at 90 kc/s and room temperature (Whitworth 1960) have been extended to study the corresponding changes in Young's modulus. It is concluded that the motion of dislocations giving rise to the amplitude-dependent damping lags in phase behind the stress by about 30° to 60°. Previously described changes in damping produced by high amplitude vibration are associated with corresponding changes in the modulus defect.

An account of some experiments on the internal friction of single crystals of NaCl at 90 kc/s and room temperature has already been published (Whitworth 1960, hereafter called I), and that paper described how the damping could be changed by vibrating the specimens at high amplitudes. There is always some uncertainty in the interpretation of such dislocation damping measurements unless the change in elastic modulus associated with the internal friction is known, but the apparatus described in I was not suitable for measuring these modulus changes. The present work was therefore undertaken to clarify this point.

The composite resonator described in I was again used, but in this case it was driven by a crystal stabilized oscillator whose frequency could be controlled to 1 part in 10^6. Both the internal friction of the specimen, δ, and the resonant frequency of the system were measured as a function of the maximum strain amplitude, ϵ, in the crystal; from the frequency measurements $(\Delta E/E)_h$, the relative decrease of Young's modulus below its value at the lowest amplitudes, was determined. In all specimens this amplitude-dependent modulus defect was found to be closely related to the amplitude-dependent part of the decrement $\delta_h = (\delta - \delta_0)$, where δ_0 is the decrement at low amplitudes. The modulus defect, $(\Delta E/E)_0$, associated with δ_0 was not measured in these experiments.

The figure shows the results of measurements of δ_h and $(\Delta E/E)_h$ as functions of ϵ for two specimens deformed in compression by 0·2% and 1% respectively. δ_h and $(\Delta E/E)_h$ are plotted on a common logarithmic

† Now at Department of Physics, University of Birmingham.

scale, and the values of δ_0 are given below the figure. The precise nature of the curves obtained varies somewhat from one specimen to another, but the principal point to note is that $r = \delta_h/(\Delta E/E)_h$ varies only slightly for quite large changes in δ_h and $(\Delta E/E)_h$. The table shows some typical values of r

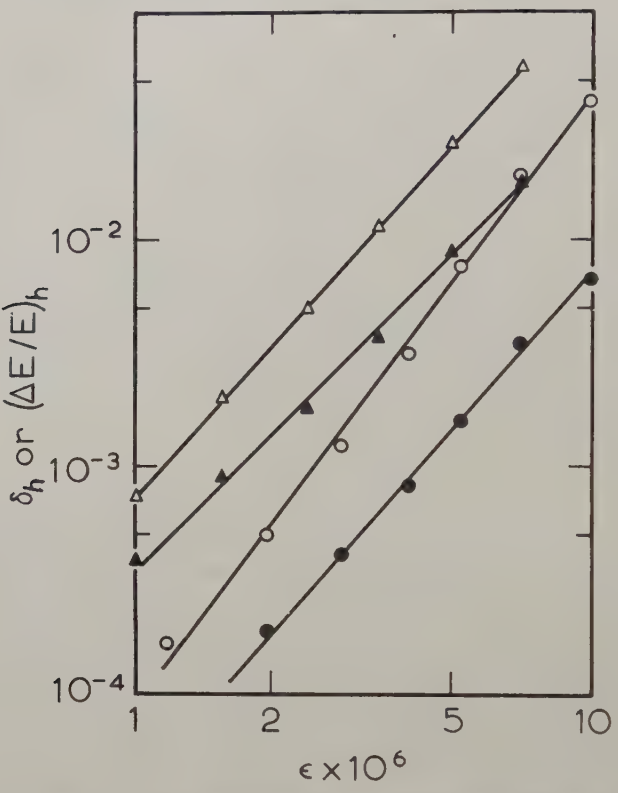

Amplitude-dependent decrement and modulus defect for two crystals.
Specimen deformed 0·2%: ○, δ_h; ●, $(\Delta E/E)_h$; $\delta_0 = 1{\cdot}7 \times 10^{-4}$.
Specimen deformed 1% : △, δ_h; ▲, $(\Delta E/E)_h$; $\delta_0 = 6{\cdot}1 \times 10^{-4}$.

for three specimens deformed by differing amounts; the values quoted are accurate to about $\pm 25\%$, and show that while r is effectively constant in the most heavily deformed crystal, it rises with ϵ in the more lightly deformed specimens. These observations are consistent with the very approximate results quoted in § 3.1 of I, and confirm the approximate values for the amplitude of motion of the dislocations calculated in that paper.

A knowledge of both $\Delta E/E$ and δ leads to information about the motion of the dislocations under the oscillatory stress, and if this motion is assumed to be sinusoidal, it can be shown that it lags behind the stress by a phase angle equal to $\tan^{-1}[(\delta/\pi)/(\Delta E/E)]$ (cf. Nowick 1953). At very low amplitudes the results of Gordon and Nowick (1956) and of Bauer and Gordon

(1960) show that $\delta_0/(\Delta E/E)_0 \sim 0{\cdot}2$ in their specimens, and this indicates that the motion of the dislocations giving rise to the amplitude-independent damping is only a few degrees out of phase with the stress. In the amplitude-dependent range, however, r is an order of magnitude larger, being $\sim \pi$, and the additional motion of the dislocations giving rise to this damping therefore lags in phase behind the stress by 30° to 60°.

In any model in which the dislocation *displacement* is a single-valued function of the stress there will be no phase lag, but the introduction of a relatively small dislocation damping term can lead to small phase differences

Typical values of $r = \delta_h/(\Delta E/E)_h$

Deformation of specimen (%)	r at $\epsilon = 10^{-6}$	r at $\epsilon = 10^{-5}$
0·2	2·0	6·0
1·0	2·0	3·4
3·5	1·7	2·3

such as those observed at low amplitudes. At the other extreme, if the dislocation *velocity* is dependent only on the applied stress there will be no modulus defect, and the motion of the dislocations will lag 90° behind the stress. The present results show that the model appropriate to the amplitude-dependent damping of NaCl lies somewhere mid-way between these two simple cases.

It was shown in I that if a specimen is deformed and then annealed at 100 to 200°C its internal friction is lower than its value determined immediately after the deformation; this was attributed to pinning of the dislocations during the anneal. It was further observed that vibration of such an annealed specimen at fairly high amplitudes increased the values of δ_h subsequently observed at lower amplitudes, and this was explained as being due to the pulling of dislocations away from pinned sites to which they do not return. Corresponding effects on the modulus defect would be expected, and they have now been observed, the values of $(\Delta E/E)_h$ being reduced by annealing and in part restored by high amplitude vibration.

Another effect described in I was a decrease in the internal friction of deformed specimens vibrated at strain amplitudes above about 3×10^{-5}. Measurements of the modulus defect before and after this high amplitude vibration treatment have shown that it too is decreased, thus confirming that the effect is due to some process which prevents the dislocations from moving under the oscillating stress. This 'pinning' is associated with the production of 'debris' by the oscillating dislocations (Davidge and Whitworth 1961).

Acknowledgments

This work was supported by a D.S.I.R. Grant for Special Research, and the author, who held a research fellowship on this grant, wishes to thank Professor J. G. Ball for the provision of research facilities in the Department of Metallurgy at Imperial College, and Dr. P. L. Pratt, the leader of the research group, for his encouragement and advice.

References

Bauer, C. L., and Gordon, R. B., 1960, *J. appl. Phys.*, **31**, 945.
Davidge, R. W., and Whitworth, R. W., 1961, *Phil. Mag.*, **6**, 217.
Gordon, R. B., and Nowick, A. S., 1956, *Acta Met.*, **4**, 514.
Nowick, A. S., 1953, *Progr. Metal Phys.*, **4**, 1.
Whitworth, R. W., 1960, *Phil. Mag.*, **5**, 425.

Precipitate Hardening in an Aluminium–Copper Alloy†

By J. G. Byrne‡ and M. E. Fine
Department of Materials Science, The Technological Institute, Northwestern University, Evanston, Illinois

and A. Kelly
Department of Metallurgy, Cambridge University

[Received January 3, 1961]

Abstract

In Al–1·7 at. % Cu the critical resolved shear stresses, tension stress–strain curves, and the dependence of the flow stress on strain rate were determined from 4·2 to 273 or 373°K for the following structures: supersaturated α solid solution, α+GP I, α+GP II, $\alpha+\theta'$, and $\alpha+\theta$. The difference between the CRSS at 4·2 and 273°K is large for the first two structures, but small with GP II, θ' or θ precipitates. With α, α+GP I, and α+GP II, a single slip system is operative over a significant portion of the stress–strain curve, and the rate of work hardening is about the same as that for pure Al. With θ or θ' multiple slip is immediately detected beyond the yield stress, the work-hardening rates are initially extremely rapid, and fall to small values after some per cent strain so that a plateau occurs in the stress–strain curves.

For supersaturated α, the strength is attributed to clustering in the solid solution.

In the cases of α+GP I and α+GP II, the zones must be sheared during plastic deformation and the strengthening arises from the atomic scrambling which occurs and the local strains near a zone which must be overcome when a dislocation moves through a zone. The variation of critical resolved shear stress with temperature and the strain-rate data are discussed in terms of the theory of thermally activated slip. Activation energies computed from the data are larger than those predicted on the basis of atomic scrambling alone.

With θ' or θ precipitate dislocations bend between the particles.

§ 1. Introduction

Four distinct stages of precipitation occur in Al base Cu alloys: Guinier–Preston zones of the first and second kinds, θ', and θ, the last being the stable precipitate. These have been extensively studied by x-ray diffraction (for reviews see Heal and Hardy 1954 and Guinier 1959) and the electron microscope (Nicholson and Nutting 1958, Nicholson *et al.* 1958–59). Commercial alloys based upon this system are heat treated to

† Based upon the Ph.D. thesis of J. G. Byrne, Northwestern University, June 1960. This research was supported by the United States Air Force Office of Scientific Research Solid State Science Division under contract Nos. AF18(600)1468 and AF49(638)-524.

‡ Present address : Dow Metal Products Co., Midland, Michigan.

contain substantially GP I or GP II; the presence of substantial amounts of θ or θ' corresponds to overageing. While these alloys have found important uses for many years, many uncertainties remain concerning the influence of the various precipitates on mechanical properties and the sources of strengthening are not well understood. Several years ago a programme was undertaken to determine the fundamental strength properties of Al base Cu alloys with various precipitates. The initial phase (Kelly and Chiou 1958) reported, for Al–1·8 at. % Cu with GP I zones and for the supersaturated solid solution, the variation of the critical resolved shear stress, and the flow stress with temperature over the range 77 to 373°K. This work has now been extended to include all four precipitates with an alloy of 1·7 at. % Cu. The temperature range of study has been lowered to 4·2°K. The effect of strain rate (10^{-5} to 10^{-3} sec^{-1}) has also been investigated.

Concurrently and independently Dew-Hughes and Robertson (1960) determined the room temperature plastic properties of single crystals of Al base Cu alloys with various precipitates as functions of Cu content. The experimental situation is now much clearer.

The purpose of the present paper is to report the experimental findings concerning plasticity of single crystals as function of structure, temperature and strain rate and to discuss these in terms of existing theory in an effort to understand the causes of the strength.

§ 2. Experimental

2.1. *Sample Preparation*

An alloy of 1·7 at. % Cu in the form of 0·260 in. diameter forged rod was provided by the Aluminum Company of America. The impurities reported by Alcoa are 0·002% Fe, 0·002% Si and 0·004% Mg. The forged rod was rolled to a thickness of about 0·060 in. and machined into tensile specimens of about 1 in. gauge length and about 0·1 in. wide in the gauge length. Single crystals were grown by first annealing at 550°C for 5 min, then plastically straining about 1·5% in tension and finally lowering at 1 cm per hour into molten salt (Houghton 430) at 550°C. The orientations of the crystals were determined to $\pm 2°$ by the back reflection Laue technique.

Heat treatment consisted of holding the specimens 15 hours at 550°C in molten salt, quenching into water at 25°C, followed immediately by an ageing treatment. Ageing treatments to 220°C were done in a circulating hot-air furnace and those above 220°C in molten salt. Resolution of GP I was accomplished by holding specimens in a bath of boiling benzyl alcohol (205°C) for 6 min.

2.2. *Plastic Deformation*

Testing was carried out with an Instron tensile testing machine at a strain rate of 10^{-4} sec^{-1} except where noted. During deformation the temperature of the crystal was controlled by immersing it in liquid helium

for 4·2°K, liquid nitrogen for 77°K, dry ice and acetone for 198°K, ice and water for 273°K, and boiling water for 373°K.

In measuring the effect of strain rate on the flow stress at a given temperature, the cross-head motion was stopped, the drive gears changed to those for the desired speed, and the cross-head motion was then resumed. During the period when the test was stopped the stress was maintained manually.

For deformation at 4·2°K a liquid helium cryostat similar to that of Blewitt *et al.* (1956) was constructed. A photograph of the parts is shown in fig. 1†. Holes drilled through the wall of the compression tube permitted liquid helium to be in direct contact with the specimen.

2.3. *Shear Modulus*

The shear modulus, G, was determined by the resonant dynamic method, utilizing a cylindrical quartz crystal vibrating in the torsional mode. The values of G at various temperatures for specimens with GP I, GP II and θ' precipitates are given in fig. 2.

Fig. 2

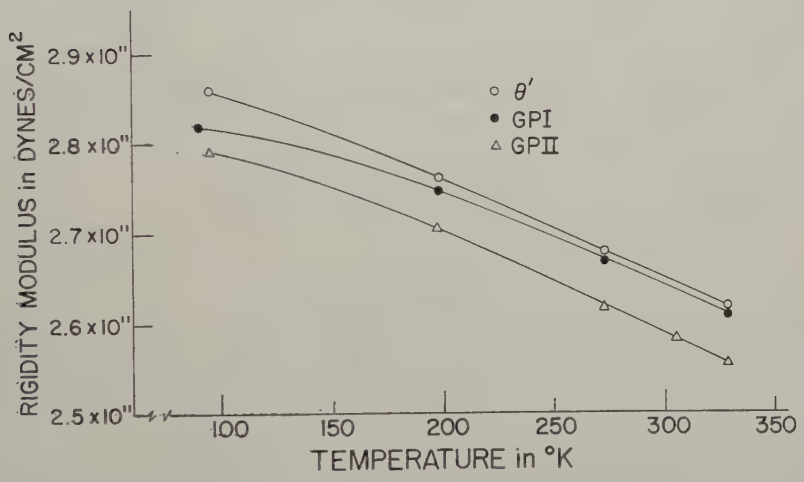

Shear modulus as function of temperature for Al–1·7 at. % Cu with various precipitates.

2.4. *Structure Determinations with X-rays*

For the identification of the precipitates after ageing, specimens of the same thickness as the tensile specimens were solution treated, quenched and aged simultaneously with the tensile specimens. They were then etched to about 0·010 in. thickness in a 10% NaOH solution and cleaned

† Figure 1 is shown as a plate.

with concentrated HNO_3. These specimens were oriented in a three-circle goniometer so that {100} planes were normal to the incident beam. Transmission Laue photographs were obtained using Mo radiation (40 kv, 10 ma, 8 hrs).

Most of our ageing treatments were based upon the comprehensive x-ray study of Silcock *et al.* (1953), to which reference should be made for details of the structures of the precipitates. Our x-ray results for the most part confirmed theirs. Guinier–Preston zones of the first kind (GP I) were produced by ageing for two days at 130°c, which gives zones of about 100 Å diameter. For Guinier–Preston zones of the second kind (GP II) a number of ageing treatments was used. One day at 190°c results in a mixture of GP II and some θ', the amount of θ' being variously estimated as 15% (Guinier 1952) and 30% (Silcock *et al.* 1953) of the maximum possible. In the present work, photometry of the θ' spots indicated 13% of the maximum amount of θ'. The thickness of the θ' plates is 80 Å (*ibid.*). 1000 hours at 130°c gives GP II plus 5 to 10% of the possible θ'; the zones are 20–30 Å thick and 500 Å in diameter while the θ' platelets are morethan 100Å thick (*ibid.*). Five hours at 190°c gives only GP II but the precipitation is not complete. In the present research some GP II was found after 4092 hours at 130°c. Relative intensity measurements indicated the presence of only about 35% of the maximum amount of θ'. Silcock *et al.* (1953) report no GP II beyond 2600 hours at this temperature.

θ' was produced by ageing one day at 240°c. This gives a platelet thickness of 300 Å; no other precipitate is present (*ibid.*). θ was formed by ageing for one day at 465°c followed by two days at 305°c; this gives a particle spacing of $3{\cdot}8 \times 10^{-4}$ cm (Shaw *et al.* 1953).

§ 3. Results

3.1. *Critical Resolved Shear Stress*

The critical resolved shear stress (CRSS) of a large number of crystals has been determined in this study (Byrne 1960). Values are plotted as a function of temperature for most of the aged states and for crystals of approximately the same orientation (fig. 3). The variation of CRSS with temperature is small for all states above about 150°k. The reverted crystals and those containing GP I show a very rapid temperature dependence of the flow stress below 150°k. The other aged states produce only a small variation in CRSS with temperature relative to the reverted and GP I states. Thus the reverted crystals or those containing GP I lose a considerable proportion of their strength on heating to room temperature. It is generally supposed that the strengthening effect of GP II precipitates is greater than that of GP I. This is not true at low temperatures, as can be seen from fig. 3, by comparison of the CRSS at 4·2°k of crystals containing GP I and GP II produced at the same temperature of ageing.

Fig. 3

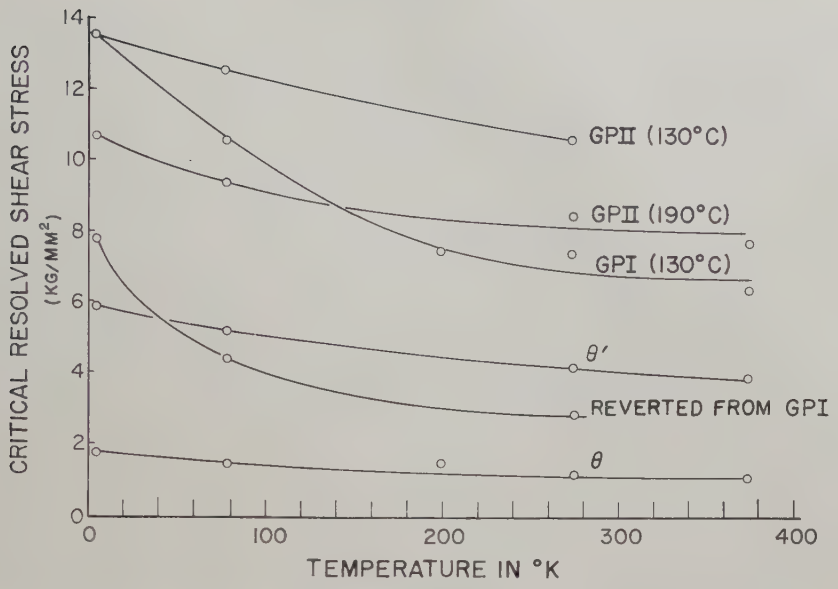

Critical resolved shear stress of Al–1·7 at. % Cu as function of temperature.

Fig. 4

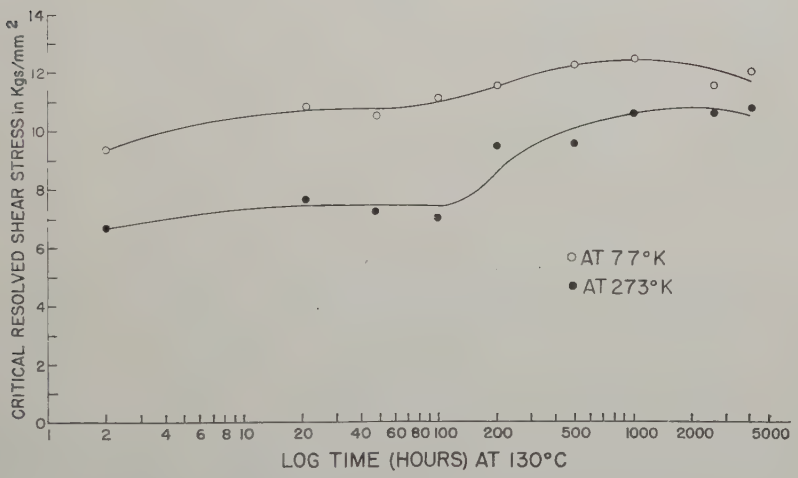

CRSS at 77 and 273°K versus ageing time at 130°C.

In fig. 4 the CRSS at 77 and 273°K are plotted against ageing time at 130°C. The hardening at early times is due to GP I and at later times GP II. The difference in the temperature dependence for crystals with mainly GP I and mainly GP II is again evident because the 77 and 273°K curves come much closer together at longer times.

3.2. *Stress–Strain Curves*

Stress–strain curves for GP I and reverted crystals are shown in fig. 5, GP II in fig. 6, and θ and θ' in fig. 7. Kelly and Chiou (1958) verified that the slip system is $\{111\}\langle 110\rangle$ for the Al–1·8% Cu alloy containing GP I. In the case of GP II, slip lines are not observed with the light microscope, nor with the electron microscope, except for large strains (Carlson and Honeycombe 1954–55, Thomas and Nutting 1957–58). This has been verified. In the present work a marked change occurred in the orientation of the crystal axes with respect to the tensile axis. The change in orientation was always found, within an error of 2°, to be consistent with slip on the $\{111\}\langle 110\rangle$ system having the maximum resolved shear stress. The Laue spots show only a small amount of asterism. In figs. 5 and 6 the resolved stress may thus be plotted versus glide strain. Slip on a single system has been assumed to occur throughout the test.

Fig. 5

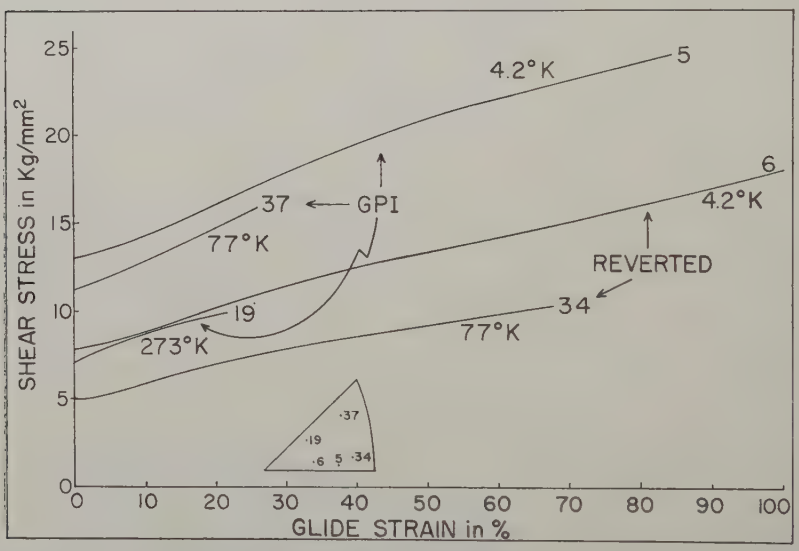

Resolved shear stress–glide strain curves for reverted crystals and crystals containing GP I.

In the case of θ and θ' being the major precipitate, deformation developed extensive asterism rather than a change in orientation. Thus slip must be occurring on several slip systems which is consistent with the change in form of the specimen during deformation. For this reason the nominal tensile stress is plotted in fig. 7.

In the testing at 4·2°K (not shown on the curves in figs. 5 to 7) sudden yielding was observed in the 'pre-plastic' and plastic ranges giving serrations in the stress–strain curves. These were accompanied by audible sounds. Serrations in the plastic region have been studied extensively

Fig. 6

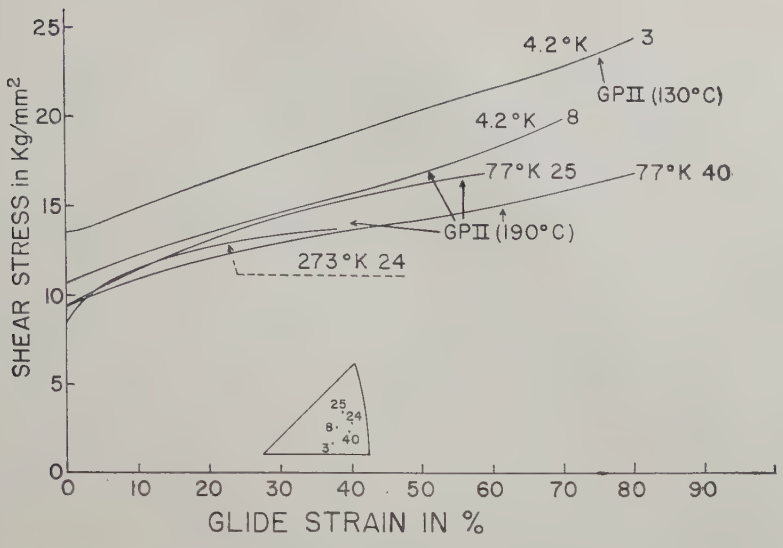

Resolved shear stress–glide strain curves for crystals containing GP II.

Fig. 7

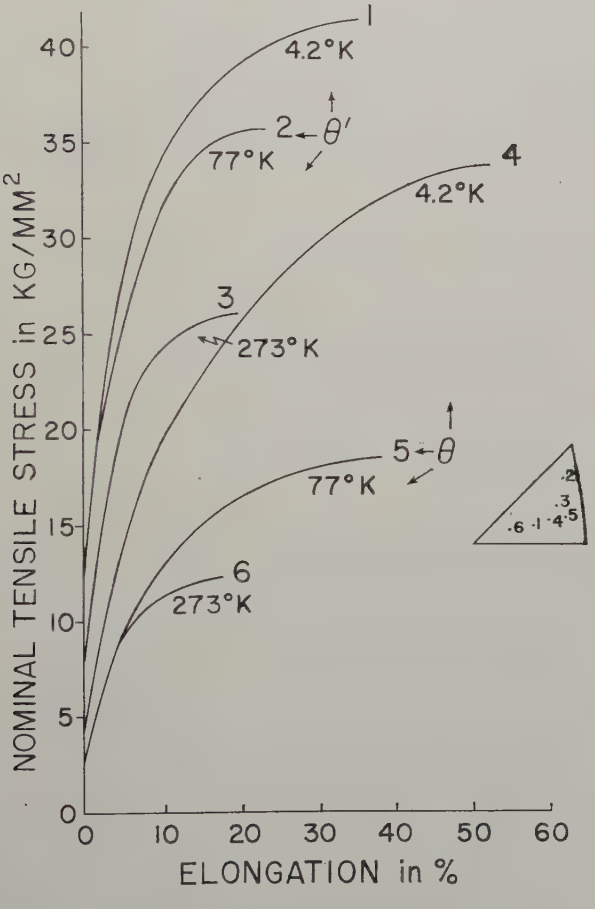

Nominal tensile stress–elongation curves for crystals containing θ and θ'.

by Basinski (1957) who attributed them to local heating from plastic deformation arising because the specific heat is so small at 4·2°K. In accord with Basinski, the magnitude of the drops in load and the spacing between them increased with elongation. The 'pre-plastic' serrations occurred only with CRSS values greater than 4·3 kg/mm^2 and therefore, did not occur with θ. Similar 'pre-plastic' serrations were shown in curves published for 2024 alloy by Basinski. The effect is not due to frozen air on the sample since the system was well purged with the He gas prior to the transfer of liquid He, and no condensation was ever noted inside the apparatus. It is believed that all the serrations observed here are due to the local heating effect.

The fractures at 4·2°K were similar to that previously recorded by Basinski (1957) in an Al–Mg alloy. They occur by shear through a highly localized region and as noted by Basinski are associated with the discontinuous yielding phenomenon. Fracture is usually preceded by several large discontinuities and results when the specimen can no longer arrest the highly localized deformation. The fracture surfaces are almost plane. Laue x-ray photographs of the fracture surface show very large amounts of asterism.

In reverted crystals and crystals air-cooled from the solution treating temperature and immediately tested, precipitation occurs during deformation (Carlsen and Honeycombe 1954–55, Kelly and Chiou 1958). The rate of strain hardening is then anomalously high. For this reason stress–strain curves for the reverted crystals are not shown in fig. 5 for test temperatures above 77°K.

It is at once clear from figs. 5, 6 and 7, that the stress–strain curves for crystals containing GP I and GP II are quite different from those of crystals containing θ' and θ precipitates. The stress–strain curves fall into two groups, those of crystals containing GP I and GP II are, at low temperatures, similar to those of pure aluminium single crystals (Staubwasser 1959, Hosford *et al.* 1960). It has been customary to define three stages of work hardening in face-centred cubic metals: Stage I is the region in the stress–strain curve where the stress increases only slightly with deformation, Stage II is the linear hardening range, and Stage III is where the curve is concave to the strain axis.

The slopes of Stage II of the low-temperature curves do not depend markedly on whether GP I or GP II is present, and their magnitude, about $G/200$, is roughly the same as that found in pure aluminium. The total increase in flow stress due to work hardening is about the same in the alloys as in pure aluminium at the same temperature.

When the principal precipitate is θ' or θ, then the curves of nominal tensile stress against elongation bear no similarity to those of an aluminium crystal of the same orientation. The initial rate of work hardening is extremely rapid for both precipitates, being about $G/10$. This is similar to that of aluminium crystals deforming on a number of slip systems (Hosford *et al.* 1960). After a certain amount of elongation, the curve levels off and becomes quite flat; no further work hardening occurs.

The complete flattening off is not apparent in Dew-Hughes and Robertson's (1960) curves but the other features are the same for crystals deformed at room temperature. From fig. 7 it is seen that the maximum stress reached depends markedly on temperature and the total amount of work hardening is very large. For crystals containing θ' the maximum nominal tensile stress depends logarithmically upon temperature obeying a relation of the form

$$\ln \sigma_{\max} = A - BT$$

where $A = 3{\cdot}72$ and $B = 1{\cdot}7 \times 10^{-3}/^{\circ}\text{K}$ for stresses in units of kg/mm^2. For the crystals containing θ the dependence of $\sigma_{\max}$ on temperature was still greater, particularly at low temperatures.

Fig. 8

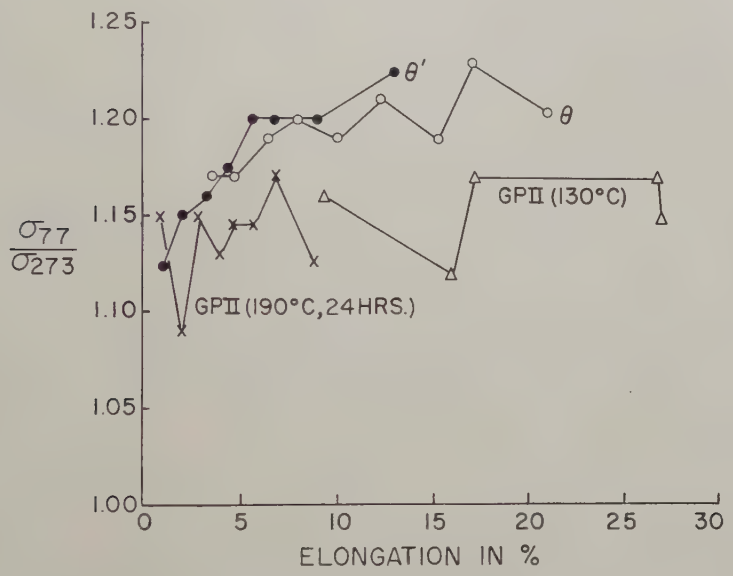

Ratio of the flow stress at 77 (σ_{77}) to flow stress at 273°K (σ_{273}) plotted against elongation for crystals containing GP II, θ' and θ.

3.3. *Temperature Transitions During Deformation*

Following the procedure of Cottrell and Stokes (1955) a large number of measurements were made of the change in flow stress accompanying a change in temperature during the deformation of these single crystals. In polycrystals and single crystals of pure metals the ratio of the flow stress at a temperature T (σ_T) to that at some standard temperature, e.g. 273°K (σ_{273}), is found to be independent of deformation at large deformations. In aluminium containing 1·8 at. % copper aged to contain GP I, Kelly and Chiou (1958) found that σ_{77}/σ_{273} initially decreased with deformation and then was roughly independent of further deformation. Later Kelly (1959) pointed out that $\sigma_{77} - \sigma_{273}$ was independent of deformation. In fig. 8, σ_{77}/σ_{273} is plotted against elongation, and in figs. 9 and 10, $\sigma_{77} - \sigma_{273}$ is plotted against elongation and σ_{273}, respectively,

Fig. 9

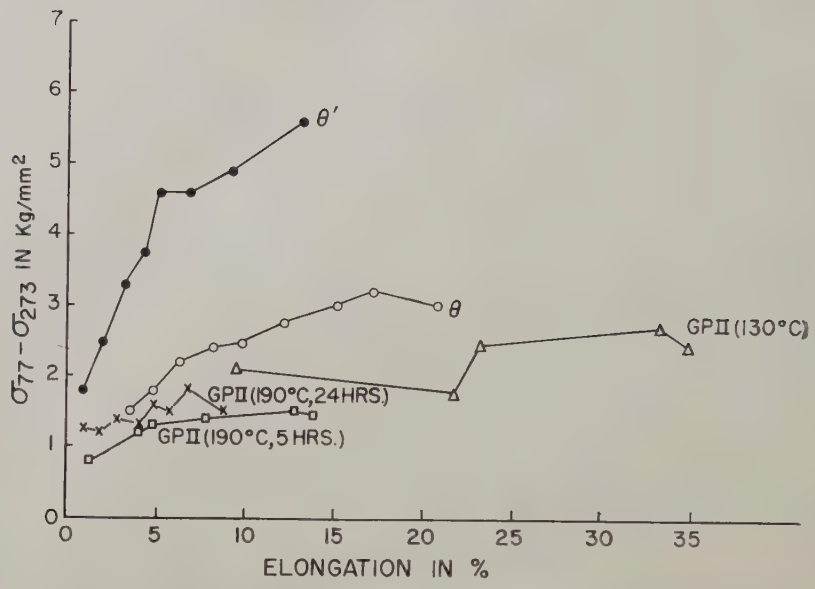

$\sigma_{77}-\sigma_{273}$ versus elongation for crystals containing GP II, θ' and θ.

Fig. 10

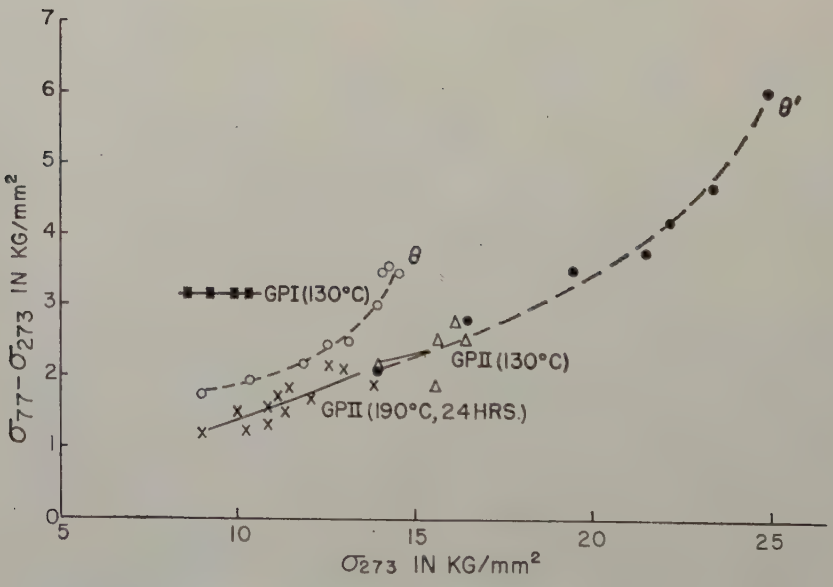

$\sigma_{77}-\sigma_{273}$ versus σ_{273} for crystals containing GP I, GP II, θ' and θ.

for representative specimens of the various states of precipitation studied in the present work. For the states containing principally GP II, σ_{77}/σ_{273} is roughly independent of elongation, and $\sigma_{77}-\sigma_{273}$ increases slightly with deformation. In the case of θ and θ', σ_{77}/σ_{273} and $\sigma_{77}-\sigma_{273}$ always increase with elongation, the changes being less for θ. For θ and θ', σ is nominal tensile stress.

Fig. 11

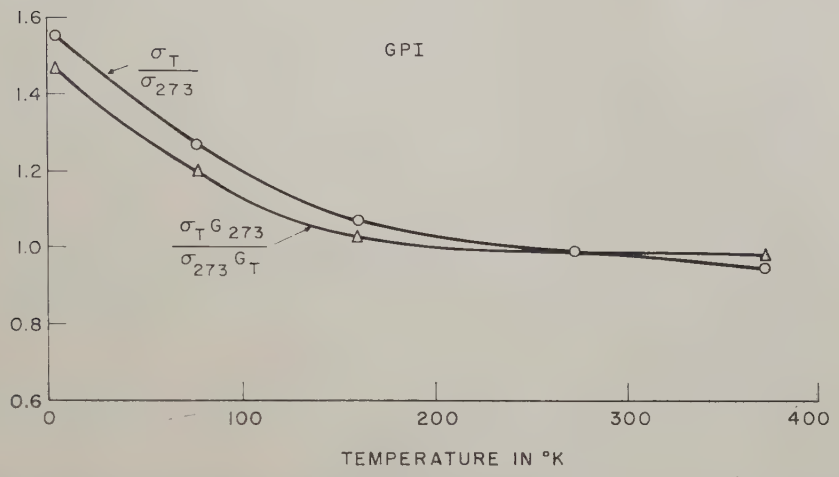

Ratio of the flow stress at T (σ_T) to flow stress at 273°K (σ_{273}) plotted against temperature for crystals containing GP I. In curve with triangle points σ_T/σ_{273} has been multiplied by G_{273}/G_T where G is shear modulus.

Fig. 12

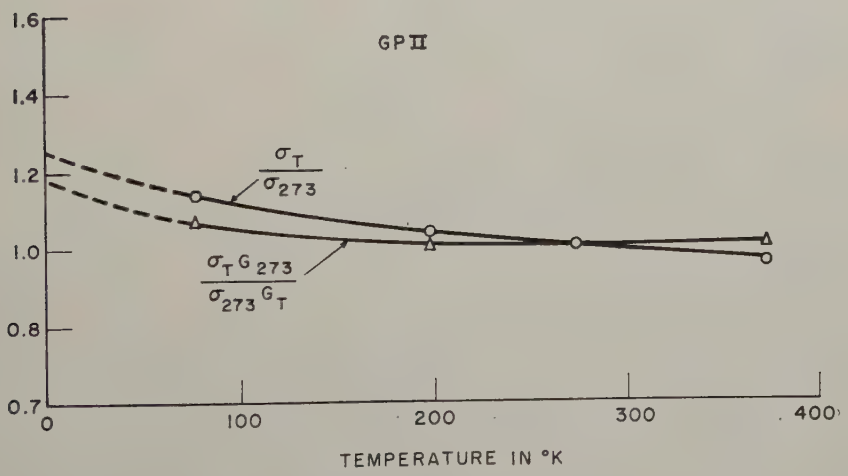

σ_T/σ_{273} and $\sigma_T G_{273}/\sigma_{273} G_T$ plotted against temperature for crystals containing GP II.

σ_T/σ_{273} and $(\sigma_T/\sigma_{273})(G_{273}/G_T)$ are plotted against temperature down to 4·2°K for GP I precipitate (fig. 11), GP II precipitate (fig. 12), θ' precipitate (fig. 13) and θ precipitate (fig. 14). When the value varied with deformation, average values for each temperature are plotted. For GP I the data of Kelly and Chiou (1958) are used for the higher and intermediate temperatures since essentially identical results for σ_{77}/σ_{273} were obtained with the present alloy.

Fig. 13

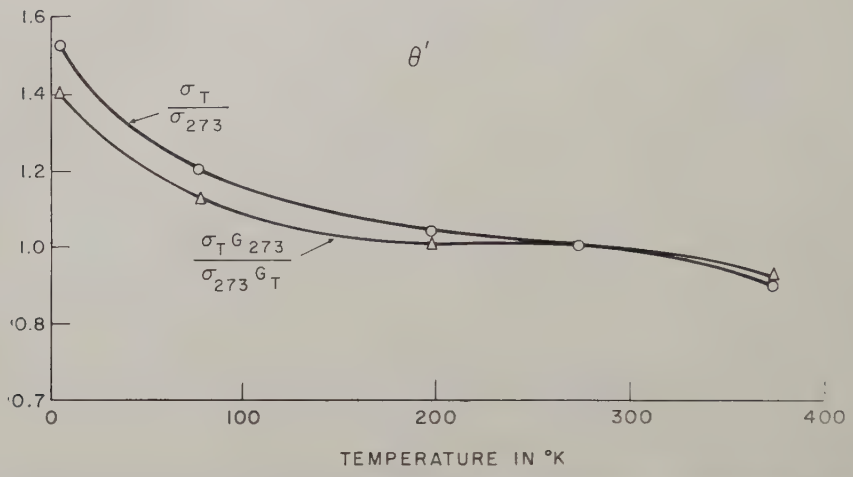

σ_T/σ_{273} and $\sigma_T G_{273}/\sigma_{273} G_T$ plotted against temperature for crystals containing θ'.

Fig. 14

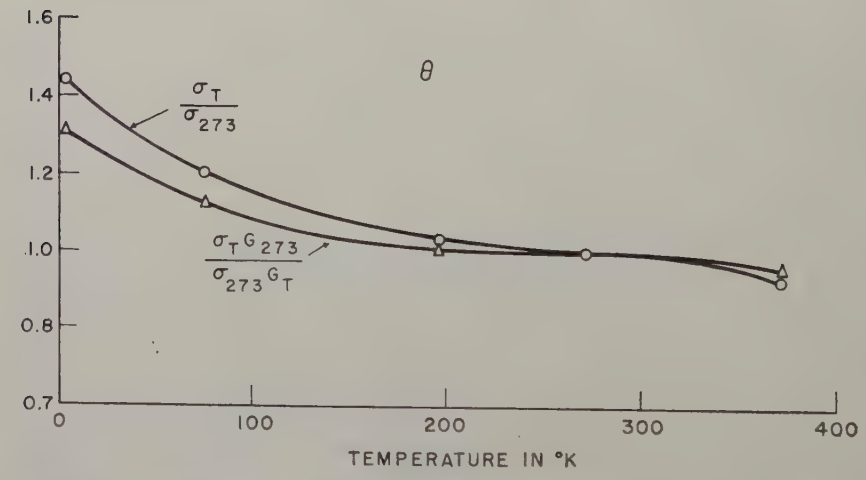

σ_T/σ_{273} and $\sigma_T G_{273}/\sigma_{273} G_T$ plotted against temperature for crystals containing θ.

No data are plotted for the reverted condition since alternate cycling between 77 and 273°K during deformation results in rapid GP I formation (Kelly and Chiou 1958).

3.4. *Strain-rate Transitions During Deformation*

Information complementary to that obtained from changing the temperature of deformation was obtained by changing the strain rate during isothermal tensile deformation and measuring the resulting change in flow stress. Changes in flow stress ($\sigma_1 - \sigma_2$) corresponding to a strain-rate transition between $\dot{\epsilon}_1$ and $\dot{\epsilon}_2$ were measured for both $\dot{\epsilon}_1 < \dot{\epsilon}_2$ and $\dot{\epsilon}_1 > \dot{\epsilon}_2$. Three strain rates were used, $3{\cdot}3 \times 10^{-5}$, $1{\cdot}65 \times 10^{-4}$ and $1{\cdot}65 \times 10^{-3}$ per sec.

Fig. 15

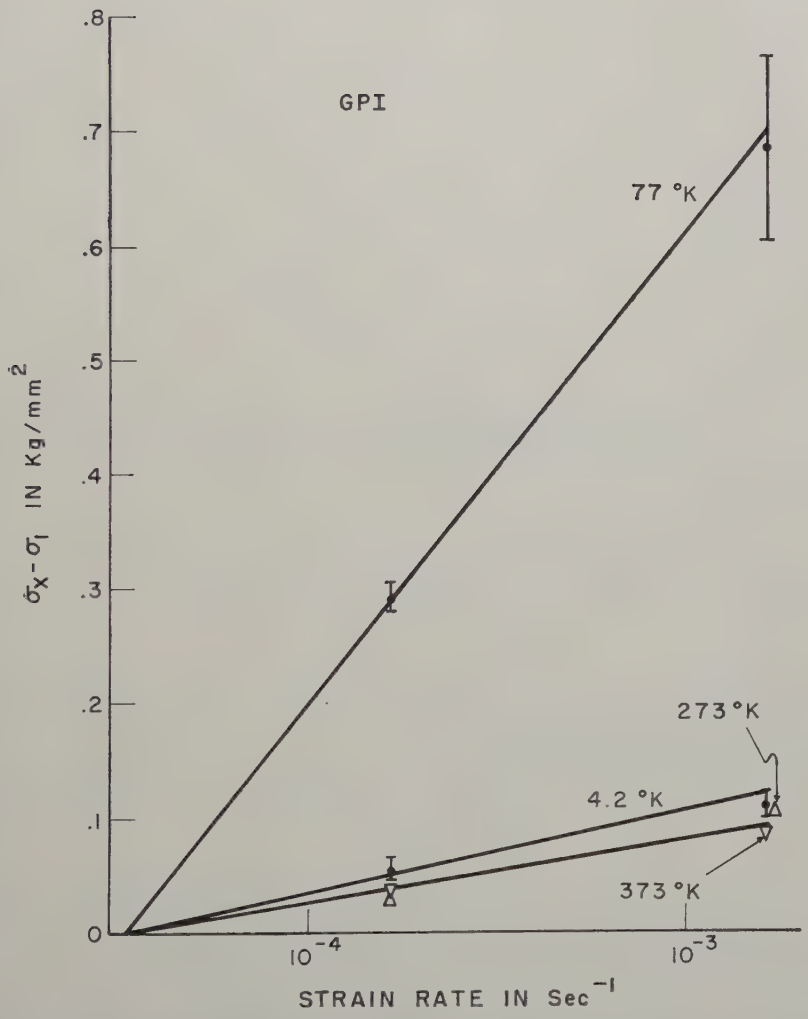

The increase in flow stress on increasing the strain rate for crystals containing GP I. $\sigma_x - \sigma_1$, where 1 refers to the slowest strain rate, is plotted as function of the log of the strain rate $\dot{\epsilon}_x$.

In figs. 15 to 19, values of $\sigma_x - \sigma_1$ (where σ_1 indicates the flow stress for the lowest strain rate) are plotted against the common logarithm of the strain rate. For GP II, fig. 16, transitions between only the two higher strain rates were performed; the zero point was established by extrapolation.

In crystals containing GP I, and in these only, yield drop effects were found on increasing the speed of deformation at temperatures above 198°K. The maximum values of $\Delta\sigma$ were then used.

As previously noted with crystals containing θ and θ', slip is not on a single system. Therefore to obtain $\Delta\sigma$ the tensile stress changes were multiplied by 0·5, an average value for $\cos\phi\cos\lambda$. For the other states the values refer to resolved shear stresses.

Fig. 16

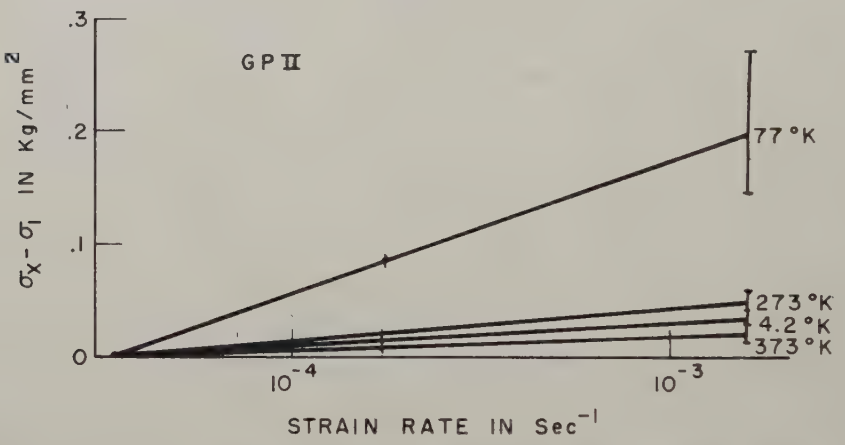

The increase in flow stress on increasing the strain rate for crystals containing GP II. See caption for fig. 15 for explanation.

The vertical lines in figs. 15 to 19 represent the spread of values. The uncertainty is shown to increase with strain rate because of the way the origin of the curve is defined.

While the strain-rate tests showed considerable scatter, the parameter

$$\frac{\sigma_x - \sigma_1}{\log \dot{\epsilon}_x/\dot{\epsilon}_1}$$

remained roughly constant throughout deformation at a given temperature; $\sigma_x - \sigma_1$ in the figures is roughly a linear function of $\log \dot{\epsilon}_x$.

The slopes of the lines in figs. 15 to 19 are observed to increase as the temperature is raised from 4·2°K to 77°K and then decrease again as the temperature of deformation is further raised. The θ' state is an exception in that the slope increases rapidly on heating above 273°K.

The large slope at 77°K of the $\sigma_x - \sigma_1$ *vs.* $\log \epsilon_x$ line compared to 4·2 and 273°K is also observed in pure metals (Wiedersich 1960, private communication) and Ag–Al solid solution alloys (Hendrickson and Fine 1961).

Fig. 17

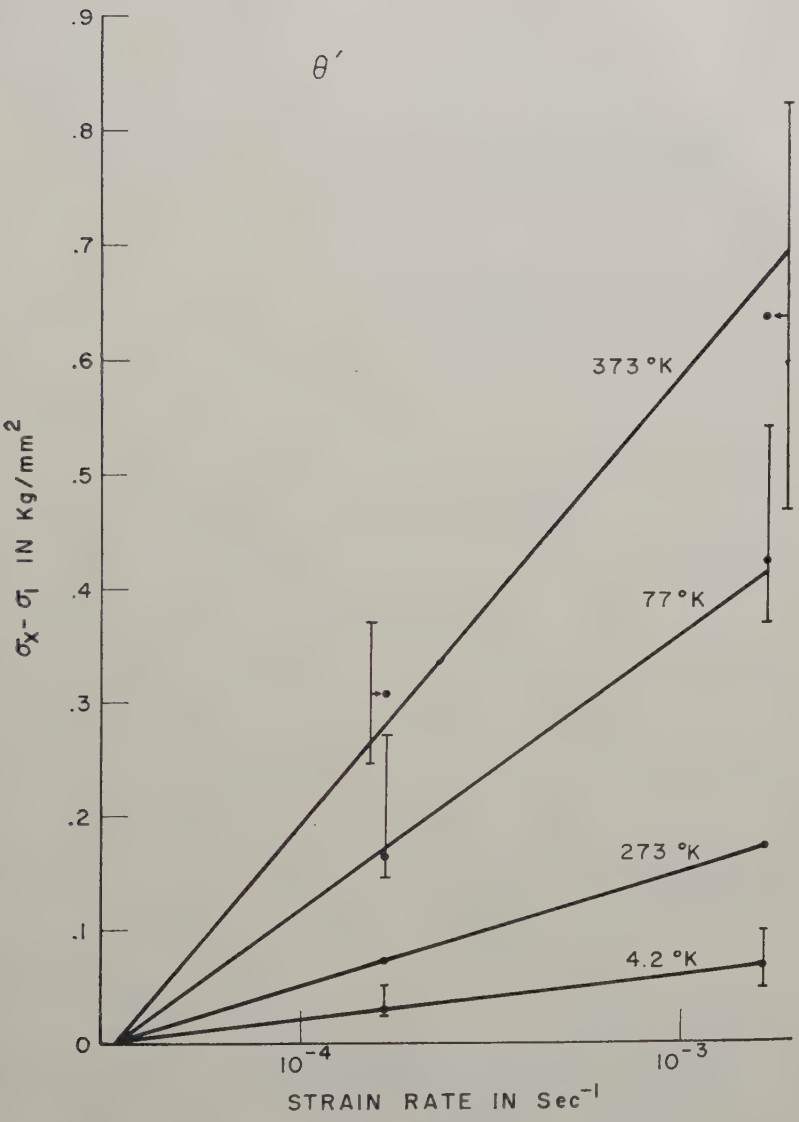

The increase in flow stress on increasing the strain rate for specimen containing θ'. See caption for fig. 15 for explanation.

Fig. 18

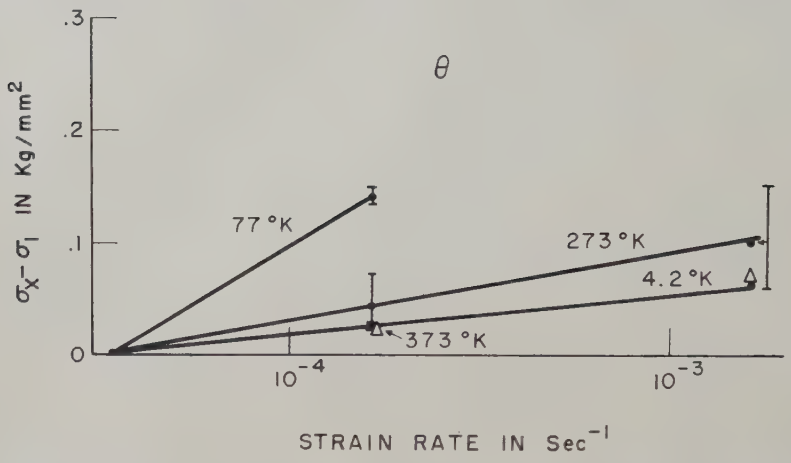

The increase in flow stress on increasing the strain rate for specimen containing θ. See caption for fig. 15 for explanation.

Fig. 19

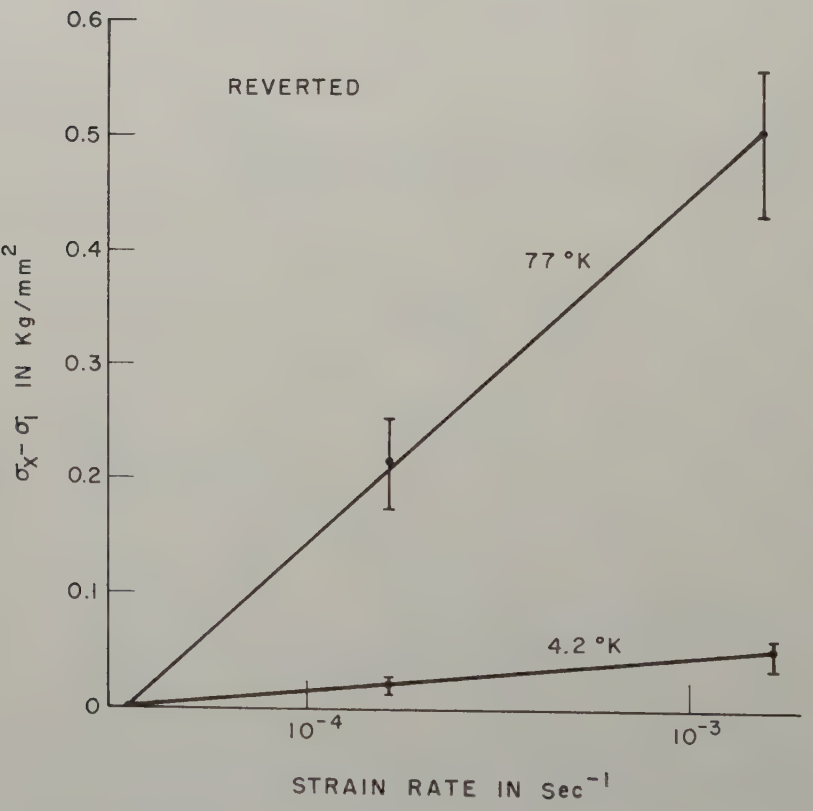

The increase in flow stress on increasing the strain rate for reverted crystals. See caption for fig. 15 for explanation.

§ 4. Discussion

4.1. *The Reverted State*

At room temperature the CRSS is low, ~ 3 kg/mm^2, and depends little on temperature (fig. 3). Below 100°K it rises rapidly to ~ 8 kg/mm^2 at 4·2°K. This effect appears characteristic of solid solutions whether supersaturated or not, see, for example, Seeger (1958). Recent studies of Cu base–Al and Ag base–Al alloys (Hendrickson and Fine 1961, Kopenaal and Fine 1961) also fit this rule. Al base–Zn alloys have been studied by Dash and Fine (1960); the temperature effect as well as the CRSS at 273°K is much smaller in the Al–Zn than in the Al–Cu alloys, suggesting that an important factor may be the mis-match in atomic size between solute and solvent. This is much greater for Al–Cu than Al–Zn.

At low temperatures the stress–strain curve is very similar to that of pure Al. Thus, the solute element affects mainly the CRSS and not the rate of work hardening provided the crystal is deformed at temperatures too low for precipitation or clustering to occur during deformation.

To account quantitatively for the magnitude of the CRSS and its variation with temperature is difficult. Friedel (1957) has proposed a theory for the CRSS and its variation with temperature based on the interaction of solute atoms with dislocations due to the stress field around the solute atoms. This theory gives for the CRSS at 0°K

$$\sigma = \tfrac{1}{4} G \epsilon f \qquad \ldots\ldots\ldots \quad (1)$$

where G is the rigidity modulus, f the volume fraction of solute, and ϵ the misfit parameter. The value of ϵf can be obtained from the measured variation of lattice parameter with composition. The theory predicts that the CRSS should vary with temperature in the manner found experimentally, as shown in fig. 3, through the effect of thermal assistance in overcoming the stress fields. However, the value given for σ from eqn. (1) is only 1 kg/mm^2, nearly an order of magnitude less than the observed value, and, hence, fails to account quantitatively for the magnitude of the CRSS.

Since the solid solution is supersaturated and tends to cluster, it seems likely that the CRSS, particularly at low temperatures, is due to the cutting of small clusters of copper atoms by dislocations. In analogy with GP I it is expected that the larger clusters would form thin discs on {100} planes and these may be important strengthening sources at all temperatures.

4.2. *Stress–Strain Curves of Crystals Containing Precipitates*

From the stress–strain curves at low temperature, shown in figs. 5, 6 and 7, it is clear that the presence of GP I and GP II affect mainly the magnitude of the critical resolved shear stress and do not greatly alter the work-hardening characteristics from those of pure aluminium or aluminium containing small amounts of other elements in solid solution.

We define the term 'friction stress' as the stress to move a single dislocation unaffected by the presence of other glide dislocations. The presence of either GP I or GP II then increases the strength of the alloy by introducing an additional friction stress opposing the motion of dislocations in the crystals. This additional friction stress is roughly constant throughout deformation. On the other hand, the precipitates θ' and θ, while affecting the CRSS less than do GP I and GP II, completely alter the work-hardening characteristics of the material. It has been shown that the deformation of crystals containing θ' and θ does not take place on a single system, but that a number of glide systems must be operative. The single crystals deform, as does a polycrystal with no external change of shape, while crystals containing GP I or GP II deform throughout, as do single crystals. These facts lead to an immediate qualitative explanation of the findings reported in § 3.3 of the effect of temperature transitions during deformation on the magnitude of the flow stress. For crystals containing GP I and GP II the increase in flow stress during deformation is not large compared to the values of the CRSS at room temperature. When the temperature dependence of the flow stress is measured as a function of strain during deformation, one measures the change of flow stress due to the temperature dependence of the friction stress plus that due to the temperature-dependent part of the increase in flow stress due to deformation. In the case of GP I the temperature dependence of the friction stress due to zones is large and masks the effect of the dislocations introduced during deformation; thus $\sigma_{77} - \sigma_{273}$ changes little during deformation.

For GP II the temperature dependence of the friction stress is much smaller and so the effect of the increase in dislocation density during deformation can be detected as an increase in $\sigma_{77} - \sigma_{273}$ (see figs. 9 and 10) during deformation. Some θ' is always present particularly with GP II produced at 190°C; this will lead to an increase in $\sigma_{77} - \sigma_{273}$.

The differences in behaviour among the crystals containing GP I, GP II, θ' and θ are strikingly seen if one plots the quantity $\sigma_{77} - \sigma_{273}$ (the temperature-dependent part of the flow stress) not against strain but against the flow stress at 273°K. This is done in fig. 10. If the increase in the temperature-dependent part of the flow stress during deformation is taken as a measure of the increase in the number of 'forest' dislocations which must be cut by gliding dislocations, as it is in all current theories of work hardening, then we see from fig. 10 that the values for GP I and GP II are much the same as for pure aluminium. This fact, in conjunction with the similarity of the stress–strain curves, is convincing evidence that the essential mechanism of work hardening in pure aluminium and in crystals containing GP I and GP II is the same. This is also true for aluminium–silver alloys containing zones and thus at least in these aluminium alloys it can be said that zone-type precipitates alter the plastic properties mainly through the introduction of an additional friction stress.

Crystals containing θ' or θ deform on a number of slip systems. This leads to an increase in the temperature dependence of the flow stress

throughout deformation (figs. 8, 9 and 10) due to the ever greater number of dislocations which must be cut by a dislocation moving on any operative glide system. As shown in fig. 10 for θ', the increase in $\sigma_{77} - \sigma_{273}$ attains a value of more than 4 kg/mm^2, indicating that the increase in density of the 'forest' is an order of magnitude greater than in pure aluminium or in crystals containing GP I or GP II alone.

Since the temperature dependence of the flow stress in crystals containing GP I and GP II is almost completely controlled by the temperature dependence of the CRSS, this means that tests involving change of strain rate during deformation can be used to investigate the strain-rate dependence of the CRSS, whereas in θ' and θ containing crystals the strain-rate dependence of the CRSS cannot be simply investigated by changes of strain rate during deformation due to the large change introduced by the deformation itself. Further, several activated processes are involved: the σ_T/σ_{273} curves turn downward at higher temperatures and with θ', $d\sigma/d\dot{\epsilon}$ is large for 373°K.

4.3. *Values of the CRSS of GP I and GP II*

In the case of crystals containing GP I and GP II the separation of the centres of precipitates cutting any slip plane, deduced from the x-ray results and confirmed by electron microscopy, is less than 150 Å and less than 300 Å respectively. The stress required to bend a dislocation to a radius of curvature ρ is $\sigma \sim Gb/\rho$. To avoid precipitates, dislocations would have to be bent to a radius of curvature of about one-half the mean separation of precipitates. This requires, in these cases, stresses of the order of magnitude of the theoretical shear strength, and an order of magnitude greater than the observed flow stress. The dislocations are thus forced to cut the zones (Kelly and Fine 1957). This has been confirmed experimentally in GP II containing crystals (Nicholson *et al.* 1960) and in other aluminium alloys containing coherent precipitates of the spacing of GP I (Jan 1955, Livingston and Becker 1958, Sato and Kelly 1961).

Comparison of the CRSS data in fig. 3 for the structures containing GP I and GP II clearly shows that increasing the size of the obstacles, which must be cut, reduces the temperature dependence of the CRSS.

The thermally activated motion of dislocations through obstacles in their glide plane has been studied by a number of workers. Assuming the barrier is cut in a single activated event and following the method due to Seeger (1954) and to Mott (1956), we write the strain rate

$$\dot{\epsilon} = \dot{\epsilon}_0 \exp\left[-U(\sigma)/kT\right] \quad . \quad . \quad . \quad . \quad . \quad . \quad (2)$$

where $\dot{\epsilon}_0$ is a constant, k and T have their usual meanings and $U(\sigma)$ is the activation energy for the cutting of a single obstacle under the influence of a shear stress σ. Solving (2) for the shear stress gives the CRSS as a function of temperature. Mott has shown that for a barrier with a rigid energy profile the dependence of U on σ is given by

$$U(\sigma) = U_0(1 - \sigma/\sigma_0)^{3/2} \quad . \quad . \quad . \quad . \quad . \quad (3)$$

for the case when the effect of thermal fluctuations is very small, and hence σ is always approximately equal to σ_0, the stress required to shear an obstacle in the absence of thermal fluctuations:

$$\sigma_0 = \frac{U_0}{4bl_0X_0}.$$

Here U_0 is the increase in potential energy of the system if an obstacle is cut at 0°K in the absence of an applied stress. l_0 is the separation of the obstacles in the glide plane and X_0 depends on the energy–distance profile of the barrier. $2X_0$ represents the distance moved by a dislocation into the barrier during the process of cutting.

Equation (3) should be used if the effect of thermal fluctuations is small. In the case when the barrier is thin and the effect of thermal fluctuations is large, we can use the approximation (Cottrell 1953, Seeger 1954)

$$U = U_0 - 4bl_0X_0\sigma. \qquad (4)$$

Substituting either (3) or (4) in (2) and defining the activation volume $v = 4bl_0X_0$ one obtains

$$\sigma = \frac{U_0}{v}\left[1 - \left\{\frac{kT}{U_0}\ln(\dot{\epsilon}_0/\dot{\epsilon})\right\}^{2/3}\right] \qquad (5)$$

or

$$\sigma = \frac{U_0}{v}\left[1 - \frac{kT}{U_0}\ln(\dot{\epsilon}_0/\dot{\epsilon})\right]. \qquad (6)$$

By differentiating (5) and (6) to obtain expressions for the strain-rate dependence of σ one obtains

$$\frac{d\sigma}{dln\dot{\epsilon}} = \frac{(kT)^{2/3}U_0^{1/3}}{3/2v(\ln\dot{\epsilon}_0/\dot{\epsilon})^{1/3}} \qquad (7)$$

and

$$\frac{d\sigma}{dln\dot{\epsilon}} = \frac{kT}{v}. \qquad (8)$$

When a dislocation cuts a zone it must overcome any misfit stresses associated with the zone, and it must change the arrangement of the atoms. Both of these must be evaluated and taken into account in any quantitative theory of zone hardening and its variation with temperature.

The zones in Al–Cu present two types of barrier. One-third of the zones lie parallel to the Burgers vector of any moving dislocation. Consideration of the structures of the zones shows that for GP I and GP II a dislocation passing through such a zone will only alter the arrangement of nearest neighbours on entering and on leaving the zone. The other zones present a much larger energy barrier and when these are cut the type of nearest neighbour is altered over the whole area of intersection of the zone and slip plane.

Equation (5) predicts a linear relation between the CRSS and $T^{2/3}$; eqn. (6) predicts a linear relation between the CRSS and T. In fig. 20 the CRSS is plotted versus $T^{2/3}$. A straight line has been drawn through

the GP II data for 130°C; the fit appears reasonably good. For GP II (190°C) containing an appreciable amount of θ' there is positive curvature at the higher temperatures. In the case of GP I the three lowest temperature points appear to fit on a straight line.

Fig. 20

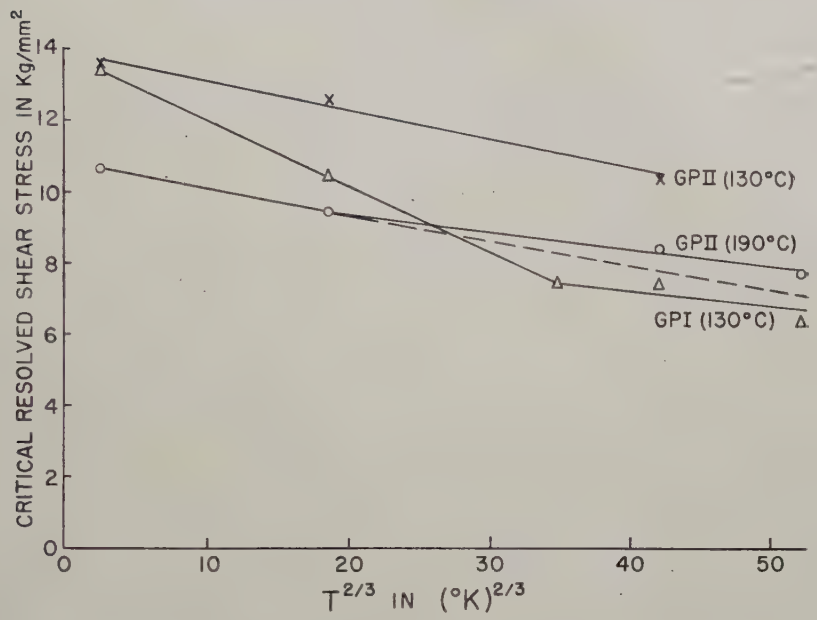

Critical resolved shear stress plotted against $T^{2/3}$ for crystals containing GP I and GP II.

Considering the data for GP I we assume that there are two kinds of barrier, one with a large U_0 and one with a small U_0. Then in fig. 20 two intersecting straight lines have been drawn through the data. We assume eqn. (5) to hold for both, but with different values of U_0. For the low temperature branch we see from eqn. (5) that at a temperature T_c where

$$U_0 = kT_c \ln \dot{\epsilon}_0/\dot{\epsilon}$$

the flow stress due to this barrier becomes zero. The critical temperature is about 150°K, see fig. 3, whence, evaluating the log term, see below,

$$U_0 \sim 0{\cdot}26 \text{ ev.}$$

The high temperature branch in fig. 20 gives a value of the flow stress at 0°K of 9 kg/mm². Whence from eqn. (5)

$$\frac{U_0}{v} = 9 \text{ kg/mm}^2$$

and from the slope of the line

$$\frac{U_0^{1/3}}{v}(k \ln \dot{\epsilon}_0/\dot{\epsilon})^{2/3} = 4 \times 10^{-2} \text{ kg/mm}^2 (°\text{K})^{2/3}.$$

We can estimate $\dot{\epsilon}_0$:

$$\dot{\epsilon}_0 = NA\mathbf{b}\nu_0$$

where N is the number of points per unit volume at which dislocations are held up at obstacles. A is the area of slip plane swept out by a dislocation per activated event, $\mathbf{b}$ the Burgers vector and ν_0 the vibration frequency of a dislocation against an obstacle. We take

$$\nu_0 = 10^{12}\ \text{sec}^{-1}.$$

A may be calculated from the known distribution of the zones. In this case it is 5×10^{-14} cm^2. We assume a value of N of 5×10^{13} corresponding to a dislocation density of 10^8 cm^{-2}, which gives a value of the ln term of 22. We then find $U_0 \sim 6$ ev and $v \sim 10^{-20}$ cm^3.

For the low-temperature branch the slope is $18{\cdot}6 \times 10^{-2}$ kg/mm^2 (°K)$^{2/3}$ and the appropriate value of the flow stress is obtained by subtracting 9 kg/mm^2 from the 0°K intercept in fig. 3 to give

$$\frac{U_0}{v} = 4{\cdot}9\ \text{kg/mm}^2.$$

Taking the same value of the ln term we then find $U_0 \sim 0{\cdot}2$ ev and $v \sim 7 \times 10^{-22}$ cm^3. The value of U_0 agrees roughly with that estimated from the critical temperature.

Additional estimates of v may be obtained from plots of $\Delta\sigma$ against $\Delta \log \dot{\epsilon}$ (fig. 15) using eqn. (7), since we can estimate U_0 from the temperature dependence of the flow stress and the term involving $(\log \dot{\epsilon})^{1/3}$ varies negligibly over the range of strain rates used. Taking $U_0 = 0{\cdot}2$ ev for temperatures of 4·2°K and 77°K, but 6 ev for 273°K gives values of v of 4×10^{-22}, 5×10^{-22} and 2×10^{-20} cm^3 for these temperatures respectively. The agreement with the values found from the temperature dependence of the flow stress is good, being always within a factor of two, and lends great support to the correctness of the analysis, when it is borne in mind that only average values can be obtained for what must in reality correspond to a range of values of both U_0 and v.

We now consider the data for GP II. The CRSS varies with temperature approximately as $T^{2/3}$ (fig. 20), and this is consistent with eqn. (5) assuming the occurrence of a single activated process. However, the strain-rate data (fig. 16) are not consistent with this analysis since the strain-rate sensitivity does not increase continuously with rise in temperature. We shall assume that there are again two types of obstacle to flow due to the different orientation of the zones, as for GP I. We assume that the obstacle responsible for the increase in flow stress as the temperature is lowered below room temperature becomes ineffective at around room temperature, and thus from eqn. (5) corresponds to an activation energy of about 0·6 ev, taking the value of the log term as 25. The increase in flow stress due to this obstacle is then the difference in flow stress between room temperature and 0°K, i.e. for GP II produced at 130°C, 2·5 kg/mm^2. We then have

$$\frac{U_0}{v} = 2{\cdot}5\ \text{kg/mm}^2$$

and from the slope, which is $7{\cdot}2 \times 10^{-2}$ kg/mm^2 (°K)$^{2/3}$, we obtain $U_0 = 0{\cdot}5$ ev and $v = 3 \times 10^{-21}$ cm^3. The value of the log term is 25 (using $A = 2{\cdot}87 \times 10^{-11}$ cm^2 and a dislocation density of 10^8 cm^{-2}).

We can also compute values of v from the strain-rate data as we did for the GP I containing crystals. We then obtain, taking $U_0 = 0{\cdot}5$ ev and using eqn. (7), $v = 2 \times 10^{-21}$ cm^2 at 4·2°K and 3×10^{-21} cm^3 at 77°K. These values show good agreement with one another and with the value found from the temperature dependence of the flow stress. If we use $U_0 = 0{\cdot}5$ ev and evaluate the strain-rate data at 273°K we obtain a value of $v = 2 \times 10^{-20}$ cm^3, which does not agree with the values obtained at the other two temperatures. It is for this reason that we suggest that there are two quite different types of barrier corresponding to the differently oriented zones in the case of GP II as in the case of GP I.

We now consider the values obtained for activation energies and activation volumes, using the above analysis. For GP I the value of U_0 of 0·2 ev we associate with the cutting of zones where **b** is parallel to the plane of the zone and 6 ev with cutting of zones where **b** is oblique to the plane of the zone; the U_0 for oblique cutting is 30 times the value for parallel cutting. The length of a zone is about 100 Å and this gives a value of about 30 atoms for the average trace of a zone intersecting a {111} plane. The agreement between the two estimates is thus very good.

For GP II the results indicate that the U_0 for **b** parallel to the plane of the zone is about 0·5 ev; it is thicker than GP I. For **b** oblique to the plane of the zone U_0 appears to be so high that the contribution to the CRSS is little affected by variation in temperature.

The consistency of the above analysis lends great support to the idea that the major contribution to the flow stress of these alloys, containing GP I or GP II is due to the work done by the applied stress in forcing dislocations through the zones. The values of v, the activation volume, are also reasonable. A crude estimate of the activation volume for zones parallel to the Burgers vector is given by $v = b^2 l_0$, where l_0 is the average separation of the zones and b the distance of closest approach of atoms. For GP I produced at 130°C, $l_0 \sim 100$ Å (Nicholson and Nutting 1958) and thus $v \sim 7 \times 10^{-22}$ cm^3. For GP II, $l_0 \sim 300$ Å (*ibid.*) and so $v \sim 2 \times 10^{-21}$ cm^3. These values agree with those deduced from the temperature dependence of the flow stress and independently from the change of strain rate during deformation.

For the zones which do not lie parallel to the Burgers vector of a dislocation the appropriate value of v will be $v \sim b l_0^2$, which gives a value of 2×10^{-20} cm^3, again in agreement with the value found from the results at room temperature.

We may now consider the value of U_0, the energy required to shear a zone. As stated previously, this will include (*a*) any stress fields around and in the zone which must be overcome and (*b*) the energy required to change the arrangement of the atoms.

A crude estimate of that part of U_0 required to change the arrangement of atoms can be made from the heat of zone formation or the heat of solution

(reversion) of the zone (Kelly and Fine 1957). For a GP I zone whose trace on the slip plane is parallel to b of the dislocation involved, U_0 is roughly $\Delta e/2$ where Δe is the heat of formation of the zone per atom of copper. Three values of Δe have been reported. These are 0·08, 0·23 and 0·14 ev per atom of copper. The first, Suzuki (1949), and second, Beaton and Rollason (1957), are heats of solution estimated respectively from differential thermal analysis on heating a sample containing GP I and from the solvus line with respect to GP I determined from hardness data. The third and most reliable (De Sorbo *et al.* 1958) is an isothermal calorimetric measurement of the heat evolved during formation of GP I. Thus a U_0 of about 0·1 ev is predicted or about half the value indicated from the measurements reported here. The estimate of U_0 from the calorimetric measurements is a lower limit since it is assumed that all copper atoms are in the zones.

For a GP II zone about 24 Å thick and with b of the slip dislocation contained in the face of the zone, U_0 is roughly $2\Delta e$ where Δe is the heat of formation of GP II per atom of copper. Two values of Δe for GP II have been reported, 0·31 ev (Beaton and Rollason 1957) and 0·14 ev (Suzuki 1949). These are rougly 1·5 times the corresponding values for GP I; GP II is a more stable phase. Assuming Δe to be 0·2 ev then a U_0 of 0·4 ev is predicted or again somewhat less than the measured value.

Additional contributions will come from the strain fields of the zones which are known to exist from x-ray examination (Gerold 1958) and from direct observation under the electron microscope (Nicholson and Nutting 1958). There will be a short-range elastic interaction between zones and a moving dislocation exactly analogous to the elastic interaction between a moving dislocation and another stationary one threading the glide plane. The magnitude of the elastic interaction is difficult to estimate without a very detailed knowledge of the stress field around and in the zones, but the low values of U_0 predicted from the change in arrangement of atoms suggests that the contribution from the elastic interaction may be of about the same order of magnitude.

Kelly (1958) and Dew-Hughes and Robertson (1960) attempted to account for the CRSS of these alloys in terms of the theory of Mott and Nabarro (1940). Dew-Hughes and Robertson claim good agreement with experiment at room temperature, by adding together various contributions to the flow stress. They conclude that at room temperature the CRSS for GP I containing crystals is satisfactorily accounted for from the theory of Mott and Nabarro, plus a small contribution from the solid solution. The theory of Mott and Nabarro cannot apply in this case without considerable modification. Firstly, the formula derived is for spherical precipitates and secondly the flow stress is identified with the mean internal stress. This is the only case when the radius of curvature to which a dislocation can be bent by the mean internal stress is equal to the separation of the precipitates. We have shown above that the measured flow stress, which is equal to the mean internal stress in this theory, is far

too small to bend a dislocation to a radius of curvature equal to the separation of those precipitates cutting the glide plane. The dislocations actually cut through the precipitates in the glide plane and hence each dislocation is subject not to the mean internal stress but to the stress due to a zone at small distances from the zone. Finally, the theory of Mott and Nabarro predicts a temperature dependence of the flow stress equal to that of the elastic constants. This is not the case.

The inapplicability of the theory of Mott and Nabarro in its current form does not mean that the stresses around a zone are unimportant, but that it is the short-range elastic interaction between dislocations and zones which are important here and not the mean internal stress.

4.4. *Alloys Containing θ′ and θ Precipitates*

The CRSS of alloys containing the θ and θ' precipitates appears to be understood at room temperature. The precipitates do not deform with the matrix and the CRSS is the stress necessary to expand a loop of dislocation between them. This is given by (Orowan 1948):

$$\sigma = \alpha G b / L \qquad . \; . \; . \; . \; . \; . \; . \; . \; . \; (8)$$

where L is the separation of the precipitates. α is the relevant constant in the theoretical expression for the line tension of a dislocation. This formula applies well over a range of spacings (Dew-Hughes and Robertson 1960). In our case for the θ precipitate L is $3{\cdot}8 \times 10^{-4}$ cm, hence σ, with $\alpha = 4$, using Cottrell's (1953) estimate of the line tension, is $0{\cdot}8\,\mathrm{kg/mm^2}$. The measured value is $1{\cdot}2\,\mathrm{kg/mm^2}$. The CRSS at 4·2°K is $1{\cdot}8\,\mathrm{kg/mm^2}$. The change can be attributed to the increase in G with temperature, the increase in strength of the equilibrium solid solution and perhaps a small increase due to the density of 'forest' dislocations.

For alloys containing θ' the same appears to be true. The separation of the precipitates is $0{\cdot}4 \times 10^{-4}$ cm (Nicholson *et al.* 1958–59), hence $\sigma = 5\,\mathrm{kg/mm^2}$; the measured value is $4{\cdot}3\,\mathrm{kg/mm^2}$. On cooling to 4·2°K there is only a small increase in CRSS of $1{\cdot}7\,\mathrm{kg/mm^2}$. This may be attributed to an increase in G ($0{\cdot}5\,\mathrm{kg/mm^2}$) and to the presence of dislocations cutting the glide plane. These may be either distributed at random or associated with the precipitate. Two types of dislocations associated with θ' have been observed (Nicholson *et al.* 1958–59): a Van der Merwe grid in the interface and a ring around the platelet and parallel to its plane. Thus, θ' is not truly coherent with the matrix; much of the misfit is adjusted by the presence of dislocations. Hardening due to misfit strains does not appear to be important here.

With regard to the stress–strain curves (fig. 7) for both θ and θ' the initial work-hardening rate is very large being about $G/10$ and roughly independent of temperature. The amounts of work hardening reach maximum values which are many times larger than the yield stresses and increase considerably on cooling.

At small strains θ particles are not deformed. This has been shown experimentally (Dew-Hughes and Robertson 1960); the precipitates are large enough to withstand the stresses on them as the dislocations expand between the particles. Following Fisher *et al.* (1953), Dew-Hughes and Robertson (1960) concluded that the initial work hardening is due to the residual loops remaining around the particles. These impose a back stress on the source. The observed temperature dependence of the initial slope is further confirmation since the back stress would only vary as G.

According to the theory of Fisher, Hart and Pry the metal work hardens until the particles are sheared. A plateau in the shear stress–shear strain curve is predicted. Hirsch (1957) suggests that the particles are avoided by cross slip. If so prismatic loops of dislocation will be formed at particles and these will give the same mean internal stress calculated by Fisher, Hart and Pry, but a reduced stress on the particle.

At large stresses at room temperature, cutting of some θ' particles is observed (Thomas and Nutting 1957–58, Koda and Takeyama 1957–58, Nicholson *et al.* 1960). θ particles are not cut at room temperature. Whether the particles are cut or whether cross slip occurs will depend upon the energies involved, and on the size, spacing, and strength of the precipitate. With θ' there is an orientation variable too, since the precipitate and matrix lattices are not in registry in all directions.

Plastic deformation of specimens containing θ and θ' do not show many slip lines (Thomas and Nutting 1957–58) indicating that slip is taking place on a fine scale. Further, Laue spots develop asterism rather than change position. Simultaneous slip on several systems is indicated; the dislocations in part appear to be undergoing cross slip to avoid the particles as suggested by Hirsch and the occurrence of the maximum in the stress–strain curve could correspond to complete replacement of the Orowan mechanism by cross slip. Since cross slip in part is aided by thermal activation a much higher maximum at 4·2°K could result. One thus expects to observe more extensive shearing of particles at low temperatures, and the maximum stress may then be reached when the particles are sheared.

Further work is necessary to completely understand with θ and θ' the very rapid rate of work hardening, the occurrence of the plateau, and its variation with temperature. These are certainly connected with slip on many systems, and a rapidly increasing dislocation density with deformation.

Acknowledgments

The authors are indebted to Professor A. H. Cottrell, F.R.S., Dr. T. H. Blewitt, Dr. J. Weertman and Dr. R. B. Nicholson for helpful discussions, and to Mr. J. Dash for his assistance in obtaining some of the experimental results.

References

Basinski, Z. S., 1957, *Proc. roy. Soc.* A, **240,** 229.

Beaton, R. H., and Rollason, E. C., 1957, *J. Inst. Met.*, **86,** 85.

Blewitt, T. H., Coltman, R. R., and Redman, J. K., 1956, *Dislocations and Mechanical Properties of Crystals* (John Wiley and Sons), p. 179.

Byrne, J. G., 1960, Ph.D. Thesis, Northwestern University.

Carlsen, K. M., and Honeycombe, R. W. K., 1954–55, *J. Inst. Met.*, **83,** 449.

Cottrell, A. H., 1953, *Dislocations and Plastic Flow in Crystals* (Oxford : University Press).

Cottrell, A. H., and Stokes, R. J., 1955, *Proc. roy. Soc.* A, **233,** 17.

Dash, J., and Fine, M. E., 1961, *Acta Met.*, **9,** 149.

De Sorbo, W., Treaftis, H. N., and Turnbull, D., 1958, *Acta Met.*, **6,** 401.

Dew-Hughes, D., and Robertson, W. D., 1960, *Acta Met.*, **8,** 147, 156.

Fisher, J. C., Hart, E. W., and Pry, R. H., 1953, *Acta Met.*, **1,** 336.

Friedel, J., 1957, *Les Dislocations* (Paris : Gauthier-Villars).

Gerold, V., 1958, *Acta cryst.*, **11,** 230.

Greetham, G., and Honeycombe, R. W. K., 1960–61, *J. Inst. Met.*, **89,** 13.

Guinier, A., 1952, *Z. Elektrochem.*, 56, 468 ; 1959, *Advances in Solid State Physics*, Vol. 9 (Academic Press), p. 294.

Heal, T. J., and Hardy, H. K., 1954, *Progress in Metal Physics*, Vol. 5 (Interscience Publishers, Inc.), p. 143.

Hendrickson, A. A., and Fine, M. E., 1961, *Trans. Amer. Inst. min. (metall.) Engrs*, **221,** 103.

Hirsch, P. B., 1957, *J. Inst. Met.*, **86,** 13.

Hosford, W. F., Jr., Fleischer, R. L., and Backofen, W. A., 1960, *Acta Met.*, **8,** 187.

Jan, J.-P., 1955, *J. appl. Phys.*, **26,** 1291.

Kelly, A., 1958, AFOSR report. TN-58-1083 ; 1959, *Acta Met.*, **7,** 811.

Kelly, A., and Chiou, C., 1958, *Acta Met.*, **6,** 565.

Kelly, A., and Fine, M. E., 1957, *Acta Met.*, **5,** 365.

Koda, S., and Takeyama, T., 1957–58, *J. Inst. Met.*, **86,** 277.

Koppenaal, T. J., and Fine, M. E., 1961 (to be published).

Livingston, J. D., and Becker, J., 1958, *Trans. Amer. Inst. min. (metall.) Engrs*, **212,** 316.

Mott, N. F., 1956, *Phil. Mag.*, **1,** 568.

Mott, N. F., and Nabarro, F. R. N., 1940, *Proc. phys. Soc., Lond.*, **52,** 86.

Nicholson, R. B., and Nutting, J., 1958, *Phil. Mag.*, **3,** 531.

Nicholson, R. B., Thomas, G., and Nutting, J., 1958–59, *J. Inst. Met.*, **87,** 429 ; 1960, *Acta Met.*, **8,** 172.

Orowan, E., 1948, *A Symposium on Internal Stresses* (London : Institute of Metals), p. 451.

Sato, S., and Kelly, A., 1961, *Acta Met.*, **9,** 59.

Seeger, A., 1954, *Phil. Mag.*, **47,** 771; 1958, *Encyclopedia of Physics*, Vol. II, part 2 (Berlin : Springer-Verlag), p. 1.

Shaw, R. B., Shepard, L. A., Starr, C. D., and Dorn, J. E., 1953, *Trans. Amer. Soc. Met.*, **45,** 249.

Silcock, J. M., Heal, T. J., and Hardy, H. K., 1953, *J. Inst. Met.*, **82,** 239.

Staubwasser, W., 1959, *Acta Met.*, **7,** 43.

Suzuki, T., 1949, *Sci. Rep. Res. Inst. Tohoku Univ.*, A, **1,** 183.

Thomas, G., and Nutting, J., 1957–58, *J. Inst. Met.*, **86,** 7.

A Dislocation at a Free Surface

By Elizabeth H. Yoffe
Cavendish Laboratory, Cambridge

[Received February 1, 1961]

Abstract

The stress field of a dislocation meeting a free surface of an elastic body is calculated for any angle of incidence and any Burgers vector.

§ 1. Introduction

Many observations have been made on dislocations lying in thin films of crystalline material. It is to be expected that the presence of the two surfaces of the film would have an effect on the behaviour of the dislocations, and this was confirmed by Eshelby and Stroh (1951) for dislocations normal to the surface, and by Head (1953) for dislocations parallel to the surface. The general case of dislocations in a semi-infinite elastic medium has been studied by Steketee (1958). His solution involves six sets of Green's functions and is not easy to apply in practice. In the present paper a straight dislocation meets a free surface of an isotropic elastic body at an arbitrary angle, and the resulting stress field is to be calculated.

§ 2. Notation

Rectangular cartesian coordinates (x, y, z) are chosen, and the elastic body is supposed to occupy the half space $z<0$, as shown in fig. 1. The dislocation lies in the (y, z) plane at an arbitrary angle α to the inward normal, the origin lies at the point where it meets the surface and the x axis is taken upwards out of the plane of the paper.

The stress field of an infinite straight dislocation so situated would contain stress components $\widehat{xz}$, $\widehat{yz}$ and $\widehat{zz}$ on the plane $z=0$. Since this plane is to be stress-free it is necessary to find the 'image' field which satisfies the elastic equations, compensates the stresses on the surface and introduces no new singularities in the region $z<0$. It is probable that singularities will be introduced in the region $z>0$.

The Burgers vector is taken in turn in the x, y and z directions with b_x, b_y and b_z denoting the magnitude of the vector in each case. A separate solution is given for each direction, and the general case, with Burgers vector in any direction, may be solved by a linear combination of these solutions.

Fig. 1

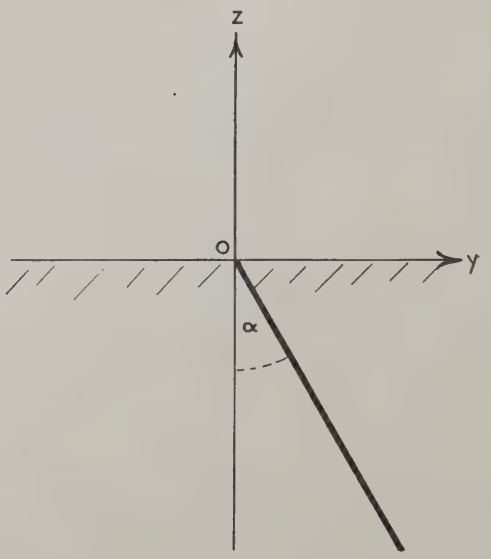

The harmonic function used in determining the ' image ' field is denoted by φ.

§ 3. Dislocation Normal to the Surface

If the dislocation meets the surface normally the angle α is zero, and at least one of the boundary conditions is automatically satisfied.

The screw dislocation gives $\widehat{zz}$ zero but shear stresses on the surface,

$$\widehat{xz} = -\frac{\mu b_z}{2\pi} \cdot \frac{y}{x^2+y^2},$$

$$\widehat{yz} = \frac{\mu b_z}{2\pi} \cdot \frac{x}{x^2+y^2}.$$

This case was solved by Eshelby and Stroh (1951) who found the ' image ' system :

$$\left.\begin{aligned} u &= \frac{b_z}{2\pi} \cdot \frac{y}{r-z}, \quad v = -\frac{b_z}{2\pi} \cdot \frac{x}{r-z}, \\ \widehat{xz} &= \frac{\mu b_z}{2\pi} \cdot \frac{y}{r(r-z)}, \quad \widehat{yz} = -\frac{\mu bz}{2\pi} \cdot \frac{x}{r(r-z)}, \end{aligned}\right\} \quad (1)$$

where $r^2 = x^2+y^2+z^2$ and μ is the shear modulus.

The edge dislocation has $\widehat{xz}$ and $\widehat{yz}$ zero with one remaining surface stress

$$\widehat{zz} = -\frac{\sigma\mu b_x}{\pi(1-\sigma)} \cdot \frac{y}{x^2+y^2} \quad \ldots\ldots (2)$$

where σ is Poisson's ratio. This case is solved by finding the harmonic function φ such that

$$\frac{\partial^2\varphi}{\partial z^2} = -\frac{\sigma\mu b_x}{\pi(1-\sigma)}\cdot\frac{y}{x^2+y^2}, \quad \text{when} \quad z=0.$$

It is related to the harmonic functions ϕ_0, ϕ_1, ϕ_2 and ϕ_3 of Neuber (1937) by the equations

$$\phi_0 = -(1-2\sigma)\varphi,$$
$$\phi_1 = 0 = \phi_2,$$
$$\phi_3 = -\frac{\partial\varphi}{\partial z},$$

and is described by Green and Zerna (1954). The solution in this case is

$$\varphi = \frac{\sigma\mu b_x}{2\pi(1-\sigma)}\left(y\log(r-z) - \frac{yz}{r-z}\right). \qquad \ldots\ldots (3)$$

The displacements of the 'image' system are then derived from φ, i.e.

$$2\mu u = z\frac{\partial^2\varphi}{\partial x\partial z} + (1-2\sigma)\frac{\partial\varphi}{\partial x}$$
$$= \frac{\sigma\mu b_x}{2\pi(1-\sigma)}\left(\frac{2xyz}{r(r-z)^2} + \frac{(1-2\sigma)xy}{(r-z)^2}\right),$$
$$2\mu v = z\frac{\partial^2\varphi}{\partial y\partial z} + (1-2\sigma)\frac{\partial\varphi}{\partial y}$$
$$= \frac{\sigma\mu b_x}{2\pi(1-\sigma)}\left((1-2\sigma)\log(r-z) - (3-2\sigma)\frac{z}{(r-z)}\right.$$
$$\left. + \frac{(3-2\sigma)y^2}{(r-z)^2} - \frac{2y^2}{r(r-z)}\right),$$
$$2\mu w = z\frac{\partial^2\varphi}{\partial z^2} - 2(1-\sigma)\frac{\partial\varphi}{\partial z}$$
$$= \frac{\sigma\mu b_x y}{\pi(1-\sigma)}\left(\frac{1}{r} + \frac{(1-2\sigma)}{r-z}\right).$$

For $z=0$ this result is in agreement with Indenborn (1959). It may be seen that the normal stress in this case is

$$\widehat{zz} = \frac{\sigma\mu b_x}{\pi(1-\sigma)}\left(\frac{y}{r(r-z)} - \frac{yz}{r^3}\right)$$

which cancels that of eqn. (2) at $z=0$. The image shear stress $\widehat{xy}$ has the surface value

$$\widehat{xy} = \frac{(1-2\sigma)\sigma\mu b_x}{2\pi(1-\sigma)}\left(\frac{x}{r^2} - \frac{2xy^2}{r^4}\right)$$

which, for $\sigma\sim\frac{1}{3}$ is equal to about 10% of the corresponding stress for a dislocation in an infinite medium.

§ 4. Oblique Dislocation, b_x

To find the stress field of a dislocation meeting the free surface obliquely it is convenient to use one of the angular dislocations described in a previous paper by the author (Yoffe 1960). This angular dislocation is composed of the original dislocation of fig. 1 and its image in the surface plane, as shown in fig. 2. The stress field of such a dislocation in an infinite

Fig. 2

elastic body is known from the previous paper and the corresponding displacements may be written down immediately:

$$
\left.
\begin{aligned}
2\mu u &= \frac{\mu b_x}{2\pi}\left(\tan^{-1}\frac{\eta}{x}-\tan^{-1}\frac{\eta'}{x}+\tan^{-1}\frac{xr\sin 2\alpha}{\eta\eta'-x^2\cos 2\alpha}\right)\\
&\quad+\frac{\mu b_x}{4\pi(1-\sigma)}\left(\frac{x\eta}{r(r-\zeta)}-\frac{x\eta'}{r(r-\zeta')}\right),\\
2\mu v &= \frac{\mu b_x}{4\pi(1-\sigma)}\left(\frac{\eta'\sin\alpha}{r-\zeta'}-\frac{\eta\sin\alpha}{r-\zeta}-\frac{y\eta'}{r(r-\zeta')}\right.\\
&\quad\left.+\frac{y\eta}{r(r-\zeta)}-(1-2\sigma)\cos\alpha\log(r-\zeta)(r-\zeta')\right),\\
2\mu w &= \frac{\mu b_x}{4\pi(1-\sigma)}\left(-\frac{\eta'\cos\alpha}{(r-\zeta')}-\frac{\eta\cos\alpha}{(r-\zeta)}-\frac{\eta' z}{r(r-\zeta')}\right.\\
&\quad\left.+\frac{\eta z}{r(r-\zeta)}+(1-2\sigma)\sin\alpha\log\frac{(r-\zeta')}{(r-\zeta)}\right),
\end{aligned}
\right\}\quad(4)
$$

where

$$\eta = y\cos\alpha - z\sin\alpha,$$
$$\zeta = y\sin\alpha + z\cos\alpha,$$
$$\eta' = -y\cos\alpha - z\sin\alpha,$$
$$\zeta' = y\sin\alpha - z\cos\alpha.$$

It is found that the shear stresses $\widehat{xz}$ and $\widehat{yz}$ derived from eqns. (4) vanish on the plane $z=0$, while $\widehat{zz}$ has the surface value:

$$\widehat{zz} = \frac{\mu b_x \cos\alpha}{2\pi(1-\sigma)}\left(\frac{2\sigma\sin\alpha}{(r-y\sin\alpha)} - \frac{y\cos^2\alpha}{(r-y\sin\alpha)^2} + \frac{(1-2\sigma)y}{r(r-y\sin\alpha)}\right). \qquad (5)$$

To remove this stress it is only necessary to find a suitable harmonic function φ such that

$$\frac{\partial^2\varphi}{\partial z^2} = \widehat{zz} \quad \text{on} \quad z=0.$$

Such a function is found to be:

$$\varphi = \frac{\mu b_x \cot\alpha}{2\pi(1-\sigma)}\left\{\zeta\log(r-\zeta) + 2(1-\sigma)r + (1-2\sigma)z\log(r-z)\right.$$
$$+ 2(1-\sigma)\cot\alpha\left[\eta\log(r-\zeta) - y\log(r-z)\right.$$
$$\left.\left. - x\left(\tan^{-1}\frac{y}{x} - \tan^{-1}\frac{\eta}{x} + \tan^{-1}\frac{xr\sin\alpha}{x^2\cos\alpha + y\eta}\right)\right]\right\}. \qquad (6)$$

A stress field is readily derived from φ as in § 3. Not all components will be written in full for reasons of space:

$$\left.\begin{aligned}
2\mu u &= z\frac{\partial^2\varphi}{\partial x\partial z} + (1-2\sigma)\frac{\partial\varphi}{\partial x} \\
&= \frac{\mu b_x\cot\alpha}{2\pi(1-\sigma)}\left\{(1-2\sigma)\frac{x}{r-\zeta} - (1-2\sigma)\frac{x}{r} + 2(1-\sigma)(1-2\sigma)\frac{x}{r-z}\right. \\
&\qquad - 2(1-\sigma)\frac{xz\cos\alpha}{r(r-\zeta)} - \frac{xz^2}{r(r-\zeta)^2} + \frac{xz\cos\alpha}{(r-\zeta)^2} \\
&\quad \left. - 2(1-\sigma)(1-2\sigma)\cot\alpha\left(\tan^{-1}\frac{y}{x} - \tan^{-1}\frac{\eta}{x} + \tan^{-1}\frac{xr\sin\alpha}{x^2\cos\alpha + y\eta}\right)\right\}, \\
2\mu v &= z\frac{\partial^2\varphi}{\partial y\partial z} + (1-2\sigma)\frac{\partial\varphi}{\partial y}, \\
2\mu w &= z\frac{\partial^2\varphi}{\partial z^2} - 2(1-\sigma)\frac{\partial\varphi}{\partial z}, \\
\widehat{xy} &= z\frac{\partial^3\varphi}{\partial x\partial y\partial z} + (1-2\sigma)\frac{\partial^2\varphi}{\partial x\partial y}, \qquad \widehat{xz} = z\frac{\partial^3\varphi}{\partial x\partial z^2}, \\
\widehat{yz} &= z\frac{\partial^3\varphi}{\partial y\partial z^2}, \qquad \widehat{zz} = z\frac{\partial^3\varphi}{\partial z^3} - \frac{\partial^2\varphi}{\partial z^2}.
\end{aligned}\right\} \qquad (7)$$

The complete stress field of the dislocation meeting the free surface is obtained from eqns. (4) and (7). It may be verified that the function φ of eqn. (6) reduces to that of (3) as $\alpha \to 0$.

§ 5. Oblique Dislocation, b_y

The dislocation with Burgers vector b_y in the y direction may be treated in a similar manner. The angular dislocation again leaves only $\widehat{zz}$ to be cancelled on the surface:

$$\widehat{zz} = \frac{\mu b_y}{2\pi(1-\sigma)} \cdot x\cos\alpha \left(\frac{\cos^2\alpha}{(r-y\sin\alpha)^2} - \frac{1-2\sigma}{r(r-y\sin\alpha)} \right). \quad . \quad . \quad (8)$$

The function φ in this case is:

$$\begin{aligned}\varphi = -\frac{\mu b_y}{2\pi(1-\sigma)} \cdot \frac{\cos\alpha}{\sin^2\alpha} \Big\{ & 2(1-\sigma)x\cos\alpha\log(r-z) \\ & -(1-2\sigma+\cos^2\alpha)x\log(r-\zeta) \\ & -(y\cos\alpha+(1-2\sigma)\eta)\left(\tan^{-1}\frac{y}{x} - \tan^{-1}\frac{\eta}{x} + \tan^{-1}\frac{xr\sin\alpha}{x^2\cos\alpha+y\eta} \right) \Big\}, \quad (9)\end{aligned}$$

which reduces to

$$\varphi = \frac{\sigma\mu b_y}{2\pi(1-\sigma)} \left(\frac{xz}{r-z} - x\log(r-z) \right)$$

when $\alpha \to 0$ for normal incidence.

The complete displacements are found by adding those of the angular dislocation to the additional 'image' terms from eqn. (9):

$$\left.\begin{aligned}
2\mu u &= \frac{\mu b_y}{4\pi(1-\sigma)}\cos\alpha \left(-\frac{x^2}{r(r-\zeta)} - \frac{x^2}{r(r-\zeta')} + (1-2\sigma)\log(r-\zeta)(r-\zeta') \right) \\
&\quad + z\frac{\partial^2\varphi}{\partial x\partial z} + (1-2\sigma)\frac{\partial\varphi}{\partial x}, \\
2\mu v &= \frac{\mu b_y}{4\pi}\left(\tan^{-1}\frac{\eta}{x} - \tan^{-1}\frac{\eta'}{x} + \tan^{-1}\frac{xr\sin 2\alpha}{\eta\eta' - x^2\cos 2\alpha} \right) \\
&\quad + \frac{\mu b_y}{4\pi(1-\sigma)}\left(\frac{\sin\alpha\cos\alpha}{r-\zeta} + \frac{\sin\alpha\cos\alpha}{r-\zeta'} - \frac{y\cos\alpha}{r(r-\zeta)} - \frac{y\cos\alpha}{r(r-\zeta')} \right) \\
&\quad + z\frac{\partial^2\varphi}{\partial y\partial z} + (1-2\sigma)\frac{\partial\varphi}{\partial y}, \\
2\mu w &= \frac{\mu b_y}{4\pi(1-\sigma)}\left(\frac{\cos^2\alpha}{r-\zeta} - \frac{\cos^2\alpha}{r-\zeta'} - \frac{z\cos\alpha}{r(r-\zeta)} - \frac{z\cos\alpha}{r(r-\zeta')} \right) \\
&\quad + z\frac{\partial^2\varphi}{\partial z^2} - 2(1-\sigma)\frac{\partial\varphi}{\partial z}.
\end{aligned}\right\} \quad . \quad . \quad . \quad (10)$$

§ 6. Oblique Dislocation, b_z

The angular dislocation of fig. 2 with Burgers vector b_z does not give zero shear stresses on the surface:

$$\left.\begin{aligned}
\widehat{xz} &= \frac{\mu b_z\cos\alpha}{2\pi(1-\sigma)}\left(\frac{x^2\sin\alpha}{r(r-y\sin\alpha)^2} - \frac{\sigma\sin\alpha}{r-y\sin\alpha} - \frac{(1-2\sigma)y}{r(r-y\sin\alpha)} \right), \\
\widehat{yz} &= \frac{\mu b_z x\cos\alpha}{2\pi(1-\sigma)}\left(\frac{y\sin\alpha}{r(r-y\sin\alpha)^2} - \frac{\sin^2\alpha}{(r-y\sin\alpha)^2} + \frac{(1-\sigma)}{r(r-y\sin\alpha)} \right), \\
\widehat{zz} &= 0,
\end{aligned}\right\} \quad (11)$$

on $z=0$. These stresses could be compensated by an 'image' system derived from another harmonic function, ψ say, if ψ can be found such that

$$\frac{\partial^2\psi}{\partial x\partial z}=\widehat{xz},$$

$$\frac{\partial^2\psi}{\partial y\partial z}=\widehat{yz},$$

on $z=0$. The displacement would then be given by

$$2\mu u=\frac{\partial}{\partial x}\left(z\frac{\partial\psi}{\partial z}+2(1-\sigma)\psi\right),$$

$$2\mu v=\frac{\partial}{\partial y}\left(z\frac{\partial\psi}{\partial z}+2(1-\sigma)\psi\right),$$

$$2\mu w=\frac{\partial}{\partial z}\left(z\frac{\partial\psi}{\partial z}-2(1-\sigma)\psi\right).$$

Fig. 3

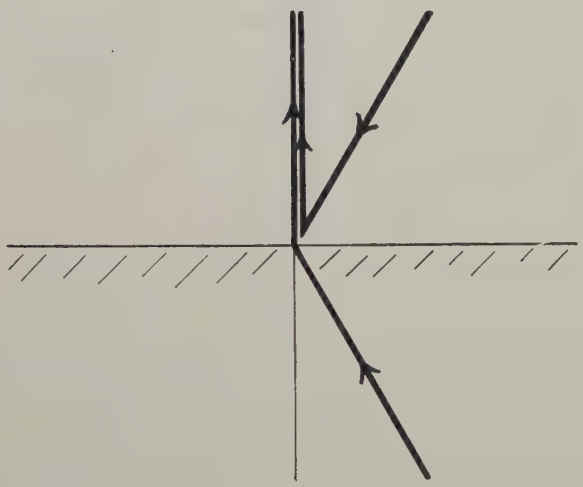

However, in this case a more direct method is to arrange two angular dislocations as in fig. 3, thereby reversing the sign of the image. The surface stresses are then given by

$$\left.\begin{aligned}\widehat{xz}&=-\frac{\mu b_z}{2\pi}\cdot\frac{y}{r^2},\\ \widehat{yz}&=\frac{\mu b_z}{2\pi}\cdot\frac{x}{r^2},\\ \widehat{zz}&=\frac{\mu b_z}{2\pi(1-\sigma)}\cdot x\sin\alpha\left(\frac{1}{r(r-y\sin\alpha)}+\frac{\cos^2\alpha}{(r-y\sin\alpha)^2}\right).\end{aligned}\right\}\quad(12)$$

The shear stresses are simply those of the normal screw dislocation in § 3 and may be cancelled by Eshelby and Stroh's solution. The direct stress

$\widehat{zz}$ is removed by the same procedure as before. The function φ is found to be

$$\varphi = \frac{\mu b_z}{2\pi(1-\sigma)}\left\{-x\sin\alpha\log(r-\zeta)+z \times\left(\tan^{-1}\frac{y}{x}-\tan^{-1}\frac{\eta}{x}+\tan^{-1}\frac{xr\sin\alpha}{x^2\cos\alpha+y\eta}\right)\right\}. \quad (13)$$

In this case φ itself vanishes as $\alpha\to 0$.

The complete solution is composed of terms derived from (13), from the two angular dislocations, and from Eshelby and Stroh's solution (1):

$$2\mu u = \frac{\mu b_z\sin\alpha}{4\pi(1-\sigma)}\left((1-2\sigma)\log(r-\zeta)(r-\zeta')-\frac{x^2}{r(r-\zeta)}-\frac{x^2}{r(r-\zeta')}\right) + \frac{\mu b_z y}{\pi(r-z)}+z\frac{\partial^2\varphi}{\partial x\partial z}+(1-2\sigma)\frac{\partial\varphi}{\partial x},$$

$$2\mu v = \frac{\mu b_z x\sin\alpha}{4\pi(1-\sigma)}\left(\frac{\sin\alpha}{r-\zeta}+\frac{\sin\alpha}{r-\zeta'}-\frac{y}{r(r-\zeta)}-\frac{y}{r(r-\zeta')}\right) - \frac{\mu b_z x}{\pi(r-z)}+z\frac{\partial^2\varphi}{\partial y\partial z}+(1-2\sigma)\frac{\partial\varphi}{\partial y},$$

$$2\mu w = \frac{\mu b_z}{2\pi}\left(\tan^{-1}\frac{\eta}{x}-\tan^{-1}\frac{\eta'}{x}+\tan^{-1}\frac{xr\sin 2\alpha}{\eta\eta'-x^2\cos 2\alpha}\right) + \frac{\mu b_z x\sin\alpha}{4\pi(1-\sigma)}\left(\frac{\cos\alpha}{r-\zeta}-\frac{\cos\alpha}{r-\zeta'}-\frac{z}{r(r-\zeta)}-\frac{z}{r(r-\zeta')}\right) + z\frac{\partial^2\varphi}{\partial z^2}-2(1-\sigma)\frac{\partial\varphi}{\partial z}.$$

§ 7. Conclusion

The expressions for the stress field of a dislocation meeting a free surface at any angle show that the 'image' system is quite simple in form. It consists of the image of the original dislocation, and a few additional elastic singularities distributed either on the image or on the outward normal from the point of incidence. It should not be impossible therefore to repeat the process and attempt to estimate the effect of a second free surface parallel to the first. This question requires further work and will not be answered here.

From casual inspection it seems unlikely that the dislocation would remain straight in all cases. In particular the straight form may sometimes be in unstable equilibrium with a tendency to bow out in the slip plane, in an attempt to lie along its image. The forces acting on the dislocation near the free surface must be calculated in each case.

Acknowledgments

The author wishes to thank Dr. P. B. Hirsch for his interest and encouragement, Dr. F. Kroupa and Professor F. R. N. Nabarro for reading the manuscript and Dr. J. Eshelby for several references and for his very

helpful criticism. Part of this work was done while in receipt of a grant from the Atomic Energy Research Establishment, Harwell.

References

Eshelby, J. D., and Stroh, A. N., 1951, *Phil. Mag.*, **42**, 1401.
Green, A. E., and Zerna, W., 1954, *Theoretical Elasticity* (Oxford), § 5.7.
Head, A. K., 1953, *Proc. phys. Soc., Lond.* B, **66**, 793.
Indenborn, V. L., 1959, *Dokl. Nauk. S.S.S.R.*, **128**, 906.
Neuber, H., 1937, *Kerbspannungslehre* (Berlin: Springer).
Steketee, J. A., 1958, *Canad. J. Phys.*, **36**, 192.
Yoffe, E. H., 1960, *Phil. Mag.*, **5**, 161.

Erratum. The author wishes to correct a misprint in the previous paper (Yoffe 1960).

The second of eqns. (3) should be:

$$\widehat{xz} = \frac{\mu b_x}{4\pi(1-\sigma)}\left(\frac{y}{r^3} + \frac{\sin\alpha}{r(r-\zeta)} - \frac{\eta\cos\alpha}{r(r-\zeta)^2} + \ldots, \quad \text{etc.}\right).$$

Mobility of Vacancy Pairs in Ionic Crystals

By K. Tharmalingam† and A. B. Lidiard‡
Department of Physics, The University, Reading, Berkshire

[Received February 13, 1961]

Abstract

Calculations have been made of activation energies for vacancy pair movements in NaCl and KCl using the approximation of a static lattice. The numerical results indicate that these energies are comparable with or greater than the activation energies for single vacancy movement. Qualitative reasons are given showing why this should be so.

The classical Born theory of ionic crystals as developed by Mott and Littleton (1938) for lattice imperfections has been used recently by Guccione *et al.* (1959) to discuss the activation energies for ionic movements into single vacancies in NaCl and KCl. It was found that observed activation energies for single vacancy movement are accurately reproduced by the theory provided that the closed-shell interactions between ions are represented by the 'Born–Mayer–Verwey' potential. This potential, of the form $A + Br^{-12}$ for interionic separations r less than the equilibrium anion–cation separation, had previously been proposed by Verwey (1946); it had been shown earlier by Verwey and de Boer (1940) to lead to a good account of the interionic distances in free molecules. Calculated activation energies were not in agreement with experiment when the 'Born–Mayer' repulsion potential was assumed, although this potential is well known to account for the low pressure compressibilities of ionic crystals. This is not surprising since the distances of approach of ions in the activated state are close to those in the molecule and much less than the normal interionic spacing in the crystal (figure).

It is evident that a substantial part of the activation energy for single vacancy movement is made up of the closed-shell repulsion between the moving ion and its two close neighbours in the activated state (ions a, b in the figure (A)). It has therefore often been assumed that the activation energies for ionic movements into a *vacancy pair* should be less than the corresponding quantities for single vacancies (figure (C)). This idea has been supported by a direct calculation for the Cl^- jump into a vacancy pair in KCl by Dienes (1948) who obtained the value 0·38 ev. The concept of mobile vacancy pairs has found favour in the rationalization of the processes of colour centre aggregation and the annealing of radiation damage (Seitz 1946, 1954). However, their direct appearance in diffusion studies has

† Now at School of Engineering, Princeton University, Princeton, N.J., U.S.A.
‡ Now at Theoretical Physics Division, A.E.R.E., Harwell, Berkshire.

remained unconfirmed until recently (Schamp and Katz 1954, Laurance 1960). Laurance studied the tracer diffusion of Cl^- in NaCl containing variable additions of $CaCl_2$ and did find a contribution which could be assigned to vacancy pairs. This contribution was governed by a total

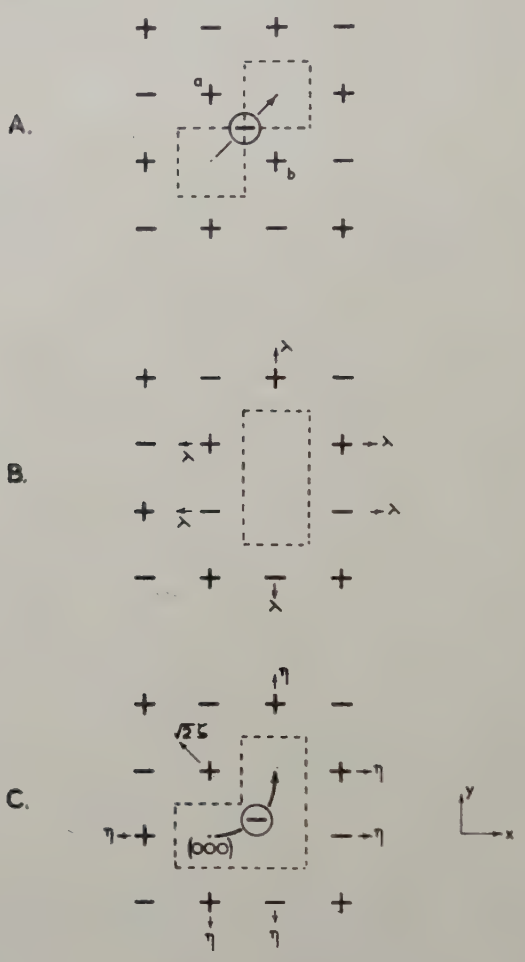

A. The activated state for a negative ion jumping into a single vacancy. B. The ground state of the vacancy pair, showing assumed relaxation of neighbours. C. The activated state showing the assumed relaxation of neighbours.

activation energy of 2·49 ev. Similar inferences have been made by Barr and Morrison (1960) from results obtained with NaCl containing $CdCl_2$ additions. Now, theoretical estimates† of the energy of formation

† Tosi and Fumi (1958). An earlier calculation for NaCl was made by Reitz and Gammel and a more recent calculation has been made on a different basis by Johnson and Parker (1960).

of vacancy pairs, E_f, using the Born–Mayer potential yield the values 1·3–1·4 ev. Hence Laurance inferred that the energy of movement is about 1·1–1·2 ev, i.e. as large as for the Cl^- jump into the single vacancy.

On account of this conflict with the intuitive idea that vacancy pairs are highly mobile we have re-examined this question theoretically. Firstly we noted that the previous calculation by Dienes used the Born–Mayer form for the closed-shell repulsions and that this form was too soft to

Activation energies ΔE for ionic movements into vacancy pairs compared with the values for single vacancies computed by Guccione *et al.* (in brackets). The calculation of ΔE has been performed at intervals of ξ of 0·02 and the components of ΔE refer to the value of ξ closest to the minimum; the values of these components are therefore approximate since although the minimum in ΔE is shallow the components vary more rapidly with ξ. For the first four entries the Born–Mayer–Verwey potential has been used to represent closed-shell interactions. The corresponding values for the energies of formation of vacancy pairs are $E_f = 1{\cdot}27$ ev (NaCl) and 1·28 ev (KCl). For the fifth entry the Born–Mayer form has been used with constants proposed recently by Tosi and Fumi: this potential is less hard than the Born–Mayer–Verwey potential and gives an energy of formation $E_f = 1{\cdot}24$ ev. For the sixth entry the Born–Mayer potential used by Dienes (1948) has been employed; this is the softest of the three potentials and gives $E_f = 1{\cdot}19$ ev. We believe the results predicted by the Born–Mayer–Verwey model to be the more reliable.

Moving ion	ΔE (ev)	ΔE_c (ev)	ΔE_R (ev)	ΔE_p (ev)	Dipole correction
Na^+ in NaCl	1·46 (0·87)	1·46 (−1·32)	−0·02 (1·83)	0·02 (0·36)	0·00
Cl^- in NaCl	1·27 (1·11)	1·67 (−1·60)	0·24 (2·29)	−0·87 (0·42)	0·23
K^+ in KCl	1·30 (1·13)	1·73 (−1·17)	−0·24 (1·92)	−0·21 (0·38)	0·02
Cl^- in KCl	1·15 (1·18)	1·70 (−1·38)	−0·07 (2·16)	−0·60 (0·40)	0·12
Cl^- in KCl	0·91	1·52	−0·03	−0·66	0·06
Cl^- in KCl	0·89 (0·64)	1·25 (−1·49)	0·28 (1·75)	−0·65 (0·38)	0·02

account for the observed activation energies for single vacancy movement. Initially therefore we carried through the calculations using the harder Born–Mayer–Verwey potential, but for comparison we have repeated them using the Born–Mayer form. The activation energies have been calculated by finding the difference in energy of the activated configuration (figure (C)) and the ground configuration (figure (B)). All 10 neighbours of the two vacancies in the ground configuration have been allowed to relax outwards by an amount λ which has been determined by minimizing the energy of the crystal. Similarly the neighbours of the three vacancies present in the activated complex have been relaxed outwards by an amount η, except for the ion at (010) which has been relaxed by an amount $\sqrt{2}\zeta$ in the direction $(-1, +1, 0)$, i.e. to the point $(-\zeta, 1+\zeta, 0)$. The position of the moving ion in the activated complex has been taken as $(\frac{1}{2}+\xi, \frac{1}{2}-\xi, 0)$. The energy of the crystal in this activated configuration has been minimized with respect to η, ζ for a range of values of ξ. The value of ξ requiring the lowest activation energy was then found; the minimum so obtained was rather shallow. As in previous calculations of this kind the energy is regarded as being composed of Coulomb interactions (monopole–monopole), E_C, closed-shell repulsions, E_R, and polarization terms. These latter include the self-energies of polarization of the ions together with monopole–dipole and dipole–dipole interactions. In the present calculations we are interested in the difference between the polarization energy of the activated state and of the ground state. The most important part of this is the energy of polarization of the moving ion and the neighbours to the vacancy complex in the monopole fields acting on them. Accordingly a polarization energy $E_p = -\frac{1}{2}\sum_i \alpha_i \boldsymbol{F}_i^2$, in which α_i is the polarizability ion i (Tessman *et al.* 1953) and $\boldsymbol{F}_i$ is the monopole field acting on it, has been included in the energy minimization programmes. A correction for dipole interactions is made after the relaxed configuration has been determined; this correction is small.

The results of these calculations are given in the table. Several points emerge.

(i) ΔE for a jump into a vacancy pair is *greater than* or close to ΔE for a jump into a single vacancy.

(ii) The contribution to ΔE from the closed-shell repulsions ΔE_R, is relatively unimportant for the vacancy pair; as expected however it is larger for the large anions than for the cations.

(iii) The Coulomb contribution ΔE_C to ΔE is positive for the vacancy pair although it is negative for single vacancies; this is due to the absence of one of the two barrier ions, a and b, which exert a strong Coulomb attraction on the ion moving into the single vacancy.

(iv) The moving ion is under the influence of a large electric field in the activated state and the associated polarization energy is an important part of the total. Since the anions are more polarizable than the cations the activation energies for anions are less: this contrasts with single vacancy movement.

(v) Tracer diffusion via vacancy pairs will be limited by the less frequent of the two jumps. We must therefore compare the experimental value of 1·1–1·2 ev for Cl^- diffusion in NaCl with the higher of the two values obtained for NaCl, i.e. 1·46 ev, which actually governs the Na^+ jump into the pair. Theory agrees with experiment that the pair is not highly mobile and the quantitative agreement is fair. We have evaluated the formation energy of vacancy pairs in our model and for this we obtained 1·27 ev which is only slightly less than the 1·3–1·4 ev used above. The total activation energy for Cl^- diffusion is then predicted to be 2·73 ev; the difference from the experimental value of 2·49 ev is perhaps within the combined error of the experiments and the theory.

(vi) A repetition of our calculations for Cl^- in KCl using the Born–Mayer potential employed by Dienes gives $\Delta E = 0{\cdot}89$ ev. The composition of this quantity shows the same features (i)–(iv) as the Born–Mayer–Verwey potential. A value of $\Delta E = 0{\cdot}91$ ev was obtained using a recently proposed modification of the Born–Mayer constants which gave a potential of intermediate hardness (Tosi and Fumi 1961). The effect of increasing the hardness of the potential is to push the saddle point of the moving ion out to larger ξ into a region of unfavourable Madelung potential and this increases the Coulomb contribution to ΔE at the expense of ΔE_R (table).

(vii) It is difficult to analyse the disagreement of these results with those of Dienes since the two calculations were carried out differently. The energy of ground-state relaxation which we obtain agrees with that of Tosi and Fumi (1958) and disagrees with Dienes. A correction for this fact would however make Dienes' predicted activation energy about zero. We also find a disagreement with his value for the polarization energy of the moving ion (his E_p'' for the rigid lattice). A correction here of about 0·7 ev seems necessary and is then such as to bring the results more into line with our own.

(viii) In conclusion, it seems clear that the mobility of vacancy pairs in alkali halides is less than or comparable with that of single vacancies. This implies a revision of the theories of colour centre aggregation at low temperature.

Acknowledgments

We wish to acknowledge the benefit of correspondence and discussion with Professor Maurer, Drs. Laurance, Fumi, Tosi, Morrison, Barr, Dienes and Johnson. One of us (K.T.) wishes to acknowledge a research grant from A.E.R.E., Harwell, who also made their Mercury computer available to us.

References

Barr, L. W., and Morrison, J. A., 1960, paper presented at N.A.S.A. Symposium on Diffusion in Solids held at Cleveland, Ohio, in October 1960.

Dienes, G. J., 1948, *J. chem. Phys.*, **16**, 620.

Guccione, R., Tosi, M. P., and Asdente, M., 1959, *J. Phys. Chem. Solids*, **10**, 162.

Johnson, C. A., and Parker, E. R., 1960, *Univ. Calif. Tech. Rep.* AFOSR–TN–60–979.
Laurance, N., 1960, *Phys. Rev.*, **120,** 57.
Mott, N. F., and Littleton, M. J., 1938, *Trans. Faraday Soc.*, **34,** 485.
Reitz, J. R., and Gammel, J. L., 1951, *J. chem. Phys.*, **19,** 894.
Schamp, H. W., and Katz, E., 1954, *Phys. Rev.*, **94,** 828.
Seitz, F., 1946, *Rev. mod. Phys.*, **18,** 384; 1954, *Ibid.*, **26,** 7.
Tessman, J. R., Kahn, A. H., and Shockley, W., 1953, *Phys. Rev.*, **92,** 890.
Tosi, M. P., and Fumi, F. G., 1958, *Nuovo Cim.*, **7,** 95; 1961, *Crystal Radii of the Alkali and Halogen Ions in the Alkali Halides* (to be published).
Verwey, E. W. J., 1946, *Rec. Trav. chim. Pays-Bas*, **65,** 521.
Verwey, E. W. J., and de Boer, J. H., 1940, *Rec. Trav. chim. Pays-Bas*, **59,** 633.

Two-phonon Infra-red Lattice Absorption in Diamond

By J. R. Hardy and S. D. Smith
J. J. Thomson Physical Laboratory, University of Reading, England

[Received February 22, 1961]

Abstract

The specimen independent infra-red absorption spectrum of diamond in the 2 μ to 6 μ region has been examined using a grating spectrometer. The results have been analysed in terms of multi-phonon processes. In particular the two-phonon absorption has been examined in detail in an attempt to deduce phonon energies for the various branches of the frequency spectrum at symmetry points in the reduced zone. Sets of lattice wave dispersion curves have been constructed from these results and are very unlike those for silicon and germanium.

§ 1. Introduction

There has recently been a considerable revival of interest in the lattice dynamics of diamond structure crystals. This was mainly stimulated by the work of Brockhouse and Iyengar (1958) who used inelastic neutron scattering techniques to determine directly the frequency (ω) wave vector ($\mathbf{q}$) dispersion relations for the plane wave normal modes of germanium. They obtained complete sets of dispersion curves only for the $\langle 100 \rangle$ and $\langle 111 \rangle$ symmetry directions, but these were sufficient to demonstrate conclusively that the interatomic forces in this crystal contained an important long-range component.

An analysis by Herman (1959) showed that one must include interactions between atoms at least as far apart as fifth neighbours to fit these results, and Cochran (1959) developed a theoretical model which demonstrated how such interactions could arise from coupling between dipole moments induced on the atoms when the lattice is distorted by a plane wave. Subsequently Brockhouse (1959) determined the dispersion curves for lattice waves propagating along a $\langle 100 \rangle$ direction in silicon. These proved to be very similar to those for germanium, and Cochran (1960, private communication) has shown that his model can be used to fit the silicon data.

It is evident that any completely satisfactory theory must reproduce the corresponding (ω vs. $\mathbf{q}$) dispersion curves for lattice waves in diamond itself. Unfortunately neutron scattering work is not at present possible owing to the large size of the crystal required, thus the actual dispersion curves are unknown for this crystal. One possible source of such

information was suggested to us by the work of Johnson (1959) on the infra-red lattice absorption bands of silicon. This was based on the theory of Lax and Burstein (1955) who showed that, although the direct absorption of radiation as single quanta of lattice vibrational energy (phonons) is forbidden, it may take place in processes involving the creation of two or more phonons. Using this theory he was able to fit the energies of all the peaks in his absorption curves using combinations of only four distinct phonon energies which he designated: transverse optical (T.O.), longitudinal optical (L.O.), longitudinal acoustic (L.A.), and transverse acoustic (T.A.). He argued that these energies were those at which the maximum density of modes occurred in each branch of the frequency spectrum which in turn would be expected to correspond to phonon wave vectors in the region of the surface of the reduced zone. Comparison with the neutron scattering data indicates that this argument is valid. Strictly there should be two T.O. and two T.A. energies since the two-fold degeneracy of these branches is only present for directions of high symmetry, but failure to resolve these implies that for most $\mathbf{q}$ vectors this splitting is not large. Thus it seemed that a similar analysis of the infra-red lattice absorption in diamond would provide corresponding information which, together with the known Raman energy (corresponding to $\omega_{TO}=\omega_{LO}$ at $\mathbf{q}=0$) and elastic constants (McSkimin and Bond 1957), could be used to construct a set of dispersion curves. It was evident that earlier data (see Lax and Burstein 1955) were much too imprecise to be interpreted in this way with any degree of certainty and a new set of measurements was therefore undertaken. These were carried out at room temperature and no attempt was made to measure the variation of absorption with temperature since Collins and Fan (1954) have shown this to be small (a consequence of the high Debye Temperature) and therefore not likely to help in assigning the various peaks unless one is prepared to use very high temperatures where one will encounter difficulties arising from the onset of graphitization of the specimen.

§ 2. Experimental

Absorption measurements were made in the wavelength range $2\,\mu$ to $6\,\mu$ on a 7500 lines per inch grating spectrometer with a Golay cell detector. No predispersing system was used; instead, second-order spectra were suppressed by a series of anti-reflected semi-conductor filters; germanium, lead sulphide and indium arsenide were used in the ranges 1·8–3·0, 3·0–3·8 and 3·8–6 μ respectively. The filters show good transparency above their absorption edges (80% transmission) and very strong rejection below, thus stray light was negligible. Two diamonds with good optical surfaces were measured—one Type I and one Type II a —giving identical results within experimental error. Reflection corrections were checked by measurements above the three-phonon cut-off (0·495 ev) where absorption in both specimens was negligible. Absorption

coefficients were calculated, correcting for multiple reflections, from:

$$T = \frac{(1-R)^2 \exp(-Kd)}{1-R^2 \exp(-2Kd)}$$

where K denotes the absorption coefficient, T the transmission, R the reflectivity, and d the specimen thickness.

§ 3. Analysis of the Results (First Stage)

The absorption spectrum is shown in fig. 1 and can be divided into two regions: (*a*) the relatively strong bands lying below 0·330 ev, with a sharp cut-off at this energy, and (*b*) the weaker, more diffuse bands

Fig. 1

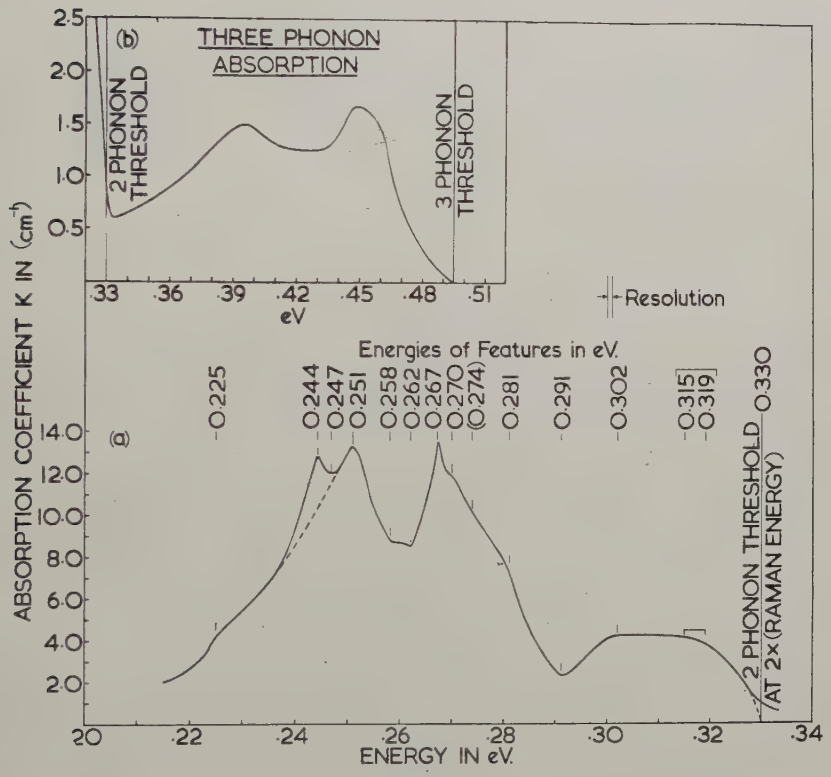

Infra-red lattice absorption of diamond. (The broken line on (*a*) indicates how the 0·251 ev peak and the 0·225 ev kink may be associated with the same absorption process.)

above this energy with a rather less well-defined high-energy cut-off at 0·495 ev. Since the known Raman energy is 0·165 ev this provides conclusive evidence that the maximum lattice frequency is that of optical

modes at $\mathbf{q}=0$ and that regions (*a*) and (*b*) are due to two- and three-phonon processes respectively, the first commencing at exactly $2\times 0{\cdot}165$ ev and the second at $3\times 0{\cdot}165$ ev. The sharp cut-off of the two-phonon absorption is particularly striking.

We shall confine our analysis to the two-phonon region since the broad three-phonon peaks are difficult to assign unambiguously. Furthermore, we shall assume that all bands are combination bands; i.e., $\hbar\omega=\hbar(\omega_1+\omega_2)$ where $\hbar\omega$ is the energy of the observed peak and $\hbar\omega_1$ and $\hbar\omega_2$ are the characteristic phonon energies involved. This is justified since (see Johnson 1959) difference bands ($\hbar\omega=\hbar(\omega_1-\omega_2)$ have essentially zero intensity when $\hbar\omega_1$ and $\hbar\omega_2\gg KT$, as is the case for diamond at room temperature.

Table 1

Observed energy of feature in ev	Assignment and phonon energies in ev	Calculated energy in ev
0·319–0·315 (shoulder)	2 T.O. $2\times(0{\cdot}158)$	0·316
0·302 (peak)	T.O. +L.O. 0·158 +0·144	0·302
0·281 (shoulder)	T.O. +L.A. 0·158 +0·123	0·281
0·267 (peak)	L.O. +L.A. 0·144 +0·123	0·267
0·251 (peak)	T.O. +T.A. 0·158 +0·093	0·251
0·244 (peak)	L.O. +T.A. 0·144 +0·093	0·237

Two-phonon cut-off at
0·330 ev $=2\times 0{\cdot}165$ ev: or twice the Raman energy.

The energies of the various features are shown on fig. 1 and in table 1 the energies of the main peaks are compared with those obtained by adding the following four energies in appropriate pairs:

T.O. $=0{\cdot}158$ ev, L.O. $=0{\cdot}144$ ev,

L.A. $=0{\cdot}123$ ev, and T.A. $=0{\cdot}092$ ev.

It will be observed that our assignment is similar to that made by Johnson (1959) for silicon. There is no clearly defined 2 T.O. peak, although the absorption curve exhibits a change of slope between 0·315

and 0·318 ev in the region of the 2T.O. energy (0·316 ev). This is not surprising since the T.O. energy is close to the Raman energy and the T.O. branches thus show little dispersion and consequently the selection rule (Lax and Burstein 1955), forbidding combinations of two degenerate branches, will ensure that the 2T.O. band is weak. Furthermore the T.O. + L.A. band at 0·281 ev is so close to the 0·267 ev L.O. + L.A. band that it appears only as a shoulder on the high-frequency side of the latter. The most striking difference is the absence of the very strong T.O. + T.A. peak present in the silicon spectrum. The analogous peak for diamond at 0·251 ev is relatively weak and this fact provides a strong indication that the distribution of T.A. modes in diamond differs drastically from that in silicon, being considerably more diffuse.

From table 1 it can be seen that we have used four energies to fit six features and have encountered the same difficulty as Johnson in that we are unable to deduce a T.A. energy which will fit both the 0·251 and 0·244 ev peaks if we use the T.O. and L.O. energies determined from the other features. Also, since the distribution of T.A. modes is believed to be more diffuse, we expect a marked variation of the frequencies of the T.A. branches over the surface of the reduced zone and it is not clear from which regions the modes responsible for the T.O. + T.A. and L.O. + T.A. peaks come.

§ 4. Analysis (Second Stage)

Because of these problems, and also in the hope of establishing the other assignments more firmly, we have carried out the following more detailed analysis which is an extension of Johnson's method and is aimed at associating specific features with specific symmetry points at the surface of the reduced zone. That this should be possible can be seen by considering eqn. (5.19) of Lax and Burstein (1955). This states that the absorption coefficient $K(\omega)$ at a frequency ω in the two phonon summation band at absolute zero is given by:

$$K(\omega) \propto \sum_{\mathbf{q}tt'} \frac{|H_{tt'}{}^{\mathbf{q}}|^2}{\omega_t(\mathbf{q})\omega_{t'}(-\mathbf{q})} \delta[\omega-\omega_t(\mathbf{q})-\omega_{t'}(-\mathbf{q})] \quad . \quad . \quad . \quad (1)$$

where $H_{tt'}{}^{\mathbf{q}}$ is a matrix element which couples modes of wave vectors $\mathbf{q}$ and $-\mathbf{q}$ from branches t and t' (assuming the wave vector of the incident *photon* is zero) and $H_{tt'}{}^{\mathbf{q}}=0$ if $t=t'$. Van Hove (1953) has shown that the distribution function of normal modes $\rho(\omega)$, which for a three-dimensional lattice is given by:

$$\rho(\omega)=\sum_t \rho_t(\omega) \propto \sum_t \int_{S_t(\omega)} \frac{dS_t}{|\nabla_{\mathbf{q}}\omega_t(\mathbf{q})|} \quad . \quad . \quad . \quad . \quad . \quad (2)$$

(where the integrations are over surfaces S_t in the reduced zone for which $\omega_t(\mathbf{q})=\omega$), has a discontinuous first derivative whenever $|\nabla_{\mathbf{q}}\omega_t(\mathbf{q})|=0$. These points are known as critical points (c.p.).

If we consider eqns. (1) and (2), the contribution to $K(\omega)$, $\Delta K(\omega)$ from a c.p. at $\mathbf{q}$ in branch t when $\omega = \omega_t(\mathbf{q}) + \omega_{t'}(-\mathbf{q})$ is given by:

$$\Delta K(\omega)d\omega \propto \frac{|H_{tt'}{}^{\mathbf{q}}|^2}{\omega_t(\mathbf{q})\omega_{t'}(-\mathbf{q})} \int_{S\omega(\mathbf{q})} \frac{dS_t}{|\nabla_{\mathbf{q}}\omega_t(\mathbf{q})|} d\omega$$

or

$$\Delta K(\omega) \propto \frac{|H_{tt'}{}^{\mathbf{q}}|^2}{\omega_t(\mathbf{q})\omega_{t'}(-\mathbf{q})} \rho_t[\omega(\mathbf{q})]$$

with a similar contribution from any singularity in the branch t' at $-\mathbf{q}$. Since there is no reason to believe that $(\partial/\partial\omega)|H_{tt'}{}^{\mathbf{q}}|^2$ is discontinuous we see that each c.p. is associated with a kink in the absorption curve. These kinks do not necessarily coincide with absorption maxima and, in practice, they will tend to be smoothed to some extent. Phillips (1956, 1959) has shown how the minimum number of c.p. implied by symmetry may be located for a given lattice and in table 1 of the (1959) article has listed the minimal set for germanium. With the exception of the T.A. c.p. at the point Σ close to the zone surface in the [110] direction, these must all be present for diamond. The c.p. at Σ are only present because both T.A. energies there are assumed to be about twice that at X, the centre of the (100) zone face, which is equivalent to a point lying outside the reduced zone along the [110] direction. This implies that $|\nabla_{\mathbf{q}}\omega_t(\mathbf{q})|$ will vanish for both branches at some point along this direction. For diamond such c.p. may well be absent from one or both T.A. branches. We shall assume that the *only* c.p. present are those implied by symmetry, an assumption which the (1959) article indicates to be valid for all diamond structure crystals. Thus we see, from table 1 of this reference, that all branches have c.p. at the origin Γ, the centre of the (111) zone face L, the centre of the (100) zone face X, and the $(1\frac{1}{2}0)$ zone corner W. The longitudinal branches are degenerate at the last two points, the transverse branches are two-fold degenerate at all c.p., and the optical and acoustic modes are separately degenerate at $\mathbf{q}=0$, the former at the Raman frequency and the latter at $\omega=0$. For the present we do not know whether there are any T.A. (Σ) singularities or not.

In table 1 it now appears reasonable to assign the T.O.+L.O., T.O.+L.A., and L.O.+L.A. features to singularities associated with c.p. at L. Combinations involving two longitudinal modes from W or X are forbidden by the degeneracy at these points. Consequently we would expect the absorption curve to show dips in the regions of twice the L.(W) and L.(X) energies which probably correspond to those observed at 0·270 ev and 0·262 ev. It is significant that the latter lies at twice 0·131 ev where there is a pronounced minimum in the defect activated single-phonon absorption (Smith and Hardy 1960) indicating a similar minimum in the density of longitudinal modes which should produce a 0·262 ev minimum in the two-phonon absorption. It seems probable that this corresponds to $2\hbar\omega$L.(W) as $|\mathbf{q}|$ is larger for this point. The

0·270 ev dip thus lies close to $2\hbar\omega$L.(X), but, as the modes are degenerate for all **q**'s of the form $(1, q, 0)$ $|q| \leqslant \frac{1}{2}$, one cannot say that this dip defines this energy precisely. However, it is unlikely to be more than 2 or 3% greater than 0·270 ev.

To analyse the T.O. + T.A. and L.O. + T.A. peaks we use Phillips' (1959) analysis of the diamond specific heat data of Desnoyers and Morrison (1958) which indicates that the T.A. mode energy for the c.p. at L is 0·063 ev. It is at once evident that the absorption peaks involving T.A. modes cannot be associated with the T.O.(L) + T.A.(L) and L.O.(L) + L.A.(L) energies which are 0·221 ev and 0·206 ev respectively, as the first of these lies close to the kink observed at 0·225 ev and the second is outside the range of our measurements. However, the presence of the 0·225 ev feature does provide additional confirmation of the value of the T.O.(L) energy used previously and of the T.A.(L) energy derived by Phillips.

Our main object now is to deduce the T.O. and T.A. energies at X and, if possible, at W, bearing in mind the fact that there may also be a T.A. c.p. at Σ. There are three features which we can use for this purpose: the sharp peak at 0·244 ev, the peak at 0·251 ev, and the kink at 0·258 ev. Two possible assignments are shown in table 2. In both cases the T.A. c.p. at X has been associated with the 0·258 ev kink and the 0·244 ev peak. The T.O. (X) energy has been assigned the maximum value consistent with that of 0·139 ev for the energy of the degenerate L.(X) modes. This last value is consistent with the condition $2\hbar\omega$L.(X) > 0·270 ev derived earlier and is favoured by the distinctive features at this energy in imperfection activated single-phonon absorption (Smith and Hardy 1960). The T.O. (X) and T.O. (L) energies are now consistent with the somewhat greater dispersion of these modes along ⟨100⟩ as compared with ⟨111⟩ directions, which is characteristic of theoretical force constant models of the diamond structure (Herman 1959). We cannot really decide in favour of either 2 (*a*) or 2 (*b*) on the basis of the present evidence. The former appears consistent, and the value of $\hbar\omega$(W) chosen for the T.O. modes is further supported by the fact that the T.O.(W) + L.(W) energy lies at 0·289 ev, close to the absorption minimum at about 0·290 ev, and one may thus see this feature as reflecting the minimum in the density of longitudinal modes believed to lie at 0·131 ev. Unfortunately there is one serious drawback; for the T.A. modes $\hbar\omega$(W) < $\hbar\omega$(X) which is implausible as $|\mathbf{q}(\mathrm{W})| > |\mathbf{q}(\mathrm{X})|$. It is this fact which leads us to favour the assignment 2*b*. This has been made using the same values for the T.O. and T.A. mode energies at Σ and W, an assumption supported by Phillips' (1959) work, and the same energy (0·158 ev) for the T.O. (Σ, W) modes as that used in assignment 2*a*. The T.A.(Σ, W) mode energy is then chosen so that the L.(Σ, W) + T.A.(Σ, W) combination lies at 0·247 ev and can be identified with the commencement of the 0·244 ev peak. The 0·225 ev kink is now unambiguously associated with the T.O.(L) + T.A.(L)

energy, and the T.A.(W)+T.O.(W) process now lies at about 0·274 ev in which region there is some slight evidence of a kink. (The 0·247 ev minimum, which appears as part of this assignment, is also to be expected on the grounds that the 2 L.A. combination is forbidden everywhere in the reduced zone and, in particular, for the 2 L.A.(L) energy or 0·246 ev.)

Table 2

(*a*) Feature (energy in ev)	Assignment and phonon energies in ev	Calculated energy in ev
0·258 (Kink)	T.O.(X)+T.A.(X) 0·153+0·105	0·258
0·251 (Peak)	T.O.(W)+T.A.(W) 0·158 +0·093	0·251
0·244 (Peak)	L.(X) +T.A.(X) 0·139 +0·105	0·244
0·225 (Kink)	L.(W) +T.A.(W) 0·131 +0·093	0·224
	or	
	T.O.(L) +T.A.(L) 0·158 +0·063	0·221
	No T.A.(Σ) c.p.	
(*b*) 0·258 (Kink)	T.O.(X) +T.A.(X) 0·153 +0·105	0·258
0·251 (Peak)	(not associated with c.p.)	
0·244 (Peak)	L.(X) +T.A.(X) 0·139 +0·105	0·244
0·247 (Minimum)	L.(W) +T.A.(W) 0·131 +0·116	0·247
(0·274 Kink ?)	T.O.(W) +T.A.(W) 0·158 +0·116	0·274

Both these last assignments are uncertain. The corresponding T.A.(Σ) singularities probably occur at almost the same energies.

It is evident that neither assignment can be sustained in detail by the present data. If one relaxes the condition $\hbar\omega$L.(W) < $\hbar\omega$L.(X), assignment 2*a* with W and X interchanged is still possible. However, if this were correct, the resultant dispersion curves would agree with those

in fig. 2. to within the limits of error. However, one can say with reasonable certainty that the T.O.(X)+T.A.(X) energy lies close to 0·258 ev, the sharp rise in absorption at this point reflecting a similar rise in the density of T.A. normal modes to be expected at the T.A.(X) energy. Also the use of this energy to fit the 0·244 ev peak to T.A.(X)+L.(X) leads to an L.(X) energy (0·139 ev) which is consistent with the previous results.

§ 5. Conclusions

The results of this analysis have been used to construct the set of phonon dispersion curves which are shown in fig. 2. The slopes of the acoustic branches at $\omega = 0$ have been derived from the elastic constants measured by McSkimin and Bond (1957). The curves have been interpolated using the zone boundary energies derived from our results, and the probable errors in these are indicated by the short vertical lines.

Fig. 2

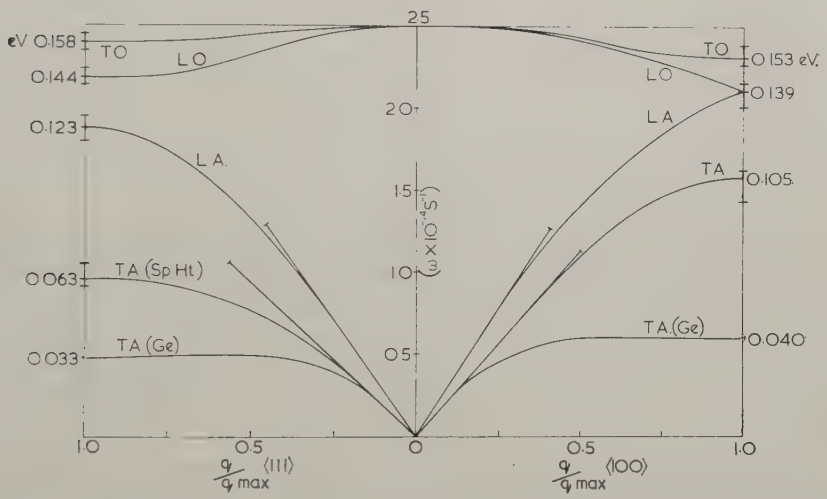

Lattice wave dispersion curves for diamond constructed from the zone boundary phonon energies derived from the absorption data. The short vertical lines indicate the probable errors in these energies.

Also shown are the T.A. branches obtained by scaling those of germanium according to the homology rule (Brockhouse 1959): $\omega\alpha(Ma^2)^{-1\cdot2}$, where M is the atomic mass and a the lattice parameter. (In the region of $\omega = 0$ the slopes have been fitted to those predicted by the elastic constants of diamond.) The discrepancy between these and our results is obviously very large and demonstrates conclusively that the interatomic forces in the two crystals are very different. The dispersion curves for diamond imply that long-range forces are *much* less

important, since it is these which are responsible for the anomalously high dispersion of the T.A. branches in germanium.

Our results are obviously somewhat tentative, and require confirmation by the more direct neutron scattering technique. Such confirmation could well be provided by very low resolution scattering work such as may be possible with crystals of a readily available size. This would define the phonon energies at c.p. to within 10 or 20% which is all one needs to check the correctness of our assignments. If these are valid, then the energies we have derived from infra-red absorption are considerably more accurate than the neutron scattering results.

Acknowledgments

We should like to express our thanks to Dr. F. A. Johnson for valuable discussions and to Miss G. Tims for carrying out the computations and plotting of the results. One of us (J.R.H.) would like to thank A.E.I. for the Research Fellowship during the tenure of which this work was carried out.

References

Brockhouse, B. N., 1959, *Phys. Rev. Letters*, **2,** 256.
Brockhouse, B. N., and Iyengar, P. K., 1958, *Phys. Rev.*, **111,** 747.
Cochran, W., 1959, *Proc. roy. Soc.* A, **253,** 260.
Collins, R. J., and Fan, H. Y., 1954, *Phys. Rev.*, **93,** 674.
Desnoyers, J. E., and Morrison, J. A., 1958, *Phil. Mag.*, **3,** 42.
Herman, F., 1959, *J. Phys. Chem. Solids*, **8,** 405.
Johnson, F. A., 1959, *Proc. phys. Soc., Lond.*, **73,** 265.
Lax, M., and Burstein, E., 1955, *Phys. Rev.*, **97**, 39.
McSkimin, H. J., and Bond, W. L., 1957, *Phys. Rev.*, **105,** 116.
Phillips, J. C., 1956, *Phys. Rev.*, **104,** 1263; 1959, *Ibid.*, **111,** 147.
Smith, S. D., and Hardy, J. R., 1960, *Phil. Mag.*, **5,** 1311.
Van Hove, L., 1953, *Phys. Rev.*, **89**, 1189.

Heat Conduction by Liquid Helium II in Capillary Tubes. II. Measurements of the Pressure Gradient

By D. F. Brewer and D. O. Edwards†
The Clarendon Laboratory, Oxford

[Received February 8, 1961]

Abstract

The pressure and temperature gradients accompanying heat flow in liquid helium II have been measured simultaneously. The experiments were made in a glass tube of 107·6 μ diameter and 10·2 cm length between 1·3°K and 1·8°K. Significant deviations from Allen and Reekie's rule were observed and are provisionally attributed to an eddy viscosity, η_e, due to turbulence in the superfluid component. An equation, based on dimensional arguments, is proposed for η_e which satisfactorily represents the experimental data available at present.

§ 1. Introduction

According to an empirical rule of Allen and Reekie (1939) the pressure gradient observed in a steady-state heat conduction experiment in helium II is proportional to the heat flow. The proportionality holds good, at least approximately, even at relatively high values of the heat current density despite the fact that the temperature gradient is then found to be a strongly non-linear function of the heat flow.

An explanation of the Allen and Reekie rule was given by Gorter and Mellink (1949) who postulated that the rapid increase in the observed thermal resistance at high heat current densities is caused by a non-linear mutual friction force acting equally and oppositely on the superfluid and normal components. With such a mutual friction term included in the hydrodynamic equations of both superfluid and normal component it is found that its effect on the pressure gradient cancels, and the pressure difference Δp observed in a cylindrical flow channel, for all values of the heat flow W, should be given by

$$\Delta p = \frac{8\eta_n l W}{\pi a^4 \rho S T} \quad . \quad . \quad . \quad . \quad . \quad . \quad . \quad . \quad (1)$$

where η_n is the normal viscosity, ρST the heat of transport per unit volume, and a and l the radius and length of the tube. The Gorter–Mellink calculation assumes that the mutual friction depends only on the temperature

† Now at the Department of Physics, Ohio State University, Columbus, Ohio.

and relative velocity v between the two fluids, that there is no restriction on the value of the superfluid velocity v_s at the wall of the channel, and that v_s may be rotational without producing any additional dissipative or viscous effects.

Recent work on non-linear processes in helium II has indicated that the Gorter–Mellink mutual friction is almost certainly due to scattering of the normal fluid excitations by turbulence in the superfluid, the turbulence consisting of a random distribution of the quantised vortex lines proposed by Feynman (1955). On this picture it seems likely that other dissipative processes may occur in the superfluid besides the mutual friction, for example it may be possible for the superfluid to interact with the channel walls by the attachment of vortex lines, or, as was suggested by Vinen (1955, and private communication), there may occur some radial transfer of momentum in the superfluid by an eddy viscosity analogous to that found in ordinary turbulence. The effect of such processes may be detected and separated from the mutual friction by testing the validity of eqn. (1) when the helium is in a turbulent condition.

Small deviations from the equation at large heat currents have already been reported in a re-analysis of the earlier data of Mellink (1947) by Vinen (1955) and Lifshitz and Andronikashvili (1959), and in some experiments on narrow channels by Keller and Hammel (1960). Some of the present measurements, which were made on the heat flow in a glass tube of 107·6 microns diameter, have already been briefly described by us (Brewer and Edwards 1958). Another series of experiments of the same kind, but using a range of tube sizes, has since been carried out in this laboratory by Bhagat and Critchlow (1961).

The present paper is one of a series describing heat conduction by liquid helium II in capillary tubes. Previous papers, following a preliminary report (Brewer, Edwards and Mendelssohn 1956), have dealt with the subcritical region (Brewer and Edwards 1959) and with the transition to non-linear conduction (Brewer and Edwards 1961 a). In a forthcoming paper we shall describe and analyse measurements of the thermal resistance in the non-linear region.

§ 2. Apparatus

A diagram of the apparatus is shown in fig. 1. The glass capillary tube C communicates at its upper end through a wide metal tube with the constant-temperature liquid helium bath. The other end is joined with platinum seals through a metal bridge tube to another glass tube S of diameter 0·8 mm in which the liquid height can be measured with a cathetometer. The arrangement of the tubes C and S shown in the diagram was chosen to allow the maximum possible difference ΔH_{obs} between levels in S and the bath (which may be positive or negative), with the restricted length of cryostat available. The tubes are thermally isolated from the bath by a metal vacuum jacket V and a glass jacket W, joined together with a copper–glass seal. The vacuum space is continuously pumped during

experiments through a metal tube which has been omitted from the diagram for simplicity. A temperature gradient across C can be established by the heater h, and measured by the carbon resistance thermometer t, which is glued in thermal contact with the metal tube connecting C and S. The capillary tube C has a diameter $2a = 107{\cdot}6$ microns and length $l = 10{\cdot}2$ cm; its Poiseuille constant, $\pi a^4/8l$, was also determined by gas flow measurements as previously described (Brewer and Edwards 1959). On applying small

Fig. 1

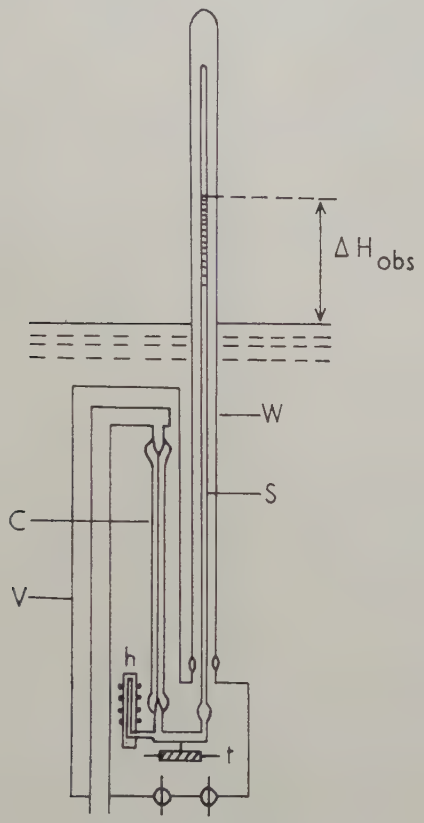

The apparatus.

heat inputs, the observed level difference, ΔH_{obs}, increases until an equilibrium is reached, when the mass flow of superfluid down the capillary is balanced by the upward flow of normal fluid. The total pressure difference ΔH is then given by the level difference ΔH_{obs}, together with the difference in vapour pressure between the liquid in S and the bath. The latter was calculated from the measured temperature difference between S and the bath, using the T_{55E} vapour pressure scale. At high heat currents the

vapour pressure correction becomes so large that the observed level difference ΔH_{obs} is negative.

To measure the bath level accurately, a second tube of the same diameter as S was used, dipping directly into the bath. Appropriate corrections for surface tension rise were made from separate experiments in water in which the rise was measured at different parts of the tube.

§ 3. Results and Discussion

Figure 2 shows the experimental results for the temperature 1·563°K, and illustrates the importance of the correction to the observed pressure gradient for the increase in vapour pressure. The directly observed quantity $\Delta H_{obs}/W$ decreases sharply at higher heat currents, whereas the

Fig. 2

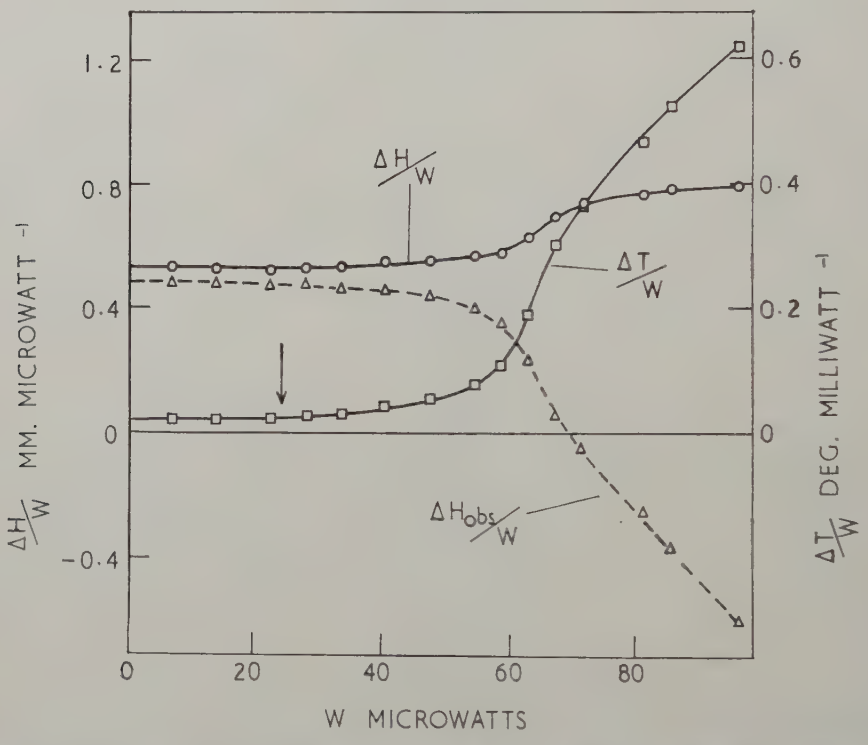

Experimental results at 1·563°K. showing the directly observed quantity $\Delta H_{obs}/W$, the corrected values $\Delta H/W$, and the thermal resistance $\Delta T/W$, as functions of heat flow W. The arrow indicates the critical heat current W_c previously determined for the same tube (Brewer and Edwards 1961 a).

corrected quantity $\Delta H/W$ increases. Values of the temperature difference across the tube have been divided by heat current to give the thermal resistance $\Delta T/W$ which is also plotted in fig. 2. The thermal resistance is

independent of W at low heat currents, and then shows a transition to strongly current–dependent values where mutual friction forces occur. These observations of $\Delta T/W$ are in complete agreement with those previously obtained with the same tube in a different experimental arrangement (Brewer and Edwards 1959, 1961 a, b). The arrow on the curve gives the critical heat current W_c as determined in the previous experiments, and is seen to be consistent with the present measurements.

During these experiments some fluctuations in the temperature and pressure were observed at intermediate heat currents just above critical, which are probably related to those found in our earlier thermal resistance measurements. None of the hysteresis observed earlier was found in the present experiments, possibly because there was appreciable vibration present, or because of small obstructions or roughness in the tube, or because in this experiment the tube was connected directly to the bath.

If Allen and Reekie's rule were followed, the graph of $\Delta H/W$ would be a line roughly parallel to the W-axis, but bending down slightly when the temperature gradient becomes large. This is seen to be true up to heat currents in excess of the critical current W_c for the appearance of mutual friction. Large deviations then occur quite sharply, and at still higher currents $\Delta H/W$ begins to level off once more.

We define an effective viscosity in these experiments given by

$$\eta_{eff} = \frac{\pi a^4 \rho S T}{8l} \frac{\Delta p}{W} \quad . \quad . \quad . \quad . \quad . \quad . \quad . \quad (2)$$

which may be considered to include dissipative effects occurring in both normal and superfluid components, but which, by the theory of Gorter and Mellink, excludes the *mutual* friction simultaneously present. This effective viscosity is plotted against the relative velocity of the two fluids, v, for three temperatures in fig. 3. At low heat currents, η_{eff} is accurately equal to the viscosity of the normal fluid, η_n, as previously determined in the same tube (Brewer and Edwards 1959), so that in this region eqn. (1) is obeyed. The slight decrease of η_{eff} with increasing velocity is due to the variation of η_n and $\rho S T$ with temperature along the tube, and agrees with the theoretical expectation, shown by the broken curves in the figure. These broken curves have been calculated from the known temperature variation of $\rho S T$ and η_n and the observed temperature gradients in each experiment, by a method described in our previous paper quoted above. The quantity represented by the broken curves, which we term η_n^{corr}, therefore represents the expected result of an experiment in which eqn. (1) is exactly true and in which the temperature gradient along the tube is the same as in the actual experiment. Arrows in fig. 3 show the critical velocities for appearance of mutual friction already determined in our previous experiments (Brewer and Edwards 1961 a), and are found to be consistent with the present observations of $\Delta T/W$, as was illustrated in fig. 2 for 1·563 °K. Thus fig. 3 shows that large contributions to η_{eff} from causes other than the

viscosity of the normal component or mutual friction occur at velocities near but generally rather larger than the critical.

To interpret the data we assume provisionally that the additional contributions to η_{eff} are due to an eddy viscosity of the superfluid, η_e, since this seems reasonable both from theory and from other experiments (see, for example, Bhagat 1960, Bhagat and Mendelssohn 1961). If we make

Fig. 3

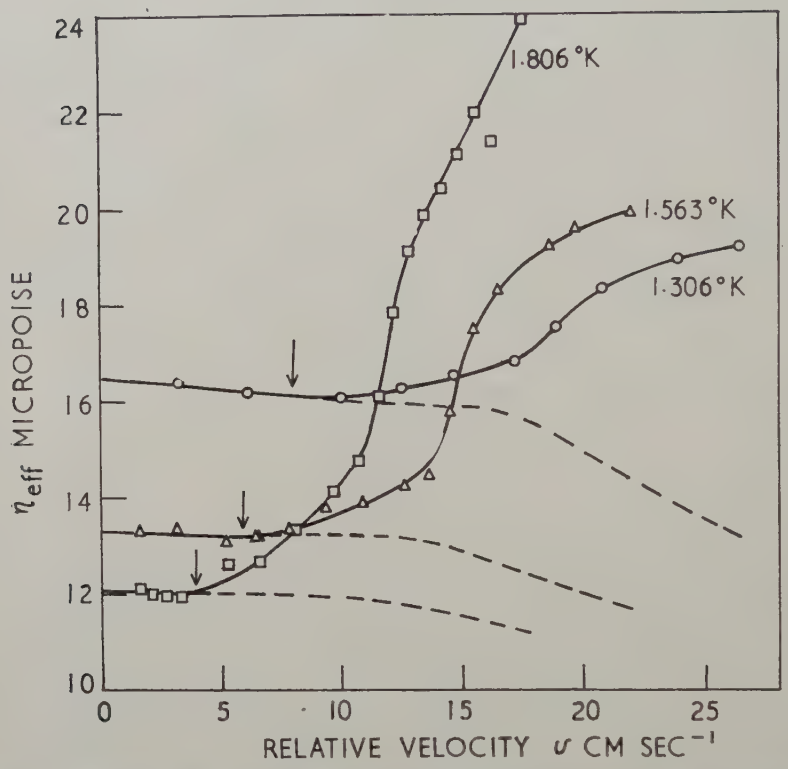

Effective viscosity η_{eff} plotted against relative velocity v of superfluid and normal fluid. ○, $T=1{\cdot}306°K$; △, $T=1{\cdot}563°K$; □, $T=1{\cdot}806°K$. The broken curves represent values of η_n^{corr} (see text). Arrows indicate the critical velocities for appearance of mutual friction previously determined in the same tube (Brewer and Edwards 1961 a).

the further, simplifying assumption that there is no restriction on the value of v_s at the wall of the channel, then it can be shown from the two fluid equations of motion that η_e is given by the difference between the broken and solid curves in fig. 3, that is

$$\eta_e = \eta_{eff} - \eta_n^{corr}. \qquad (3)$$

As mentioned in the Introduction, the eddy viscosity is understood to arise from the motions of the random distribution of vortex lines in the

superfluid component, and it may be expected to depend rather directly on the length of vortex line per unit volume present in the liquid. A plausible equation for η_e from dimensional arguments is

$$\eta_e = \rho \frac{\hbar}{m} f(DL_0^{1/2}) \quad . \quad . \quad . \quad . \quad . \quad . \quad . \quad . \quad . \quad (4)$$

where $2\pi(\hbar/m)$ is the quantum of circulation around a vortex line, ρ the liquid density and $f(DL_0^{1/2})$ a dimensionless but possibly temperature dependent function of vortex line density, L_0, and tube dimension, D. (The length D will be defined as the ratio of tube cross section to perimeter

Fig. 4

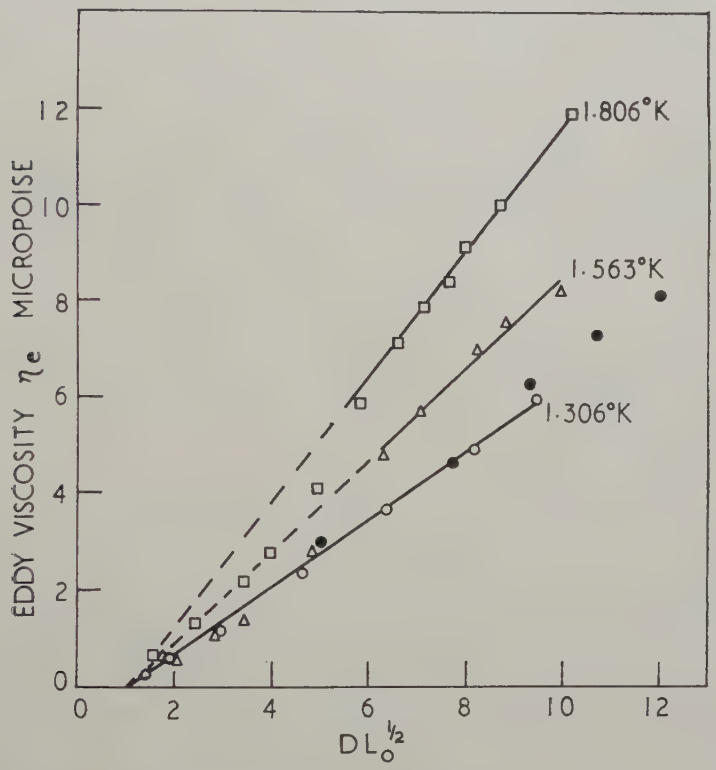

Eddy viscosity η_e plotted against the dimensionless number $DL_0^{1/2}$ (see eqns. (4) and (5) and text). ○, $T = 1{\cdot}306°\text{K}$; △, $T = 1{\cdot}563°\text{K}$; □, $T = 1{\cdot}806°\text{K}$. Closed circles ● represent results calculated from the measurements of Bhagat and Critchlow (1961).

so that it may be applied to tubes of various shapes.) There is no need to include any dependence on the fluid velocity v in eqn. (4) since there is another relation between L_0 and v determining the magnitude of the mutual friction. Values of L_0 have been derived from the present measurements using the

theory of mutual friction developed by Hall and Vinen (1956) and Vinen (1957) and the experimental values of the temperature gradient. In fig. 4 we plot η_e against the dimensionless number $(DL_0^{1/2})$, in order to determine the form of the function f. It is interesting that the value of η_e is apparently zero up to $(DL_0^{1/2}) \approx 1$ and then increases almost linearly with $DL_0^{1/2}$. Moreover, the magnitude of η_e at a given value of $(DL_0^{1/2})$ does not depend strongly on temperature. Since $L_0^{-1/2}$ is of the order of the spacing between vortex lines, values of $(DL_0^{1/2})$ equal to or less than unity represent situations where the average line spacing is of the order of or greater than the dimensions of the channel. It is natural to expect that the behaviour of both the mutual friction and eddy viscosity should change in this region. Measurements on the mutual friction at low heat current densities (Brewer and Edwards 1961 b) have shown that the vortex line theory of Vinen, based on the assumption of a homogeneous, random distribution of vortex lines, breaks down (as may be expected) when $(DL_0^{1/2}) \gtrsim 1$, and the variation of L_0 with v is then completely different from that at higher vortex line densities.

The present experiments can therefore be explained by postulating an eddy viscosity in the superfluid, with no constraint on the value of v_s at the channel wall. The magnitude of this proposed eddy viscosity is given approximately by

$$\eta_e \approx \zeta_1 \rho \frac{\hbar}{m} [(DL_0^{1/2}) - \zeta_2], \quad DL_0^{1/2} > \zeta_2 \quad . \quad . \quad . \quad . \quad (5)$$

where ζ_1 and ζ_2 are dimensionless numbers ($\zeta_1 \approx 0{\cdot}05$, $\zeta_2 \approx 1$), only slightly dependent on temperature. As can be seen from fig. 4, there are systematic deviations from this linear equation for small values of $(DL_0^{1/2})$ at the two higher temperatures.

Equations (4) or (5) predict a definite relation between the proposed eddy viscosity η_e and tube size. We are unable to verify this prediction from our own measurements since only one tube of 107·6 micron diameter was investigated. However, Bhagat and Critchlow (1961) give simultaneous values of the mutual friction and pressure gradient for a tube of 297 microns diameter at 1·41°K, which have been plotted as closed circles in fig. 4. It is satisfactory that these independent points also lie on a straight line and are in good agreement with the values at our closest temperature, 1·306°K. The only other available data which might be used to test eqn. (5) or the more exact eqn. (4) are the results of Mellink (1947) re-analysed by Lifshitz and Andronikashvili (1959); these are in rather rough agreement with our proposed equations, but since they refer to radial flow in a disk-shaped slit, they are not exactly comparable with our own. The measurements of Keller and Hammel (1960) were made with very large temperature differences across the tube, and are again rather difficult to interpret.

Acknowledgments

The authors are grateful to Dr. K. Mendelssohn, F.R.S., for his interest in the work, to Dr. W. F. Vinen for some stimulating discussions and

particularly for pointing out the importance of the Allen and Reekie rule, and to Dr. S. M. Bhagat for a copy of his paper with Dr. P. R. Critchlow before publication. The work has been supported by Research Fellowships from the Nuffield Foundation (D.F.B.) and the Pressed Steel Company (D.O.E.).

References

Allen, J. F., and Reekie, J., 1939, *Proc. Camb. phil. Soc.*, **35,** 114.
Bhagat, S. M., 1960, *Proc. phys. Soc., Lond.*, **75,** 303.
Bhagat, S. M., and Critchlow, P. R., 1961, *Cryogenics*, **2,** 39.
Bhagat, S. M., and Mendelssohn, K., 1961, *Cryogenics*, **2,** 34.
Brewer, D. F., and Edwards, D. O., 1958, *Low Temperature Physics and Chemistry* (Madison: University of Wisconsin Press), p. 12.
Brewer, D. F., and Edwards, D. O., 1959, *Proc. roy. Soc.* A, **251,** 247; 1961 a, *Phil. Mag.*, **6,** 775; 1961 b, *Phil. Mag.* (in print).
Brewer, D. F., Edwards, D. O., and Mendelssohn, K., 1956, *Phil. Mag.*, **1,** 1130.
Feynman, R. P., 1955, *Progress in Low Temperature Physics* (Amsterdam: North-Holland Publishing Co.), **1,** 36.
Gorter, C. J., and Mellink, J. H., 1949, *Physica*, **15,** 285.
Hall, H. E., and Vinen, W. F., 1956, *Proc. roy. Soc.* A, **238,** 215.
Keller, W. E., and Hammel, E. F., 1960, *Ann. Phys. (U.S.A.)*, **10,** 202.
Lifshitz, E. M., and Andronikashvili, E. L., 1959, *A Supplement to Helium* (Chapman and Hall), p. 121.
Mellink, J. H., 1947, *Physica*, **13,** 180.
Vinen, W. F., 1955, *Cong. de Phys. des Basses Temp.*, Paris, p. 60; 1957, *Proc. roy. Soc.* A, **242,** 493; *Ibid.* A, **243,** 400.

CORRESPONDENCE

The Determination of Dislocation Densities in Thin Films

By R. K. Ham

C.S.I.R.O., Division of Tribophysics, University of Melbourne

[Received March 1, 1961]

I wish to describe (1) a new method of estimating the density of dislocations observed in a thin metal film by electron microscopy, and (2) an investigation of the sources of random error in estimates of the mean density corresponding to a particular treatment.

(1) Bailey and Hirsch (1960) have described a method of estimating the density of dislocations. They measure the total projected length R_p of dislocation line in a given area A on a typical micrograph. Then, on the assumption that the dislocation segments are randomly orientated with respect to the plane of the film, the dislocation density is $\rho=(4/\pi)R_p/At$, where t is the thickness of the film.

A disadvantage of this method is the labour of measuring R_p. However, an estimate of R_p may be obtained easily by making use of the results of Smith and Guttman (1953). They showed that if a set of random lines with a total length L is marked on A, and the number of intersections N which dislocations make with the grid lines is measured, then $R_p=\pi NA/2L$, giving $\rho=2N/Lt$, provided N is large enough.

The two methods of finding R_p have been compared for 20 micrographs taken from thin films of a specimen of aluminium cold-rolled to about 9% reduction. The new method proved to be about ten to twenty times faster in measuring time alone. Five lines drawn in random directions on a plate taken at $\times 20\,000$ gave enough intersections (about 50), and it was not necessary to enlarge the micrographs, as it was for the direct measurement of R_p. The mean difference between the dislocation densities (of about $2\times10^9/\text{cm}^2$) estimated by the two methods was $\simeq 4{\cdot}1\times10^7/\text{cm}^2$, the standard deviation of the mean difference being $\simeq 3{\cdot}6\times10^7/\text{cm}^2$. Hence there was no significant difference between the two methods.

(2) As part of another programme, the new method has been used in a preliminary investigation of the sources of random error in determinations of dislocation density. Three specimens of aluminium were prepared at each of three levels of deformation, namely 18, 45 and 88% reduction, by cold rolling. A thin film was prepared from each specimen and two micrographs taken from each of two grains. The specimens were treated in three groups, all levels being represented in each group. In this way

systematic variation during the measurement was shown to be absent. The dislocation density was determined for each micrograph, and an analysis of variance made of these data. In what follows, references have been given to specific sections of Davies (1958) which describe the procedure. For each level of deformation the specimens, grains, and micrographs form a hierarchic classification with three sources of variation (§ 6.3). The additive property of variance (§ 6.11) was used in the separation and estimation of components of variance associated with specimens, grains, and micrographs. These estimates are given in the table. The variance of the mean dislocation density (§ 6.11) based

Level	Components of variance		
	Between specimens, S_s^2	Between grains, S_g^2	Between micrographs, S_m^2
18	0	0·87	0·68
45	0	6·03	2·14
88	1·07	0·17	1·23

on n_s specimens, n_g grains per specimen and n_m micrographs per grain is $S_s^2/n_s+S_g^2/n_sn_g+S_m^2/n_sn_gn_m$. Hence it is seen from this formula and the estimates in the table that at levels 18 and 45 the most efficient way to reduce the error in the mean is to take more than two grains per specimen ; two specimens and two micrographs per grain are enough. At level 88, however, the most efficient procedure is to take more specimens. The variance estimates are fully efficient, but since they are based on few observations these suggestions should be regarded as a guide to the design of further investigations.

Acknowledgments

I wish to thank Mr. W. B. Hall of the C.S.I.R.O. Division of Mathematical Statistics for invaluable advice, and Mr. J. F. Nicholas for reading the manuscript.

References

Bailey, J. E., and Hirsch, P. B., 1960, *Phil. Mag.*, **5**, 485.

Davies, O. L., 1958, *Statistical Methods in Research and Production*, 3rd edn. (London: Oliver and Boyd).

Smith, C. S., and Guttman, L., 1953, *J. Metals, N.Y.*, **5**, 81.

The Positive Ion Bombardment of Evaporated Single Crystal Gold Films

By E. Gillam and M. Phillips
The General Electric Company Limited, Central Research Laboratories, Hirst Research Centre, Wembley, England

[Received June 5, 1961]

§ 1. Introduction

It has been reported on several occasions (Ogilvie 1959, Gillam 1959 and Ogilvie and Thomson 1961) that the bombardment of a metal surface with positive ions of low energy (from 4000 to 10 ev) results in the formation of crystallites which are considerably misoriented with respect to the crystal structure before bombardment. This was inferred from experiments in which flat specimens were electropolished to form holes, and transmission electron diffraction patterns were taken through thin regions of the metal round the edge of a hole. The pattern from a polished but unbombarded specimen consisted of sharp spots, if it was large grained or a single crystal. In the diffraction pattern of the same specimen after ion bombardment, the spots had become arced, and the pattern was similar to those obtained by Hirsch *et al.* (1955) in beaten and etched gold foil. A misorientation of 35° has recently been reported when 130 ev argon ions bombarded a silver single crystal (Ogilvie and Thomson 1961).

More detailed investigations of these effects can be carried out by transmission electron microscopy. The technique of observing dislocations and other defects used by Whelan *et al.* (1957), Bailey (1960) and many others, seems a promising way of finding out how ion bombardment causes these changes in the crystalline texture. Dislocation loops have been shown to arise from the neutron bombardment of copper (Silcox and Hirsch 1959) and from the bombardment of copper with high energy α-particles (Barnes and Mazey 1960) in this way. In all the experiments mentioned so far, 'electropolishing to holes' was used to produce the thin films required in the microscope.

In the experiments to be described, evaporated single crystal gold films were used instead of electropolished specimens. These had the advantage of being of uniform thickness, and a large area of such specimens was thus available for inspection; with electropolished specimens the part examined is wedge-shaped, and only small sections near the holes are available. Extinction contours and impurities from the polishing bath can also be a nuisance with polished specimens. Evaporated films are frequently objected to because they have different properties from bulk specimens, but

the misorientation effects due to ion bombardment should also appear in films, as the effects are thought to occur in a layer of about 100 Å thickness and this should be observable in a film some 500 Å thick after bombardment.

§ 2. Experimental Method

Single crystal gold films were prepared by the method of Bassett and Pashley (1959). A layer of silver at least 1000 Å thick was evaporated on the (100) face of a freshly cleaved rock-salt crystal held at 250–300°C, and the gold was immediately evaporated on the silver. The rock-salt was dissolved in water and the silver in concentrated nitric acid, and a coherent single crystal gold film remained. Gold films made in this way were examined in a Siemens Elmiskop 1 electron microscope and found to be of the same general appearance as that described by Bassett and Pashley.

The ion bombardment of the film took place in a low pressure argon discharge similar to the type used in the experiments mentioned previously. A cylindrical anode of aluminium with open ends was used with a magnetic field of about 500 gauss directed along its axis. A hot tungsten filament at one end of the cylinder and the specimen at the other acted as cathodes. The greased cone and socket joins in the glassware used in earlier experiments to make the system demountable were abandoned, as evidence of carbon contamination appeared in the first micrographs. Thus the system could be baked and the gaseous impurities in the glass and electrodes pumped away before the argon was introduced. The baking temperature was 500°C. The pressure during the ion bombardment was $0{\cdot}6 \times 10^{-3}$ torr which was sufficiently low to prevent sputtered material being scattered back to the specimen.

Backus (1949) discusses this discharge system, in which most of the ions bombard the specimen normal to its surface with energies slightly less than that given by the anode voltage. The ion bombardment with a discharge voltage of 300 volts lasted for 1 hour and the current density was 0·15 mA/sq. cm. The film which was initially 2000 Å thick appeared to be much thinner in the microscope and was probably about 500 Å thick. This would correspond to an approximate sputtering ratio of the order of 0·1 atoms removed per incident positive ion, under these conditions.

§ 3. Results

Figure 1† is a micrograph showing the appearance of a film after the above treatment. The whole of the field is covered with specks and there are a few dislocation rings. Barnes and Mazey (1960) found similar spots after α-particle bombardment of copper. Figure 2 shows the diffraction pattern taken from the same part of the specimen, and the noticeable feature is that the arcing of the spots which had been expected did not appear. There were no edges in the sections of the film examined in this case.

† All figures are shown as plates.

Some of the films, however, lay across the grids in such a way that an edge of the film was seen in a grid hole. Figure 3 shows a diffraction pattern taken from an area including such an edge, and misorientations of the kind found previously in diffraction patterns are seen. It seems therefore that these are a feature, not of the ion bombardment, but of the twisting and bending of the specimen in the very thin fragile region of an edge. Moving to an adjacent grid hole on the same specimen which did not contain an edge, diffraction patterns were obtained similar to fig. 2. For a gold film bombarded in a 130 volt discharge, the observations were similar.

Further support for the view that edge effects have been misleading was obtained by making an evaporated gold film in which a wire placed in front of the rock-salt prior to the evaporation resulted in a thin edge being formed on the unbombarded film. Once again, well away from the edge, the diffraction pattern was that of a single crystal, but fig. 4 shows the 'misorientation' effect occurring near the edge.

It remains to be explained why the misorientations have not been found before ion bombardment in diffraction patterns of films made by electropolishing, but have been observed after ion bombardment. This is possibly because the thin areas round the electropolished hole were in fact not thin enough, and the edges were not at this stage bent. Ion bombardment caused a further thinning of the edge and may then have also been instrumental in bending it.

The nature of the defects from which the specks in fig. 1 arise has not been studied in detail. Ion bombardment is expected to produce vacancies and interstitials in equal numbers, some of which can combine to form clusters. Collapse of the lattice and the formation of dislocation loops can then occur. Annealing at 350 °C for 10 min resulted in a disappearance of the specks and the formation of complex dislocation networks. Figure 5 shows a resulting micrograph.

References

Backus, J., 1949, *Gaseous Electrical Discharges in Magnetic Fields* (New York: McGraw-Hill), p. 353.

Bailey, J. E., 1960, *Phil. Mag.*, **5**, 833.

Barnes, R. S., and Mazey, D. J., 1960, *Phil. Mag.*, **5**, 1247.

Bassett, G. A., and Pashley, D. W., 1959, *J. Inst. Met.*, **87**, 449.

Gillam, E., 1959, *J. Phys. Chem. Solids*, **11**, 55.

Hirsch, P. B., Kelly, A., and Menter, J. W., 1955, *Proc. phys. Soc., Lond.* B, **68**, 1132.

Ogilvie, G. J., 1959, *J. Phys. Chem. Solids*, **10**, 222.

Ogilvie, G. J., and Thomson, A. A., 1961, *J. Phys. Chem. Solids*, **17**, 203.

Silcox, J., and Hirsch, P. B., 1959, *Phil. Mag.*, **4**, 72.

Whelan, M. J., Hirsch, P. B., Horne, R. W., and Bollmann, W., 1957, *Proc. roy. Soc.* A, **240**, 524.

Note on the Scattering of Electrons by Stacking Faults in Lithium

By J. S. Dugdale and D. Gugan†
Division of Pure Physics,
National Research Council, Ottawa, Canada

[Received June 17, 1961]

There is considerable interest in the problem of the electrical resistance due to stacking faults in pure metals (for references see, for example, Howie 1960) but at present the experimental evidence for the magnitude of this resistance is scanty. We have already noted that in pure sodium the dominant residual electron scattering is *not* due to stacking faults (Basinski *et al.* 1959); a consideration of the electrical resistivity of the low-temperature phase of lithium leads us to conclude that stacking-fault scattering is small in lithium also.

When lithium is cooled below about 80°K a hexagonal close-packed phase begins to form by the martensitic mechanism (Barrett 1947, 1951, 1956. Barrett and Trautz 1948). According to Barrett "it would be appropriate to describe the structure of the spontaneously formed low-temperature phase as a nearly random placement of each successive layer of atoms in the hollows of the layer just below, or alternatively as an f.c.c. structure with very imperfect stacking of (111) planes" (1951, p. 354). This implies that the stacking-fault density may be nearly as high as one plane in three. At 4°K approximately 90% of the material has transformed to this 'hexagonal' phase, the rest being untransformed b.c.c. material (Hull and Rosenberg 1960, Barrett 1951, Martin 1960).

Typical values for the resistivity of such 'pure' lithium specimens at 4°K, where the scattering is essentially all residual scattering, are between 1 and $1{\cdot}5\times10^{-8}$ ohm cm. If we assume that the residual resistivities of the two phases are equal and attribute *all* the resistivity of the close-packed phase to stacking faults then, since the mean free path of electrons at room temperature is about 10^{-6} cm, we deduce that at 4°K it is about 10^{-3} cm in such samples. In the extreme case that every third plane is a faulted plane the distance between stacking faults is about 10^{-7} cm and the probability of reflection at an individual stacking fault is approximately 10^{-4}‡. In this estimate we have taken the free electron Fermi velocity for the electrons; this should not introduce a serious error. We are also assuming the scattering from one stacking fault to be independent of that from another; according to Howie (1960) this should be true if they are further apart than one lattice spacing.

---

† Now at the H. H. Wills Physics Laboratory, University of Bristol.
‡ We are assuming that the stacking faults are effectively infinitely wide.

It might be argued that perhaps in the resistive specimens less than 90% of the b.c.c. phase transforms and, being free from stacking faults, short-circuits the h.c.p. phase. If this were a large effect it would show itself in the temperature region around 80°K where we can compare the resistivity of the two-phase mixture with that of the pure b.c.c. phase. We deduce from such measurements (cf. Dugdale and Gugan 1961) that even if only 50% transforms the reflection coefficient can hardly exceed 10^{-3}. In fact, however, there seems no reason to doubt the figure of about 90%. The amount transformed appears to be insensitive to the amount of strain in the specimen before transformation (Martin 1960) and, moreover, our resistance measurements were made on a variety of specimens (bare wires with diameters between 0·5 and 5 mm and with different heat treatments) which all gave similar results.

As noted above, we concluded earlier that stacking-fault scattering in sodium was small but this was hardly surprising because even in the hexagonal phase this metal approximates well to a free-electron metal (Dugdale and Gugan 1960). On the other hand, it has been argued that in a metal with a distorted Fermi surface the reflection coefficient should be fairly high (cf. Ziman 1960), and for copper a value of about 0·2 has been calculated (cf. Howie 1960). The Fermi surface in lithium is thought to be highly distorted in the b.c.c. phase (cf. Cohen and Heine 1958) and in the close-packed phase the situation may well be similar. It is therefore interesting that the reflection coefficient for the scattering of electrons by stacking faults is apparently so small in lithium. However, as the next letter shows, it is perhaps possible to account for the small value on the basis of existing theories of the scattering of electrons by stacking faults.

Acknowledgments

We are grateful to Dr. Z. S. Basinski for valuable discussions and to Dr. L. M. Clarebrough for drawing our attention to the problem.

References

Barrett, C. S., 1947, *Phys. Rev.*, **72,** 245 ; 1951, *Imperfections in Nearly Perfect Crystals* (New York : John Wiley) ; 1956, *Acta cryst.*, **9,** 671.

Barrett, C. S., and Trautz, C. R., 1948, *Trans. Amer. Inst. min. (metall.) Engrs*, **175,** 579.

Basinski, Z. S., Dugdale, J. S., and Gugan, D., 1959, *Phil. Mag.*, **4,** 880.

Cohen, M. H., and Heine, V., 1958, *Advanc. Phys.*, **7,** 395.

Dugdale, J. S., and Gugan, D., 1960, *Proc. roy. Soc.* A, **254,** 184 ; 1961, *Cryogenics* (in the press).

Howie, A., 1960, *Phil. Mag.*, **5,** 251.

Hull, D., and Rosenberg, H. M., 1960, *Cryogenics*, **1,** 27.

Martin, D. L., 1960, *Proc. roy. Soc.* A, **254,** 444.

Ziman, J. M., 1960, *Electrons and Phonons* (Oxford : Clarendon Press).

A Possible Explanation of the Results of the Preceding Note Regarding Scattering of Electrons by Stacking Faults in Lithium

By A. Howie
Cavendish Laboratory, Cambridge

[Received July 5, 1961]

In the preceding letter it is reported that samples of h.c.p. lithium, containing an estimated density of 10^7 cm^{-1} of independently scattering stacking faults, have a resistivity of about 1×10^{-8} ohm-cm. The resistivity to be associated with unit stacking-fault density is therefore 1×10^{-15} ohm-cm and may be compared with a value of 2×10^{-13} ohm-cm recently measured for stacking faults in gold (Cotterill 1962). This latter figure is in quite good agreement with the lower of two estimates made for copper by Howie (1960) on the basis of a wave-matching calculation and is thought to be typical of copper, gold and silver. The apparent difference of about two orders of magnitude between the resistivity of stacking faults in lithium and of stacking faults in the noble metals may result from several causes.

(1) Lithium, as the authors of the preceding note point out, is regarded as being less free-electron-like than sodium. It is however almost certainly more free-electron-like than the noble metals. Estimates of the size of the band gap at the (110) Brillouin zone boundaries in b.c.c. lithium (Ham 1960) seem to be only about half to one-third of the value for the gap at the (111) zone boundary in copper (Pippard 1957). This would imply that in lithium the value (suitably averaged over the Fermi surface) of the most important diffracted wave intensity is between one-quarter and one-ninth of what it is in copper and the resistivity of stacking faults which is essentially a diffraction effect might be expected to fall by a similar factor (Ziman 1958).

(2) In the noble metals, the electrons most strongly scattered by a stacking fault on a (111) plane were found (Howie 1960) to be those diffracting from (111), ($1\bar{1}1$) and (11$\bar{1}$) planes, i.e. electrons travelling at about 70° to the direction of normal incidence on the fault. In the h.c.p. structure however the situation is quite different. Electrons travelling normal to the fault and diffracting from planes parallel to the fault would be unaffected by the fault (since these planes are merely sheared at the fault). Electrons diffracted by (10$\bar{1}$0) pyramidal planes would be affected by the fault but would generally be travelling almost parallel to the faults and hence would not encounter them so often. It would be necessary to consider diffraction from higher order inclined planes such as (10$\bar{1}$1) for which the associated Fourier component of the lattice potential may

be very small. It does not seem impossible that further reduction in scattering by as much as a factor of 5 or so could occur purely as a result of the different geometry in the h.c.p. system.

(3) The estimate of a stacking-fault density of 10^7 cm^{-1} (equivalent to a fault on every third plane) with the faults scattering independently seems dangerously large. Even in highly deformed sodium, where the f.c.c. and h.c.p. phases appear to be relatively closer in energy than in lithium, Barrett (1956) estimated from x-ray studies that only 1 plane in 5 was faulted while in unworked samples the faulting was less. A faulting density involving 1 plane in 10 might therefore be a more reasonable figure to assume for the case in question.

The suggestion (Howie 1960) that faults more than one layer apart should scatter independently was made for copper and it is likely that faults would interact over greater distances in more free-electron-like metals. The assumption of genuinely independent scattering from arrays of parallel faults should moreover evidently be applied with the greatest caution since any approach to a regular arrangement of faults must lead to cooperative effects. The h.c.p. structure could for instance be regarded as f.c.c. with a fault on every second plane and a very large resistivity would be expected for perfect crystals of this structure if the faults were imagined to scatter independently.

It seems possible therefore that a figure for the resistivity associated with unit density of stacking fault in h.c.p. lithium as low as 4×10^{-15} ohm-cm could be understood without any modification to our picture of the way in which stacking faults scatter electrons and that the remaining discrepancy between this figure and the one quoted earlier may result from an over-estimation of the effective stacking fault density.

Acknowledgments

I am grateful to Drs. Dugdale and Gugan for affording the opportunity to comment on their observations and to Mr. Cotterill for permission to quote his results prior to publication.

References

Barrett, C. S., 1956, *Acta cryst.*, **9**, 671.
Cotterill, R. M. J., 1962, *Phil. Mag.* (to be published).
Ham, F. S., 1960, 'The Fermi Surface' (Proceedings of Cooperstown Conference), p. 9.
Howie, A., 1960, *Phil. Mag.*, **5**, 251.
Pippard, A. B., 1957, *Phil. Trans.* A, **250**, 325.
Ziman, J. M., 1958, *Nuovo Cim.* Suppl., **7**, 353.

A Systematic Error in the Determination of Dislocation Densities in Thin Films

By R. K. Ham and N. G. Sharpe
Division of Tribophysics, Commonwealth Scientific and Industrial Research Organization, University of Melbourne, Victoria, Australia

[Received July 17, 1961]

The methods of estimating the density of dislocations in thin films described by Bailey and Hirsch (1960) and Ham (1961) both depend on the assumption that the dislocation segments are randomly orientated with respect to the plane of the film. Bailey and Hirsch have suggested that when a bulk specimen is thinned dislocations may shorten their lengths by re-orientating themselves so as to lie more nearly normal to the plane of the film. A. K. Head (private communication) has pointed out that this departure from randomness in the distribution of dislocation orientations might be detected by counting the number of intersections which dislocations make with the surfaces of the film. If the dislocations are randomly orientated with respect to the plane of the film, then the dislocation density (i.e. length of line per unit volume) obtained is $\rho' = 2N'/A$, where N' is the number of intersections with both surfaces whose total area is A (Frank 1957). Shortening of the dislocations in the way suggested by Bailey and Hirsch will cause ρ' to be greater than the density ρ obtained by the random line method described by Ham, which counts intersections of dislocations with planes normal to the film.

The dislocation density has been determined both by surface intersection counts and by the random line method for the same areas on 20 micrographs taken from thin films of a specimen of aluminium cold-rolled to give about 9% reduction in thickness. The mean density obtained with random lines was $\rho = 1{\cdot}78 \times 10^9$ cm/cm^3, while that obtained with surface counts was $\rho' = 2{\cdot}18 \times 10^9$ cm/cm^3. Thus the mean difference between the densities determined by the two methods was 4×10^8 cm/cm^3. The standard deviation of the mean difference was $1{\cdot}75 \times 10^8$ cm/cm^3, so that the difference between the two results is significant (at the 3·5% level) and ρ' is greater than ρ. Hence the distribution of dislocation orientations is biased in favour of the direction normal to the film, as suggested by Bailey and Hirsch.

This means that the true dislocation density in the film (in the absence of other systematic errors, e.g. invisibility of certain dislocations) must lie between ρ and ρ'. Since the difference between ρ and ρ' is about 20% then the error in either ρ or ρ' is about 10%.

It may also be noted that the dislocation re-orientations which can occur during the preparation of a thin film will not affect the number of

surface intersections. Thus the result of the surface count ρ' gives an estimate of the true dislocation density *in the bulk* (again in the absence of other systematic errors, e.g. loss of dislocations during thinning from the bulk) if the dislocations are randomly orientated in the bulk, or if the orientations of the surfaces examined are selected at random. Hence the random line result underestimates the bulk density by about 20%.

Surface counting has a further advantage over the other methods in that it does not depend on a determination of the thickness of the film. Unfortunately it becomes very difficult to count surface intersections for dislocation densities higher than about 3×10^9 cm/cm^3.

References

Bailey, J. E., and Hirsch, P. B., 1960, *Phil. Mag.*, **5,** 485.
Frank, F. C., 1957, *Proc. phys. Soc., Lond.*, B, **70,** 1022 (book review).
Ham, R. K., 1961, *Phil. Mag.* (in the press).

REVIEWS OF BOOKS

Elements of Maser Theory. By Arthur A. Vuylsteke. (Van Nostrand, 1961.) [Pp. 363.] Price £3 11*s.* 6*d.*

This is a remarkable book, and both the author and his employers, General Motors Corporation, are to be congratulated on their foresight in anticipating that there would be a need for a comprehensive account of the general background of theory needed to understand masers. The author (and your reviewer) believes that a new branch of technology, quantum electronics, is about to develop, and that unlike semi-conductors, for example, classical analogues are unlikely to appear. Thus those who are going to be responsible for designing the new devices will be faced with the need to have a really good understanding of quantum mechanics and statistical mechanics. The attempt is made, in this book, to satisfy this need and, in consequence, many pages are devoted to what might be called the standard book-work of modern theoretical physics. The readers' requirements are always kept in mind and although I feel that the average British physics graduate will be hard pushed to absorb all the material presented, he really hasn't any option if he proposed to contribute to the development of masers and quantum electronics. Further, once he has mastered the subject, he will have achieved something worthwhile. I would certainly recommend this book to anyone who is prepared to work hard to understand masers. K. W. H. S.

Computing Methods and the Phase Problem in X-ray Crystal Analysis. By R. Pepinsky, J. M. Robertson and J. C. Speakman. (Pergamon Press, 1961.) [Pp. 326.] Price £3 3*s.* 0*d.*

A conference of crystallographers was held in Glasgow in August of last year to discuss computing methods and methods of solving the ' phase problem '—in other words, how to reconstitute the image of an object when the phases of the waves diffracted by it are unknown. The present book is a summary of the proceedings.

Usually such books are not very successful: they tend to record work at an inappropriate stage of development; the papers often do not hang together; and the discussions, illuminating as they may have seemed to the participants at the time, may look rather trivial in the cold light of print. This book, however, emerges as better than the average. It is extremely useful to know what various people are doing in the field of computation, for their methods are not usually published in the ordinary journals.

Of the 28 chapters in the book, nine are devoted to the phase problem. These are chiefly concerned with so-called ' direct methods '—that is, finding the phases by utilizing relations that are likely to exist between the various orders of diffracted beams. Other methods discussed are the ' heavy-atom ' method, in which the phases are taken to be those of a predominant atom in the crystal; the isomorphous-replacement method, in which comparison is made between two isomorphous crystals; and anomalous dispersion, in which use is made of the change in phase produced when the radiation has a wavelength near to an absorption edge of one of the atoms. Nothing at all is included about recent uses of Fourier transforms.

The book will form a useful addition to the library of the practising x-ray crystallographer. H. L.

The Theory of Neutral and Ionized Gases. Edited by C. De Witt and J. F Detoeuf. (New York: John Wiley & Sons, Inc., 1960.) [Pp. 469.] Price £7 0*s*. 0*d*.

The 1958 and 1959 Les Houches Summer Schools in Theoretical Physics were devoted to the theory of many-body systems. The 1958 Summer School considered the quantum mechanics of such systems and its proceedings have by now become a recognized *vade-mecum*. The 1959 Summer School was devoted to the discussion of the statistical mechanics of systems of interacting particles and the volume reviewed here constitutes its proceedings. Unfortunately these proceedings have taken about half a year longer to be published than the 1958 ones, but now that they have appeared, they should also soon become part of the all too scarce number of compendia on the theory of many-body systems.

Once again the directors of the Les Houches Summer Schools succeeded in attracting a number of theorists who themselves contributed greatly to the subject matter under discussion. The longest contribution is the first one by Montroll in which he discusses ensemble theory, cluster integral theory, transport processes, random walk, phase transitions, and the Ising problem. This is followed by Van Hove's lectures on non-equilibrium processes, and a series of lectures by Delcroix, Kruskal, Kaufman, and Denisse on various aspects of plasma theory. The volume is completed by a discussion by Schatzman of plasma-physics as applied to astrophysics.

Unfortunately the editors have not supplied an index which would have appreciably enhanced the already considerable value of this book. Surely, if these lectures are worth publishing—which they certainly are—they are worth publishing with an index. D. ter Haar.

Balthasar van der Pol: Selected Scientific Papers. (2 volumes.) Edited by H. Bremmer and C. J. Bouwkamp. (Amsterdam: North Holland Publishing Company, 1960.) [Pp. xvi+1339.] Price £6 13*s*. 0*d*.

Balthasar van der Pol's scientific papers range over a wide field in the border region between Physics, Electrical Engineering and Mathematics. They include papers of fundamental importance to which workers in the appropriate fields need to make frequent reference and there must be many who will want to have these volumes on their shelves.

The topics covered may be divided broadly into three groups. First, there are the papers on the propagation of radio waves including the famous series on propagation over a spherical earth with finite conductivity. Second, there are the papers on thermionic valves including studies of relaxation oscillations and the two well known papers written in collaboration with Sir Edward Appleton. Third, there are the mathematical papers which cover such topics as operational calculus, theory of numbers, Tchebycheff polynomials and Jacobi functions.

These volumes are very well reproduced from the original journals by a photographic process. About 71% of the material is in English, 13% in Dutch and the remander about equally in French and German. Van der Pol's doctoral thesis, in Dutch, is included, but the editors point out that most of the material is repeated elsewhere in English. Two plates show photographic reproductions from van der Pol's manuscript notes. K. G. B.

Relativity. The General Theory. By J. L. Synge. (North-Holland Publishing Company, 1960.) [Pp. 505.] Price £5 10*s*. 0*d*.

This is the companion volume to Professor Synge's *Relativity: the special theory* (1956) but it can be read independently. Like the earlier book, it is a major addition to the literature.

In a general way, the ground covered is about what we should expect of a comprehensive treatise. However, the approach and development and the selection of particular topics within the general scope are all highly individualistic. Synge exploits more recondite resources of differential geometry than those that are at the command of most other writers. He combines the physics and the geometry almost axiomatically and without appeal to the outworn traditional heuristic arguments. He gives a many-sided analysis of the field equations and their consequences. He considers many applications of the general theory but mainly for the sake of the principles or methods they illustrate rather than the immediate particular results. While he expressly does not aim at completeness in his treatment of the ground covered, he provides an extensive bibliography (64 pages) that includes references to numerous topics not dealt with in the text.

The work is the outcome of Synge's unrivalled experience of relativity in research, teaching and collaboration with younger colleagues. As we have come to expect, the presentation is spiced by Synge's mordant wit. His book will be of immense value to all workers in relativity and it will be a special boon to those beginning to do research in the field. The only readers on whom its merits would probable by wasted are those who are quite without previous knowledge of the theory. W. H. McC.

Resonance Absorption in Nuclear Reactors. By Lawrence Dresner. (Pergamon Press, 1960.) [Pp. 131.] Price £2 0*s*. 0*d*.

This book is extremely useful, containing a comprehensive summary of the theory and a comparison of theory with experiment. It is divided into eight chapters, commencing with a short historical review and two chapters on the theory of resonance absorption in an homogeneous medium. The interesting part of the book, from the point of view of people interested in reactor design physics, is contained in the subsequent chapters on heterogeneous resonance integrals. These chapters contain a description of the approximate analytic theory for estimating the resonance absorption in a lattice structure. It is shown how, with certain assumptions, the calculation in the heterogeneous case can be reduced to that of the homogeneous case. The argument is more satisfying from a logical point of point, than the theory previously used to justify the form of the empirical relations fitted to the experimental results.

The use of the purely numerical Monte Carlo method is not discussed in detail, although some results are quoted. It would have been interesting to compare the Monte Carlo results with the approximate analytic ones for a greater variety of cases. The comparison with theory and experiment illustrate the usefulness of Hellstrand's series of experiments.

This book should be welcomed, it will be very useful to reactor design physicists. J. H. T.

Radio Waves in the Ionosphere. By K. G. Budden. (Cambridge: University Press, 1961.) [Pp. 542.] Price £4 15*s*. 0*d*.

The propagation of radio waves through the inhomogeneous, anisotropic ionosphere presents problems of considerable complication, especially when the electron concentration changes appreciably within the space of one wavelength. The results of work on these problem are spread over a wide range of papers so that it is not easy to obtain a clear picture of what has been accomplished. Moreover, the mathematical apparatus involved is complicated, so that many physicists and engineers find difficulty in understanding clearly how the problems have been approached and what the results are.

Dr. Budden's book provides, in a very clear form, an exposition of these matters and a clear statement of what has been accomplished. His ability as a teacher is evident from the way in which he introduces each part of the subject from first principles, and explains any less familiar mathematical concepts.

The book can be unreservedly recommended to all who are concerned with the theory of radio waves in the ionosphere. For those familiar with the subject it will suffice to list some of the section headings to indicate its value:

" Slowly varying media ", " W.K.B. solutions ", " Ray theory for oblique incidence ", " The Booker quartic ", " The ray velocity and the ray surface ", " The general problem of ray tracing ", " Coupled wave equations ", " The Z-trace ", " The coupling echo ", " Coupling between upgoing and downgoing waves ", " The phase integral method ", " Reciprocity."

It will also form a valuable text-book for anyone setting out to study some of the more complicated aspects of electro-magnetic wave theory, and for them the examples included at the ends of the separate chapters should prove useful.

The dedication of the book " To the memory of Douglas R. Hartree " is a happy and most appropriate one. J. A. R.

Electrical Noise. Fundamentals and Physical Mechanism. By D. A. Bell. (D. van Nostrand, 1960.) [Pp. 342.] Price £2 10*s.* 0*d.*

This is an excellent book which will undoubtedly be warmly welcomed by engineers, research workers and teachers in a wide variety of fields. The author's intention was to give a complete and coherent account of the present state of knowledge and he has amply succeeded in this scholarly, closely reasoned and yet readable volume.

In the first few chapters a very thorough account is given of the fundamentals of noise theory, namely equipartition, statistical mechanics and Nyquist's theorem. Succeeding chapters deal with noise in various types of valve, photo-multipliers and more recent devices including masers and parametric amplifiers. This is followed by a detailed discussion of current noise in semi-conductors, noise in thin films and Barkhausen noise. Some mention is also made of radiation detectors and measuring techniques although space forbids other than an outline of the principles involved. Throughout, the text is liberally dressed with references to original papers which provide a full, if not exhaustive, bibliography.

It is difficult to criticize this book without niggling at a few details and it deserves far better treatment than this. A. H.

Quantum Theory of Atomic Structure, Vol. 2. By J. C. Slater. (McGraw-Hill Publishing Company Ltd., 1960.) [Pp. 439.] Price £5 1*s.* 0*d.*

This book is one of the best attempts to lead the advanced student easily into the sophisticated theory of the quantum structure of atoms. At the same time it provides a very useful collection of reference data and applications of advanced techniques. It might be regarded as for the specialist and for reference but it is not the compendium of theorems that this might seem to imply. There is an air of teaching the reader to do it for himself. Professor Slater writes as if he thinks you can do quite a lot of advanced theory on an odd piece of paper and this book will show you how. The content, however, is really quite heavy and, for example, one finds a very informative review of Racah's methods for complex spectra but without all the details of his papers.

The main contents are the mathematical theory and an account of quantitative predictions of atomic multiplet levels, together with many reference tables, the theoreties of magnetic properties and hyperfine structure and the treatment of the fractional parentage theory of *an* configurations by projection operators. Finally there is a complete bibliography of all theoretical investigations on atomic structure.

It will be a most valuable book for those who research or lecture on atomic structure and it should be in all science libraries. S. F. B.

Introduction to Mechanics, Matter, and Waves. By U. Ingard and W. L. Kraushaar. (Addison-Wesley Publishing Company Inc., 1960.) [Pp. 672.] Price £2 13*s*. 0*d*.

This textbook is based upon a year's course in general physics at MIT, and it covers mechanics, dynamics, wave motion, elementary properties of matter, the kinetic theory of gasses, and a little thermodynamics, starting essentially from scratch. As is common with such American texts it assumes a concurrent course in mathematics, so that the mathematical standard of the book becomes more advanced as it progresses; calculus is used freely throughout the latter half. The basic concepts, such as force, energy and so on, are discussed very carefully, with the aid of many excellent diagrams illustrating actual or conceptual experiments, and the argument is developed from these as far as such relatively sophisticated topics as Rutherford scattering, coriolis force, gyroscopic motion, the Maxwell–Boltzman distribution, entropy and probability, and the Bernoulli effect. There are a number of problems after each chapter. In general the presentation is good, and the book seems likely to be a useful one.

T. E. F.

The Theory of Transition-Metal Ion. By J. S. Griffith. (Cambridge: University Press, 1961.) [Pp. x+453.] Price £4 15*s*. 0*d*.

Transition metal compounds are interesting because of the great variety of their properties, chemical, optical and magnetic. Basically these all derive from an incomplete electron shell. There are many energy levels of an ion within a relatively small energy range. The electron charge distribution is therefore flexible and can adapt itself to its environment in such a way as to lower the energy, thereby making a particularly stable complex. There are many levels separated from the ground state by energy differences in the range afforded by quanta of visible light. Light is therefore selectively absorbed, giving transition metal compounds their colour, and on a more sophisticated level, their interesting and complex absorption spectra. The magnetic moments of individual electrons in the ion are not forced by the exclusion principle to cancel each other out, and the ion therefore has a magnetic moment.

Since the pioneer work of Van Vleck in the 1930s, more and more attention has been devoted to those interesting phenomena and to the theories which unify them. Professor Griffith's book is both timely and admirable. It brings together the various physical and chemical properties of transition metal ions in a comprehensive manner and relates them to a well-developed theoretical framework. The exposition is admirably lucid. General principles are first outlined and then specified problems are worked out in fair detail. Nowhere is the reader bogged down by a surfeit of generality, though by the end of an argument he may have been led to a very general point of view. Professor Griffith prefers to treat a problem first approximately, and later to point out what modifications are required to incorporate the features which were neglected.

Five chapters are devoted to theoretical ground work. This covers ground which is to be found elsewhere, and makes the book rather bulky. However, this approach has the merit of making the book self-contained and giving it unity. Some of the results presented, particularly in the chapter on groups, are new. The general theory is always economically set out for the purpose in hand. The remainder of the book is devoted to a more detailed discussion of various aspects of transition metal ions as follows: complex ions; crystal-field theory and the weak-field coupling scheme; the strong-field coupling scheme; paramagnetic susceptibilities; optical spectra and thermodynamic properties; paramagnetic resonance.

M. H. L. P.

An Introduction to Applied Anisotropic Elasticity. By R. F. S. Hearmon. (Clarendon Press; Oxford University Press, 1961.) [Pp. 136.] Price £1 15*s*. 0*d*.

After assuming that the reader has a knowledge of the fundamentals of theoretical elasticity, the first part of this book gives an authoritative discussion of the stress–strain relations in aelotropic media. The effects of symmetry are described in full, and there is a chapter on single crystals, sheet materials and polycrystalline aggregates.

In later chapters, the author has collected, from many sources, solutions to a large number of problems in anisotropic elasticity. In a few cases solutions are given out of context and are, therefore, hard to follow. However, the comprehensive list of references makes it easy to refer to the original work. In a chapter on wave propagation, recent research work is described, but one gains the impression that the presentation could be simplified if a more general approach were adopted.

The book fills a gap and it will be found very useful, not only by the engineer or physicist, but also by the mathematician working in this field. V. T. B.

Dispersion Relations. Edited by G. R. Screaton. (Oliver & Boyd, 1961.) [Pp. 290.] Price £2 15*s*. 0*d*.

This volume contains the lecture notes of the Scottish Universities Summer School on Dispersion Relations arranged by N. Kemmer in August 1960.

The first chapter is by J. D. Jackson and gives an introduction to dispersion relation techniques that is suitable for a reader having only an elementary knowledge of quantum field theory. In the second chapter J. C. Polkinghorne gives an account of the basic techniques used to establish analyticity properties in perturbation theory. This is balanced by a discussion of analyticity properties of scattering amplitudes based on axiomatic field theory given by W. Thirring. The mathematical foundations of quantum field theory are discussed in a short chapter by J. M. Jauch.

The four remaining chapters give an excellent introduction to the problems of applying dispersion theory to physical processes. M. J. Moravcsik discusses the use of the 'nearest singularity' approximation with particular reference to nucleon–nucleon scattering. G. F. Chew gives a very readable account of the ambitious programme directed towards basing a theory of strong interactions on double dispersion relations and unitarity; this includes a discussion of the Mandelstam representation and partial wave dispersion relations. W. R. Frazer gives an account of the more limited problem of the nucleon form-factor, based on the two-pion approximation. S. Fubini describes the use of single variable dispersion relations in pion physics.

This book gives an excellent introduction to the important subject of analytic structure and elementary particle physics. It is suitable for reading at graduate level following an elementary course on quantum field theory. R. J. E.

[*The Editors do not hold themselves responsible for the views expressed by their correspondents.*]

Fig. 2

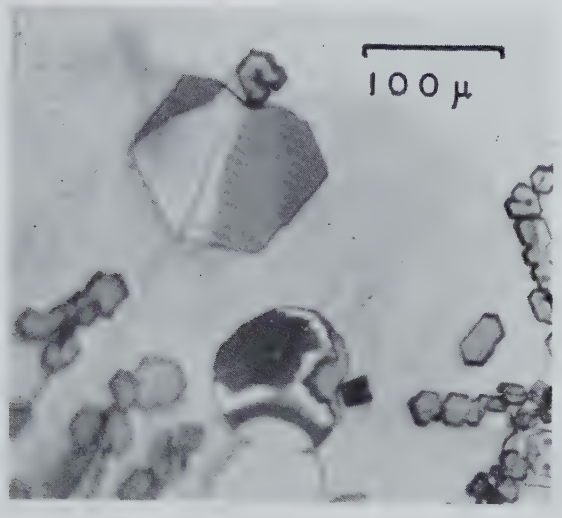

A large crystal (top) showing changes of hue as it grows across a series of shallow steps of height 300 to 800Å. The lower crystal, thickening by layers spreading over its surface, is becoming polygonal.

Fig. 5

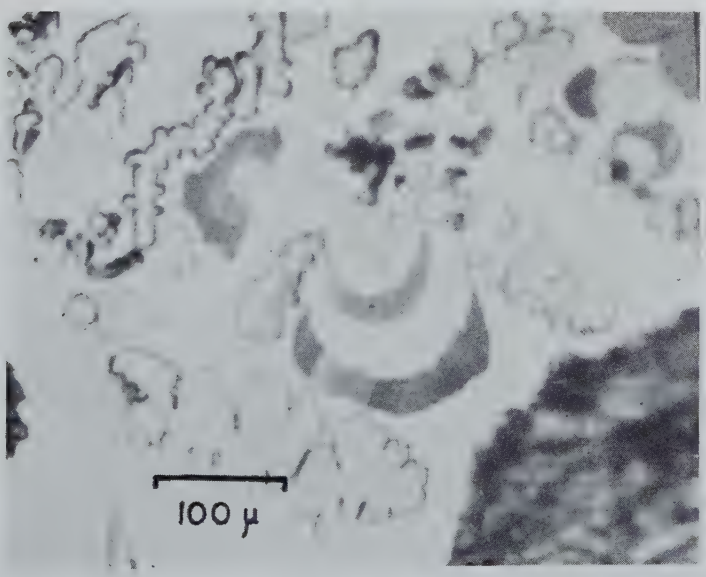

Layers of thickness 300 to 1200Å spreading over crystal surfaces after initiation at the edge. Temperature $-16{\cdot}5°$C. Excess vapour density $0{\cdot}4 \times 10^{-6}$ g cm^{-3}.

Fig. 8

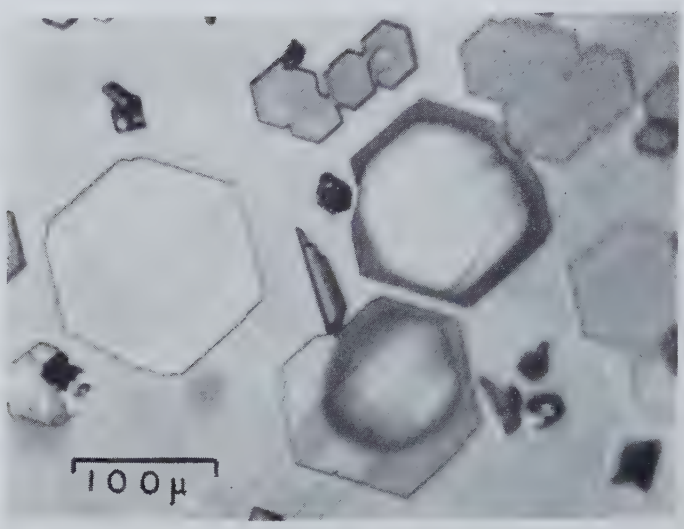

Layers of thickness 1200Å growing around the crystal edges, after initiation by contact with thicker crystals.

Fig. 9

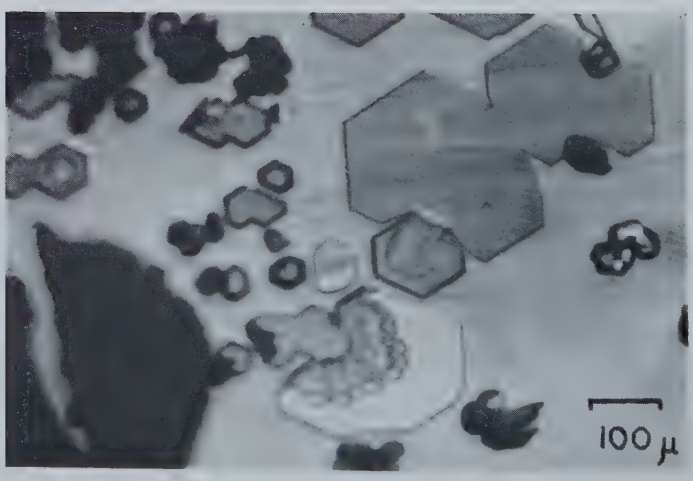

An irregularly shaped layer growing over an ice surface.

Fig. 10

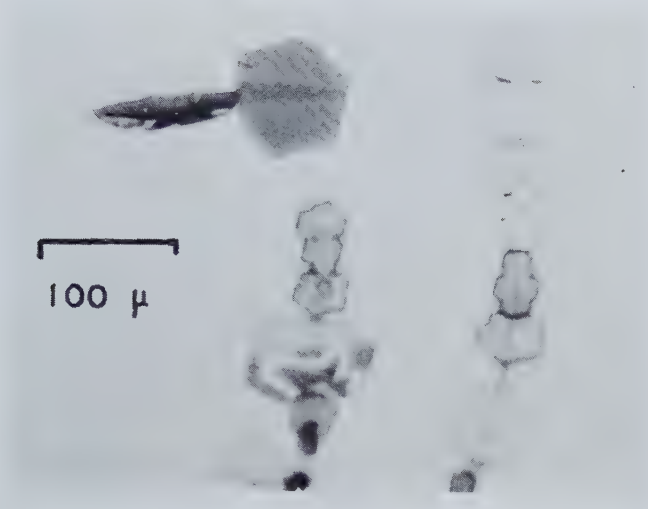

A dendritic layer with growth maxima in ⟨11$\bar{2}$0⟩ directions. Note that all crystals are growing on steps in the substrate.

Fig. 15

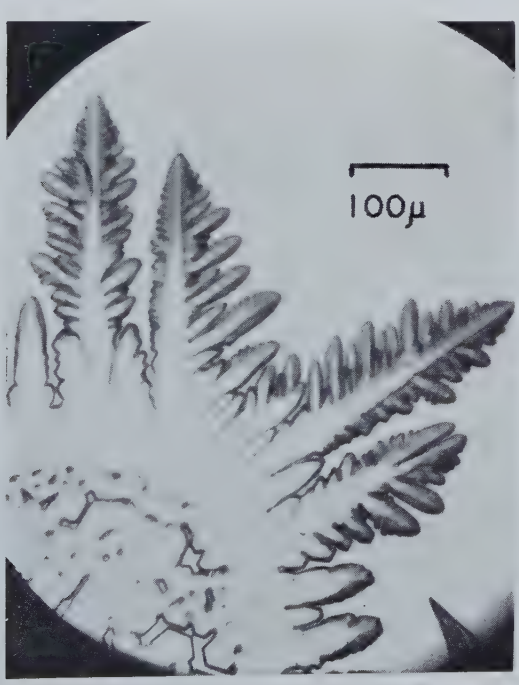

Dendritic growth of ice crystals on a freshly cleaved mica surface.

Fig. 1

Photomicrograph (×140) of a natural octahedron surface showing a low-angle pyramidal trigon X and a steep-sided flat-based trigon Y.

Fig. 2

Fizeau fringes across a steep-sided flat-based trigon (×400).

Fig. 3

Fizeau fringes across a low-angle pyramidal trigon (×400).

Fig. 5

Photomicrograph (×28) showing low-angle pyramidal trigons and steep-sided trigons.

Fig. 1

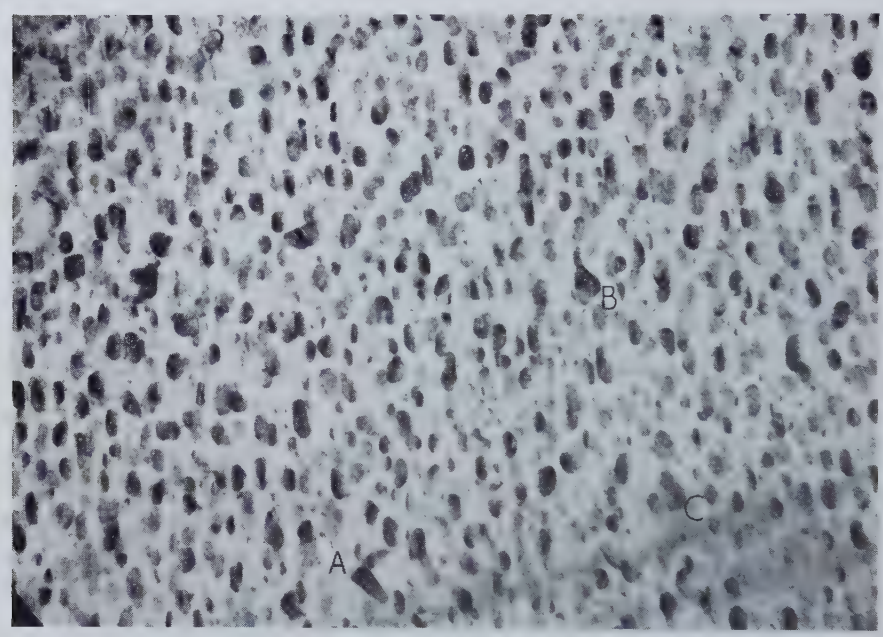

(*a*)

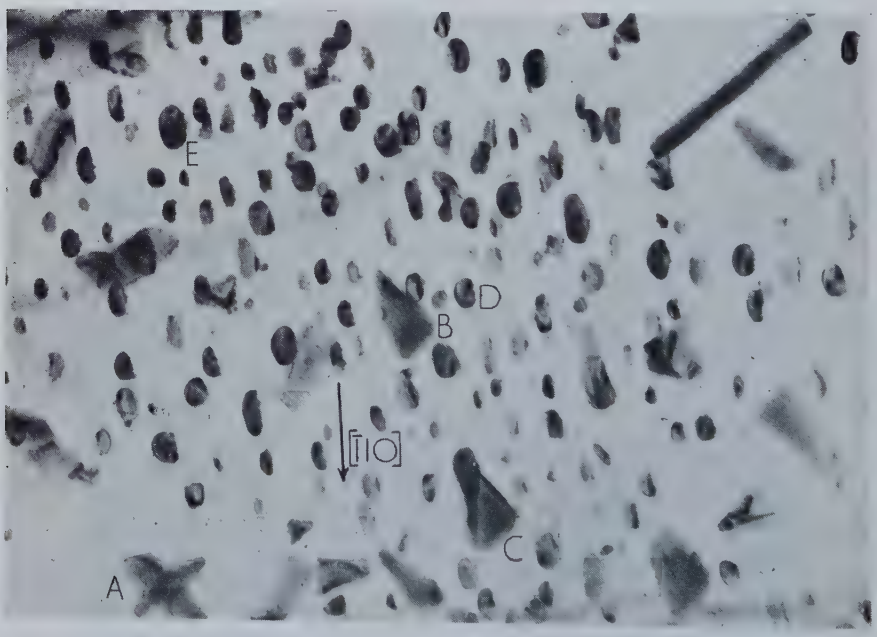

(*b*)

(*a*) Initial precipitation in Al+4% Cu alloy aged for a few minutes at ~270°C. The majority of the precipitates are θ' and are believed to be at the foil surfaces. (*b*) Same area at ~340°C. Note the coarsening. Large precipitates A, B and C are θ. Foil surface near (112). ×30 000.

Fig. 2

(*a*)

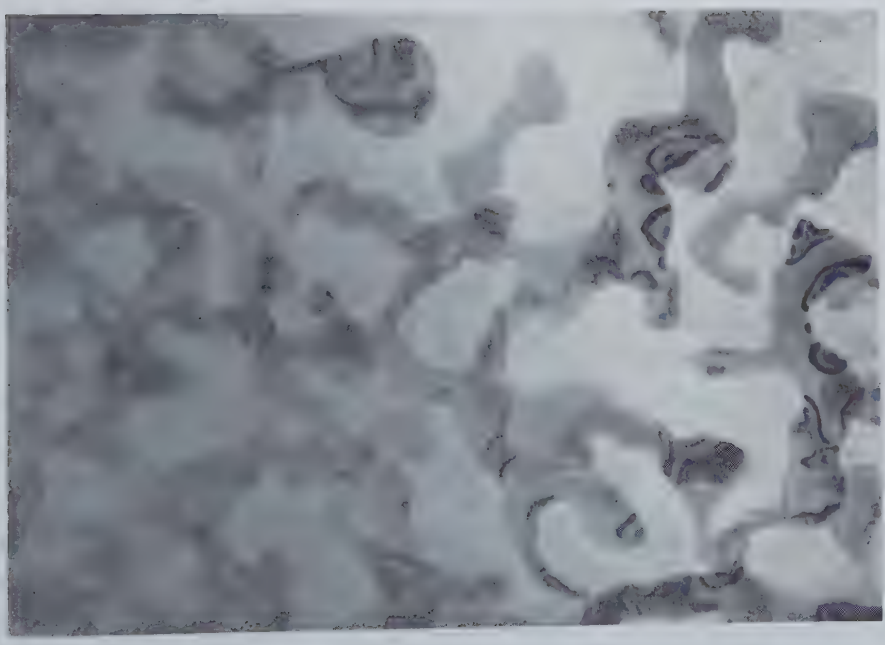

0·5μ (*b*)

(*a*) Precipitation at ~270 c characteristic of a foil with near (100) surface. The large θ' precipitates viewed edge-on are known to have nucleated in the interior on dislocations. The irregular precipitates of lower visibility are θ', and are thought to lie at the (100) surfaces. (*b*) Same grain at ~330 c showing extended precipitate patterns of θ phase. The extended patterns are believed to be at the surfaces. ×30 000.

Fig. 3

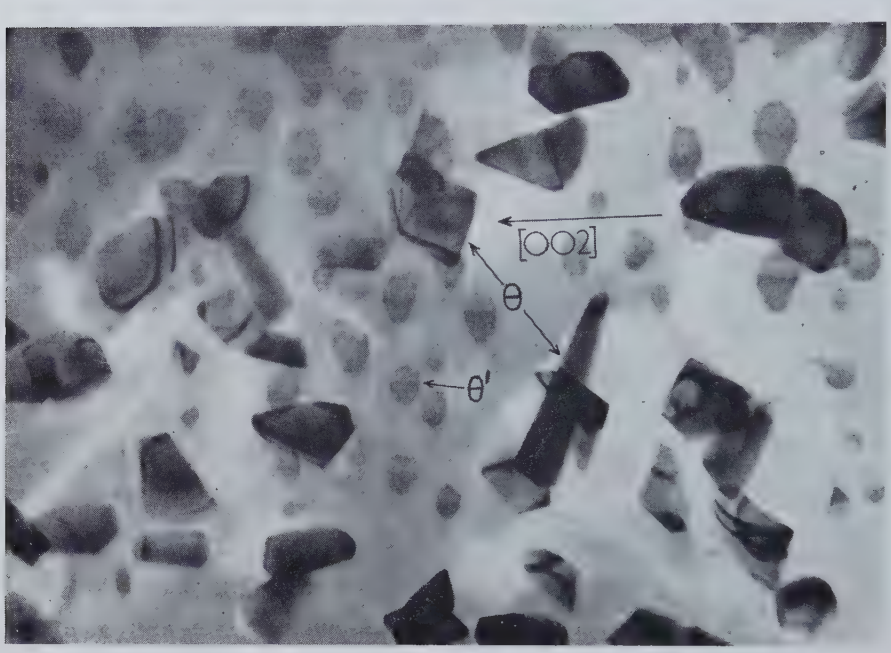

Region with near (110) surface showing θ and θ' precipitates at $\sim$320°c. $\times$30 000.

Fig. 4

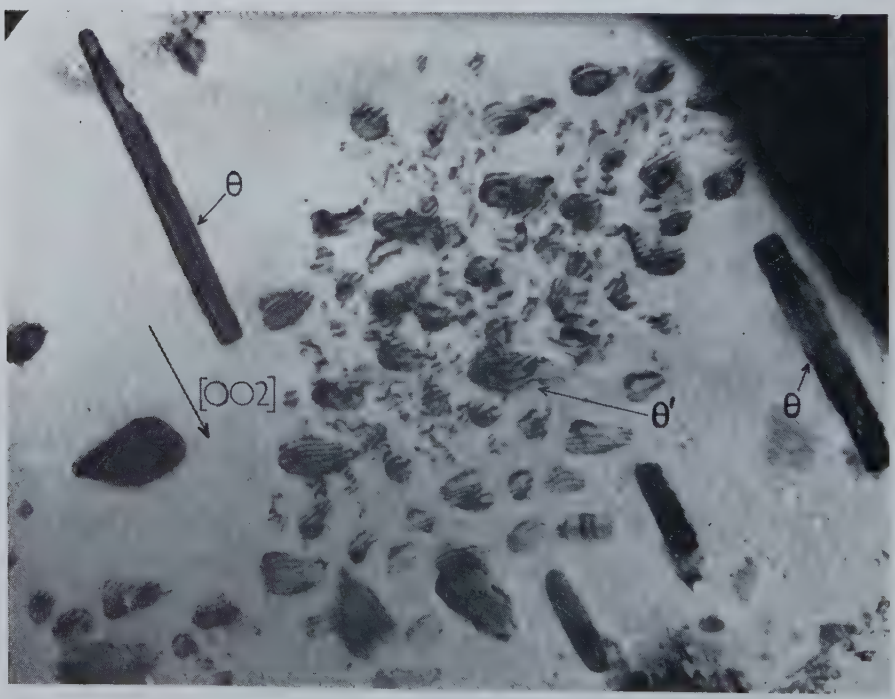

0·5μ

(110) area at $\sim$320°c, showing θ and θ' precipitates. $\times$30 000.

Fig. 5

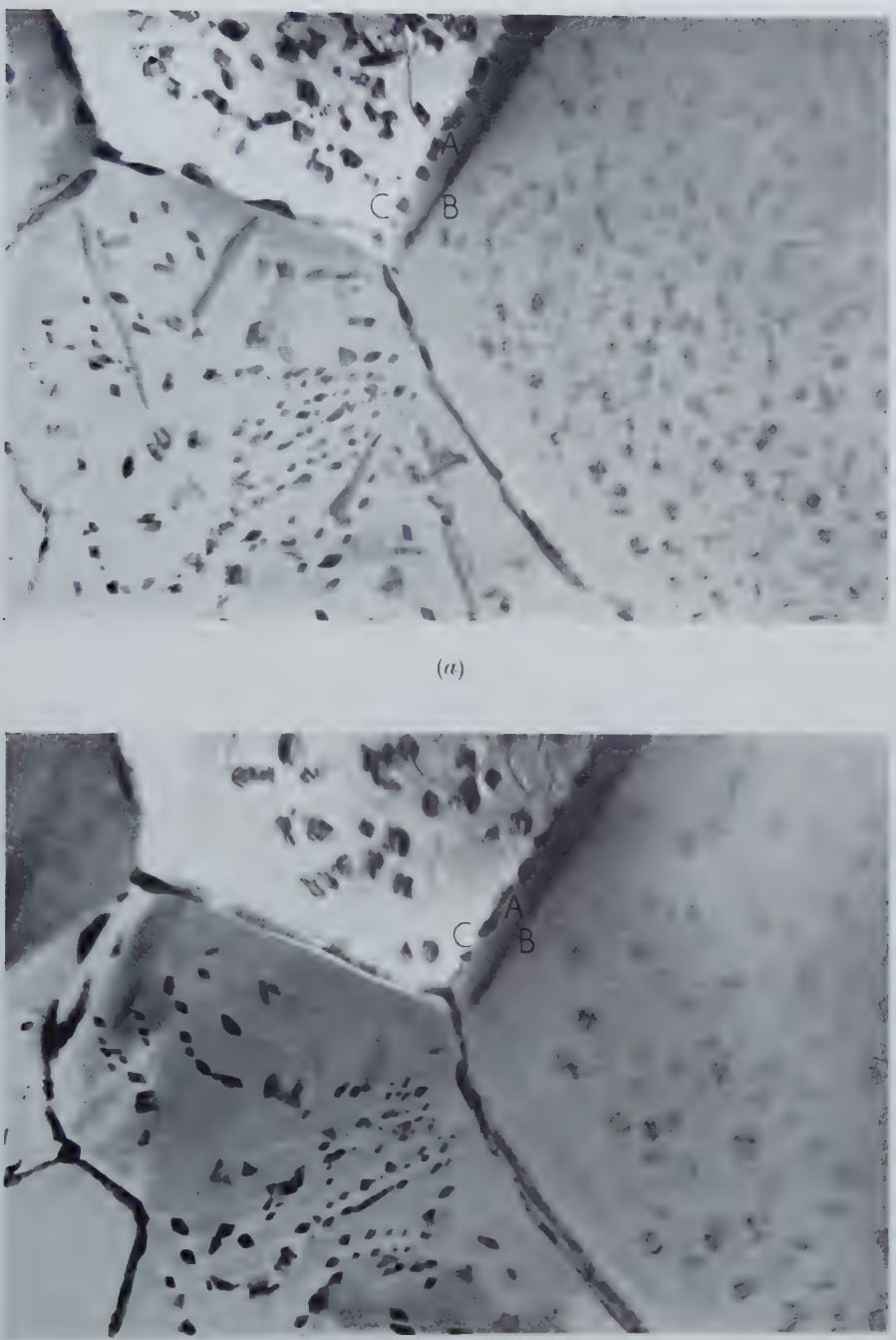

(*a*)

(*b*)

Examples of precipitates at ~300 c near a triple grain boundary junction. A, inclined grain boundary with preferential precipitation at the surfaces B and C. Note the regions denuded of precipitates near the grain boundaries; (*a*) refers to the second precipitation, (*b*) refers to the third precipitation. ×15 000.

Fig. 6

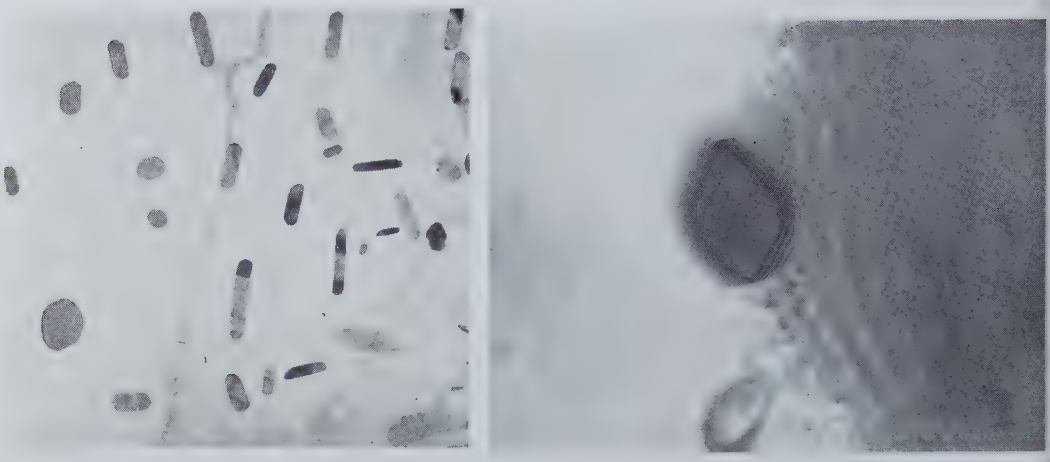

(*a*) θ precipitates in a thin region. The precipitates run right through the foil. Temperature ~430°C. ×10 000. (*b*) θ precipitate running right through the foil. Note the inclined boundary showing thickness interference fringes. ×30 000.

Fig. 7

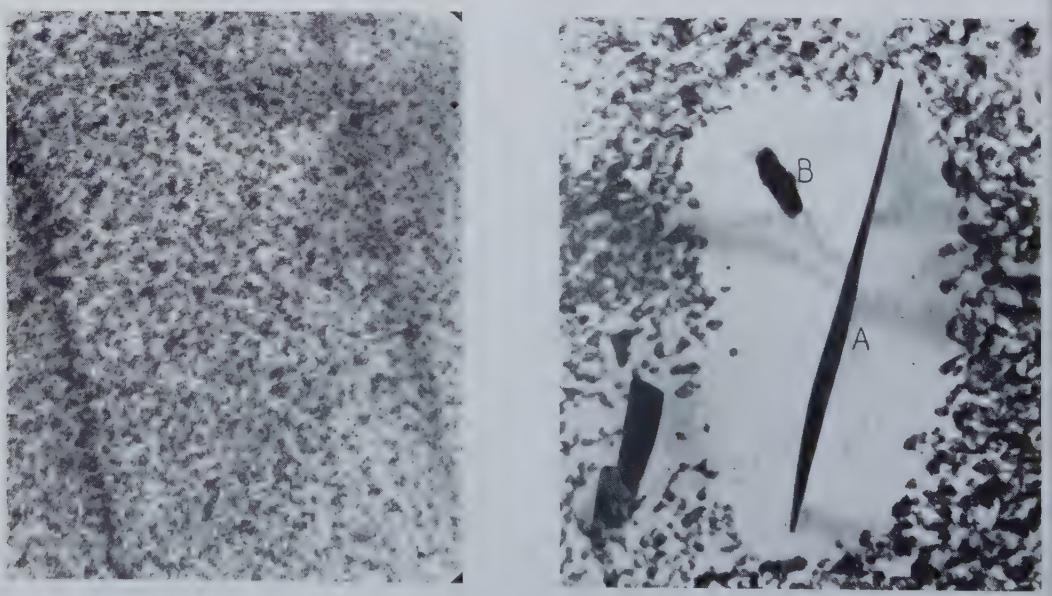

(*a*) Region showing initial precipitates after 30 min. at ~250°C. The precipitates are probably θ'. ×20 000. (*b*) Same region after a small temperature rise, showing growth of large precipitates surrounded by a denuded zone. The precipitates A and B are probably θ. ×10 000.

Fig. 8

0·5μ

Thin foil aged for 10 min. at 270°c in high vacuum prior to examination. Compare with fig. 1. ×30 000.

Fig. 9

0·5μ

Thick region of the same specimen as fig. 8 after the same ageing treatment and a further electropolish. The θ' precipitate patterns are probably the result of nucleation at helical dislocations. ×26 000.

Fig. 10

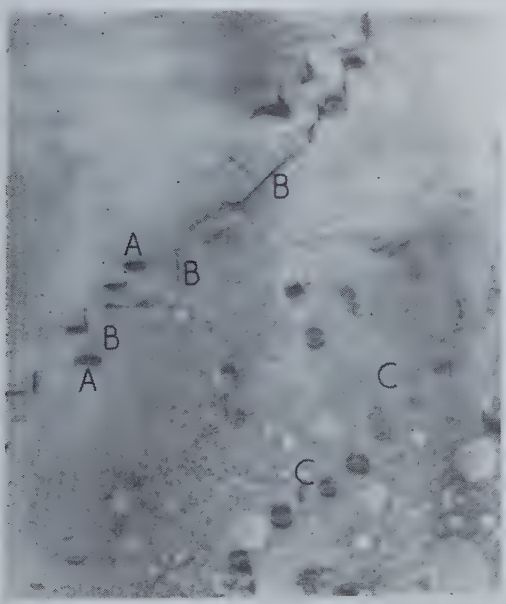

Examples of precipitation at helical dislocations. Aged in bulk for 2 min at 270°c. Note the precipitates A and the dislocation B. ×26 000.

0·5μ

Fig. 11

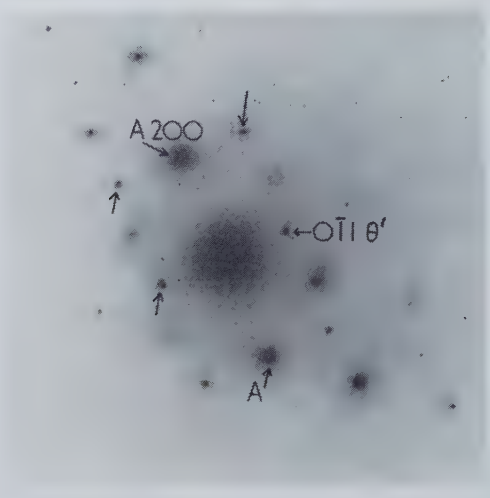

Selected area electron diffraction pattern from a thin foil aged at ~270°C, showing cross-grating pattern from θ' marked with arrows. A, 200 matrix and θ' reflections. Foil surface near (011).

Fig. 12

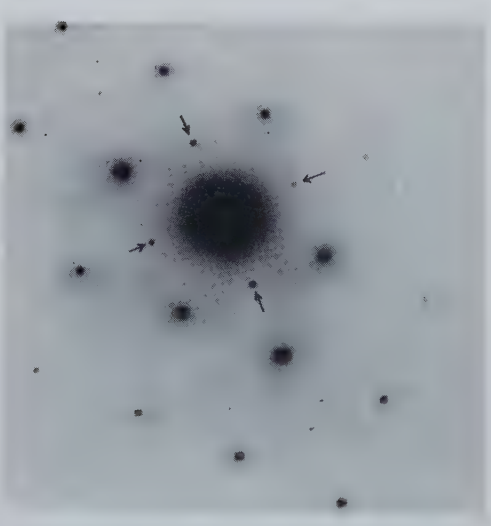

(*a*)

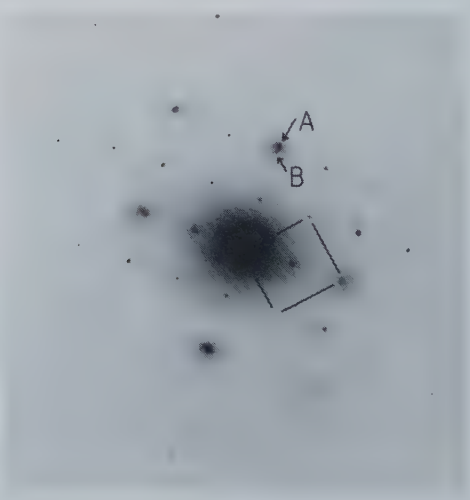

(*b*)

(*a*) θ' reflections of type 110 (marked with arrows) from precipitates in a foil of (001) orientation similar to fig. 2 (*a*). Ageing temperature ~250°C. (*b*) Diffraction pattern from the same grain at ~330°C, showing θ cross-grating pattern. *a*-axes of θ phase are outlined. Note the 200 type matrix reflection A, and the 220 type θ reflection B.

Fig. 13

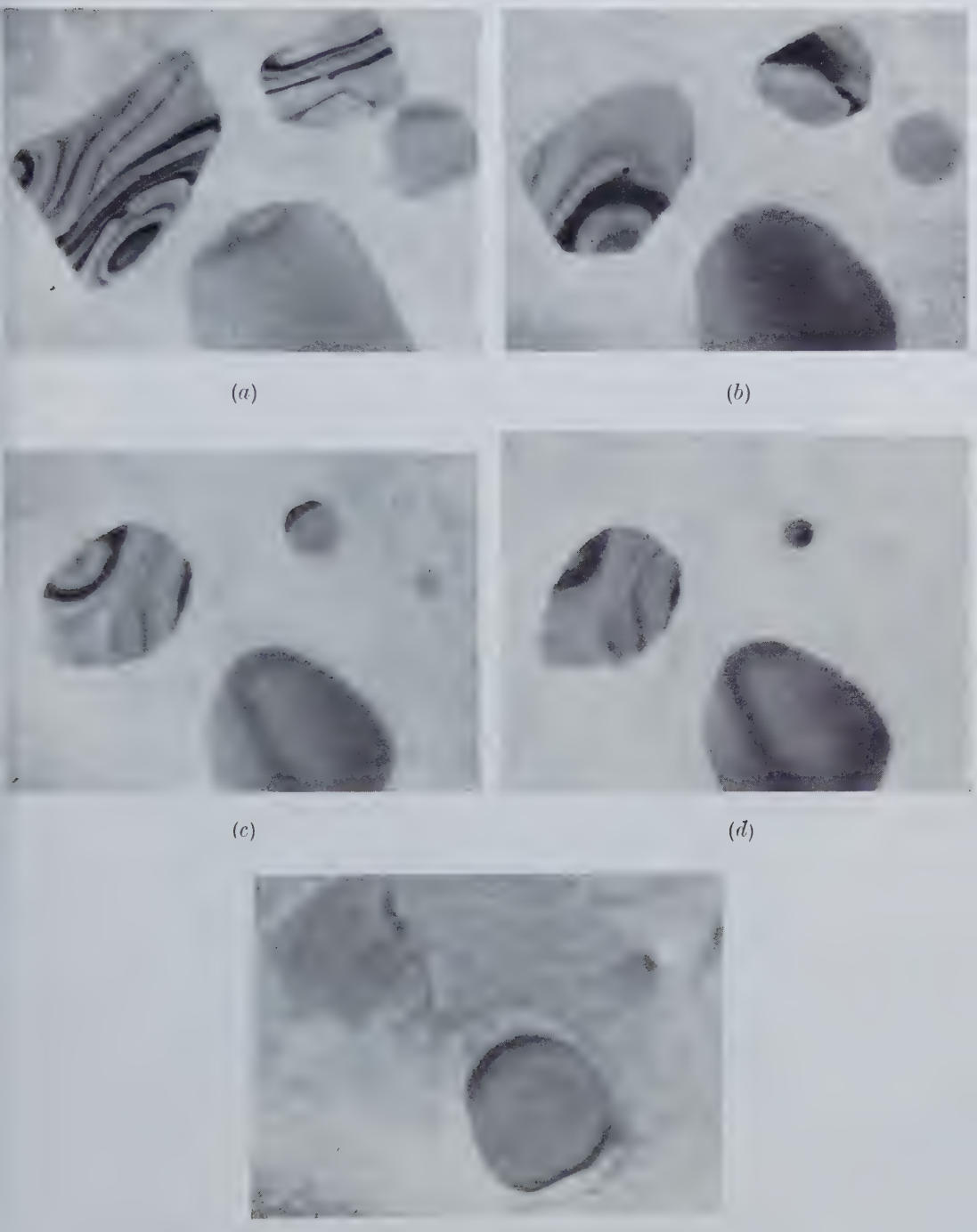

Sequence of micrographs showing dissolution of θ precipitates as the temperature is raised between 400 and 500°c. Note the rounding-off of the angular-shaped precipitates. Foil surface is (100). ×30 000.

Fig. 1

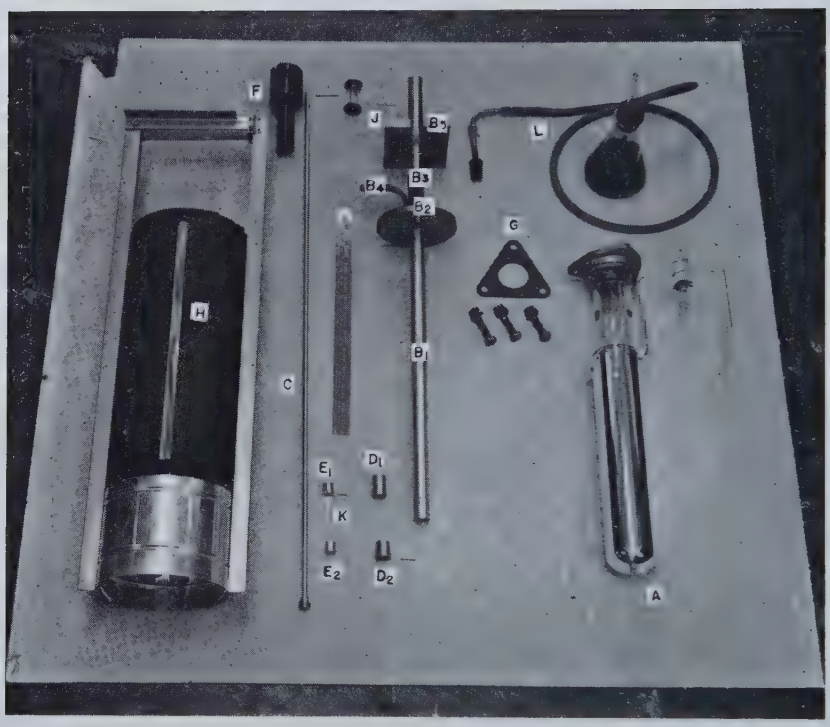

Apparatus for tensile testing at 4·2°K. A, vacuum jacketed helium dewar ; B_1, compression tube ; B_2, flange for attaching helium dewar ; B_3, attachment for helium transfer tube ; B_4, exhaust opening ; B_5, flange for attaching to Instron ; C, tension tube ; D_1 and D_2, fixtures for holding specimen grips ; E_1 and E_2, grips for holding specimen ; F, adaptor for attaching tension tube to Instron ; G, neoprene gasket ; H, nitrogen dewar ; J, helium gas inlet for purging ; C fits into opening in J ; K, typical specimen ; L, bubbler for helium gas outlet.

Fig. 1

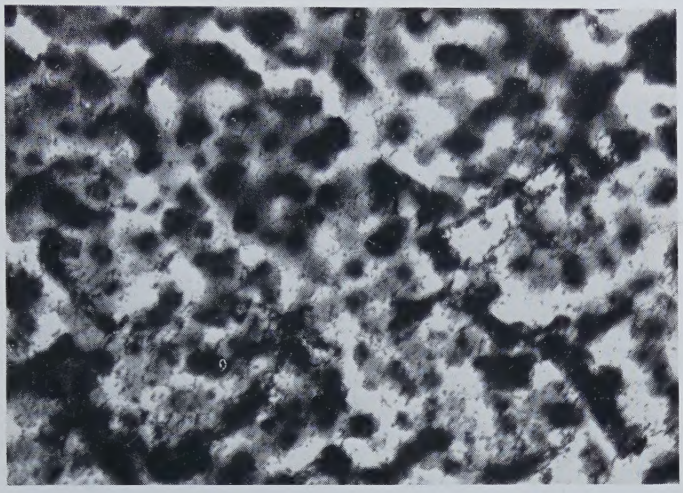

Single crystal gold film bombarded with 300 ev argon ions. ×40 000.

Fig. 2

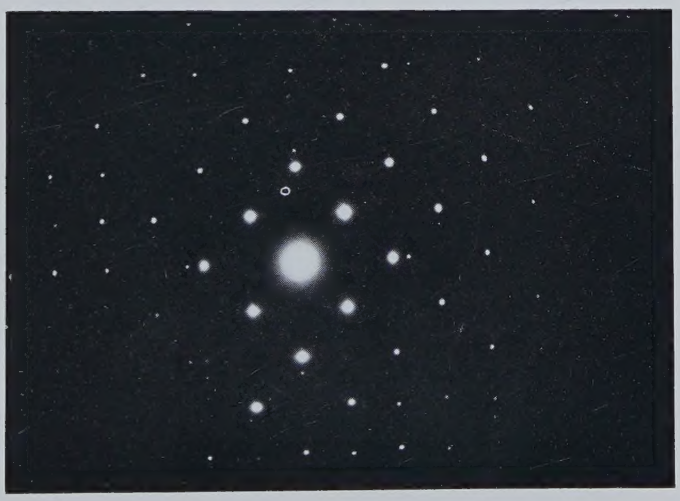

As fig. 1, selected area 5 microns in diameter.

Fig. 3

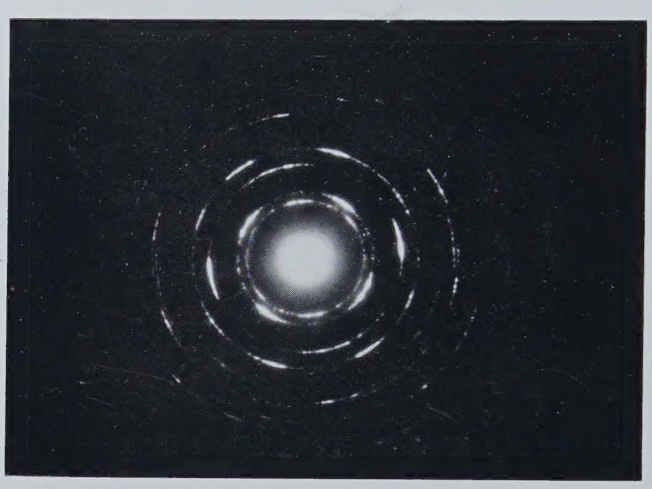

Diffraction pattern at edge of bombarded specimen. 5 microns.

Fig. 4

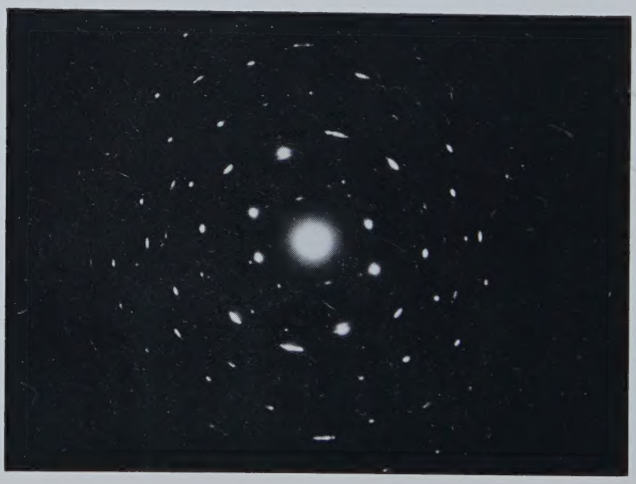

Diffraction pattern at edge of unbombarded specimen. 5 microns.

Fig. 5

Gold film annealed at 350°c after ion bombardment. $\times 100\,000$.